Alkynes in covalent enzyme inhibitors: down the kinetic rabbit hole

Mons, E.

IC50
Ub
Kinact

Chapter 6

The Versatility of Substituted Propargyl Warheads in Ub-ABPs

Adapted from:

Mons, E.; Kim, R.Q.; van Doodewaerd, B.R.; van Veelen, P.A.; Mulder, M.P.C.; Ovaa, H. Exploring the Versatility of the Covalent Thiol–Alkyne Reaction with Substituted Propargyl Warheads: A Deciding Role for the Cysteine Protease. *J. Am. Chem. Soc.* **2021**, *143*, 6423-6433. doi:10.1021/jacs.0c10513.

Abstract. Terminal nonactivated alkynes are nowadays considered the golden standard for cysteine-reactive warheads in activity-based probes (ABPs) targeting cysteine deubiquitinating enzymes (CysDUBs). In this work, we study the versatility of the thiol–alkyne addition reaction in more depth. Contrary to previous findings with UCHL3, we now show that covalent adduct formation can progress with substituents on the terminal or internal alkyne position. Strikingly, acceptance of alkyne substituents is strictly CysDUB-specific as this is not conserved among members of the same subfamily. Covalent adduct formation with the catalytic cysteine residue was validated by gel analysis and mass spectrometry of intact ABP-treated USP16CD^{WT} and catalytically inactive mutant USP16CD^{C205A}. Bottom-up mass spectrometric analysis of the covalent adduct with a deuterated propargyl ABP provides mechanistic understanding of *in situ* thiol–alkyne reaction, identifying the alkyne rather than an allenic intermediate as the reactive species. Furthermore, kinetic analysis revealed that introduction of (bulky/electron-donating) methyl substituents on the propargyl moiety decreases the rate of covalent adduct formation, thus providing a rational explanation for the commonly lower level of observed covalent adduct compared to unmodified alkynes. Altogether, our work extends the scope of possible propargyl derivatives in cysteine targeting ABPs from unmodified terminal alkynes to internal and substituted alkynes, which we anticipate will have great value in the development of ABPs with improved selectivity profiles.

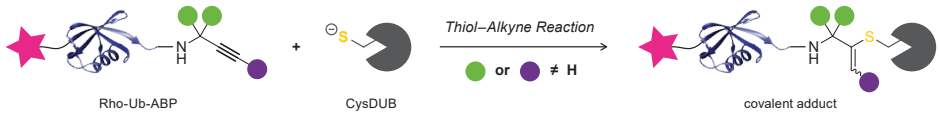

1. Introduction

Ubiquitination is a post-translational modification (PTM) which regulates many cellular processes.[1-3] Aberrant ubiquitination has been observed in numerous diseases, rendering the enzymes involved as attractive targets for drug design.[4-8] Ubiquitination involves ligation of Ubiquitin (Ub), a small 76-amino acid protein, onto the target protein by the E1-E2-E3 ligase machinery. Deubiquitinating enzymes (DUBs) reverse this process by cleavage of the native isopeptide bond between the Ub C-terminus and the target protein Lys (lysine) residue, or between the distal and proximal Ub in poly-Ub chains.[8-9] Cysteine DUBs are classified by their catalytic domain, which contains a catalytic cysteine residue essential for their proteolytic function. There are currently six known classes of human cysteine DUBs; USP, OTU, UCH, MJD, MINDY, and ZUFSP.[1, 10] Their proteolytic activity can be monitored with activity-based probes (ABPs), which covalently trap active enzymes by formation of a covalent bond between an electrophilic warhead on the ABP and the nucleophilic cysteine residue in the targeted enzyme.[11-13] Cysteine DUB ABPs have been utilized to monitor DUB activity during infection, in disease and/or upon inhibitor treatment,[14-17] to identify new DUB (classes) and catalytic cysteine residues in newly discovered DUBs,[18-21] and to visualize Ub binding in crystal structures of covalent adducts.[22-23]

Terminal nonactivated alkynes were believed to be unreactive towards (nontargeted) thiols under physiological conditions, and are therefore widely applied as bioorthogonal handles.[24-26] However, in 2013 two independent groups[27-28] discovered that propargylamide on the C-terminus of ubiquitin(-like modifiers; Ubl) can act as a latent electrophile, forming an irreversible covalent adduct with the catalytic cysteine thiol of cysteine proteases that normally cleave the native Ub(l)-Lys isopeptide bond (**Figure S1A**). The propargyl (**Prg**) moiety has since been utilized in various covalent Ub(l)-based ABPs, and is considered the golden standard for DUB ABPs because of its high stability, ease of synthesis and lack of intrinsic reactivity with nontargeted thiols.[17-18, 29] Formation of a Markovnikov-type thiovinyl bond between active site cysteine thiol and internal (quaternary) alkyne carbon has been confirmed with numerous crystal structures of Ub(l)-**Prg** ABPs bound to human and viral cysteine proteases (summarized in **Table S1**). Recently we showed that the thiol–alkyne reaction can be extended to small molecule inhibitors; a small recognition element is sufficient to initiate covalent thiovinyl bond formation between the cathepsin K catalytic cysteine thiol and the inhibitor alkyne moiety.[30]

The covalent thiol–alkyne addition forming a Markovnikov-type thiovinyl adduct is a newly discovered reaction for which several reaction mechanisms have been proposed (**Scheme 1**). A radical-mediated thiol–yne mechanism was quickly excluded because covalent adduct formation was not prevented by absence of light and/or addition of radical scavengers, and would have resulted in the *anti*-Markovnikov-type thiovinyl bond adduct with terminal C1 carbon (**Scheme 1A**).[31-32] Ekkebus *et al.*[27] and Sommer *et al.*[28] both propose a proximity-driven *in situ* thiol(ate)–alkyne addition that involves direct nucleophilic attack of the catalytic cysteine thiol(ate) to the alkyne internal C2 carbon (**Scheme 1B**). However, it was not possible to exclude the possibility that nucleophilic addition actually occurs with a more reactive allenic isomer, present at the enzyme active site in equilibrium with the unreactive terminal alkyne (**Scheme 1C**).[33-34] Alternatively, Arkona *et al.*[35] propose an enzyme-templated

stepwise reaction with stabilization of a secondary carbanion intermediate in the oxyanion hole to overcome the thermodynamically unfavored bond formation (**Scheme 1D**). This stepwise reaction mechanism would be similar to cysteine/serine protease-mediated proteolysis of native amide bonds that involves stabilization of the anion intermediate in the oxyanion hole, *via* interactions with polar residues such as glutamine or by H-bonds with backbone amides.[36-37]

To date, the scope of the thiol–alkyne addition with nonactivated alkynes has been limited to unsubstituted terminal propargylamide; Ekkebus *et al*. report that substituting the hydrogens on either the terminal C1 carbon (CH) or the internal C3 carbon (CH_2) of the propargyl moiety in Ub-**Prg** mitigates covalent bond formation with UCHL3 (**Figure 1**).[27] The lack of reactivity was contributed to mechanistic components, like an important role for the terminal alkyne proton, or formation of a reactive allene intermediate at the active site. Alternatively, we now hypothesize that the lack of reactivity with substituted propargyl derivatives is resultant from specific steric interactions at the UCHL3 active site, and as such not representative for the prospective reactivity with other cysteine DUBs. Variation in the warhead has been reported to affect the adduct formation pattern in cell lysate while keeping the ubiquitin recognition element unchanged,[19] although we would like to note that in those cases the nature of the warhead was changed rather than introduction of (bulky) substituents to the same electrophile.

In this work we show that restrictions on propargyl substitution are DUB-dependent rather than a general property of the *in situ* thiol–alkyne reaction. We selected a panel of substituted alkynes that are incorporated in DUB ABPs, and explore their reactivity both in lysate and on an extensive set of recombinant cysteine DUBs. Formation of a covalent adduct with substituted alkynes is subsequently validated with USP16. Furthermore, we investigate the consequences of substituents on the rate of covalent adduct formation, since introduction of electron-donating substituents on internal and terminal alkyne carbons reduces alkyne electrophilicity. Together, these results illustrate the possibilities and flexibility of the *in situ* thiol–alkyne addition, thereby improving our understanding of its underlying reaction mechanism and expanding the scope of this reaction to substituted and internal alkynes.

2. Results and Discussion

Design and synthesis of ABPs with substituted alkyne warheads. Cysteine DUB activity can be probed by replacing the Ub C-terminal carboxylate (G76) with an electrophile positioned in alignment with the native isopeptide bond (**Figure S1A**), thus covalently trapping the catalytic cysteine residue.[38-40] The binding affinity of the truncated C-terminal Ub peptide at the active site is low, therefore full-length Ub is used as recognition element in cysteine DUB targeting ABPs.[41-42] In order to elucidate the scope of alkyne substituents in the thiol–alkyne reaction, we prepared a panel of substituted alkynes which were coupled to the C-terminus of fully synthetic Rho-Ub_{1-75} thus generating new ABPs targeting cysteine DUBs (**Figure 2**, **Figure S1B**). Substituents were introduced on the terminal C1 carbon (**2** & **3**), internal C3 carbon (mono-substitution; **4** & **7**, or double substitution; **5** & **8**), as well as alterations on the Ub backbone (amide) (**9** & **10**).

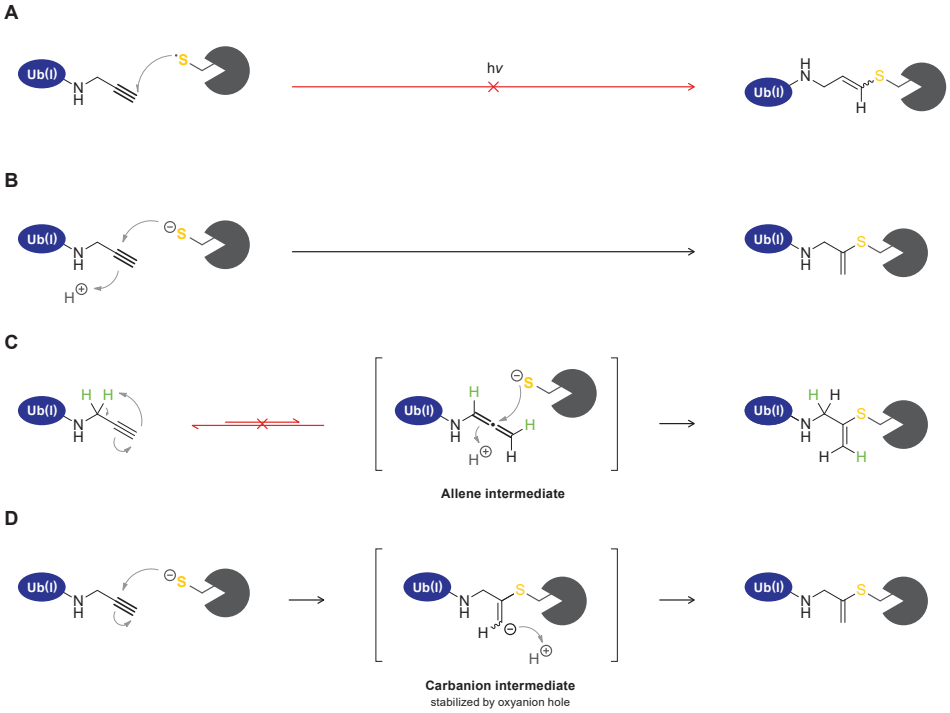

Scheme 1 | Proposed reaction mechanisms for nucleophilic thiol–alkyne addition forming covalent thiovinyl bond between cysteine protease and alkyne. **(A)** Radical-mediated thiol–yne reaction. Excluded because this would form an anti-Markovnikov-type product with alkyne C1 carbon atom.[31-32] **(B)** Proximity-driven *in situ* thiol(ate)–alkyne addition.[27-28] Direct nucleophilic attack on internal C2 alkyne by cysteine thiol is supported by mutagenesis experiments with SENP1; only catalytic Cys603 was essential to form covalent adduct with SUMO2-**Prg**.[28] **(C)** Spontaneous or enzyme-initiated isomerization (tautomerization) of the terminal alkyne moiety to a thiol-reactive allenic intermediate prior to nucleophilic addition.[27] Excluded in this work by MS analysis. **(D)** Enzyme-templated thiol–alkyne addition *via* a secondary carbanion intermediate that is stabilized in the protease oxyanion hole, proposed by Arkona *et al*.[35] Contradicted by mutagenesis with SENP1; Q597A mutation of important glutamine residue in oxyanion hole did not mitigate covalent adduct formation with SUMO2-**Prg**,[28] but this does not exclude the role of stabilizing H-bonds with backbone amides.

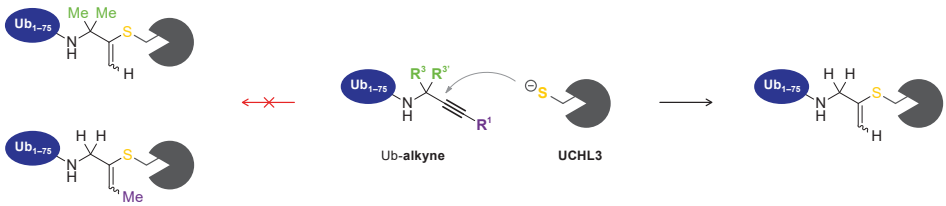

Figure 1 | Covalent adduct formation between catalytic cysteine thiol of recombinant cysteine protease UCHL3 and the alkyne quaternary C2 carbon of Ub-**Prg** is mitigated when hydrogens are substituted on the propargyl terminal (C1) or internal (C3) carbon.[27]

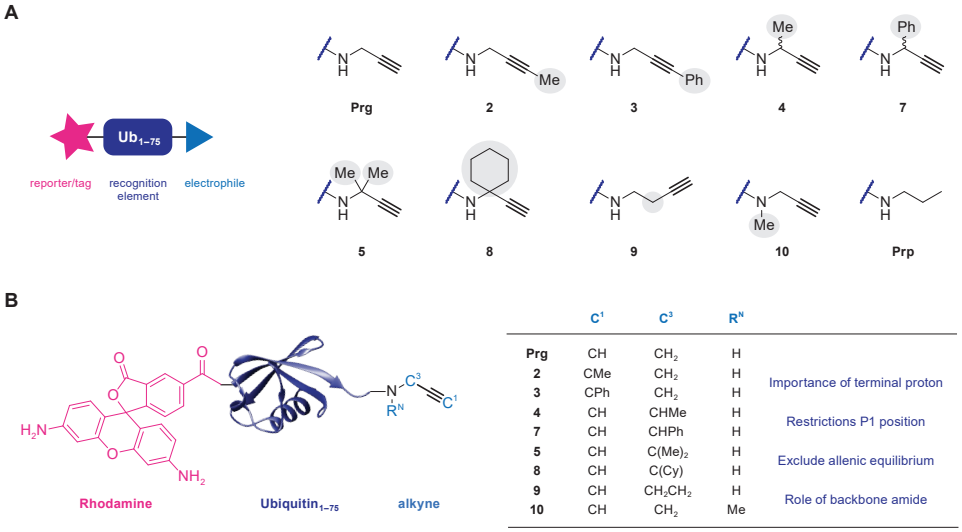

	C^1	C^3	R^N	
Prg	CH	CH_2	H	
2	CMe	CH_2	H	Importance of terminal proton
3	CPh	CH_2	H	
4	CH	CHMe	H	Restrictions P1 position
7	CH	CHPh	H	
5	CH	$C(Me)_2$	H	Exclude allenic equilibrium
8	CH	C(Cy)	H	
9	CH	CH_2CH_2	H	Role of backbone amide
10	CH	CH_2	Me	

Figure 2 | Panel of substituted alkynes incorporated in activity-based probes (ABPs) targeting cysteine DUBs. **(A)** Synthetic Ubiquitin lacking the C-terminal glycine residue ($Ub_{1–75}$ or UbΔG) was modified with fluorescent Rhodamine (Rho) moiety on the N-terminus as reporter tag, and with propargylamide (**Prg**) or propargylamide derivatives **2-10** as cysteine thiol-reactive electrophiles on the C-terminus. General synthetic scheme can be found in **Figure S1B**. **(B)** Substituents were introduced on the terminal C1 carbon, internal C3 carbon, and on the Ub backbone amide. Propylamide (**Prp**) is a noncovalent control.

In detail, terminal methylated alkyne **2** and terminal phenylated alkyne **3** were designed to investigate the importance of the terminal proton on C1. The mono-methylated alkyne **4** and mono-phenylated alkyne **7** (increased bulkiness) with a single substituent on the C3 carbon were included to gain further insight in restrictions at the Ub C-terminus (P1 site in substrate nomenclature). The double substituted quaternary C3 derivatives *geminal*-3,3-dimethylated alkyne **5** and cyclohexylated alkyne **8** were included to examine the option of a reactive allene intermediate rather than a reactive alkyne (as presented in **Scheme 1C**). Adduct formation with these quaternary C3 alkynes would exclude the formation of a reactive allene isomer prior to nucleophilic thiol addition, as it is not possible to deprotonate a quaternary C3 carbon. Furthermore, we included butargyl **9** and *N*-methylated alkyne **10** to examine the role of the Ub backbone (amide). The longer linker between the amide and the reactive carbon in butargyl **9** excludes conjugating effects by the Ub amide (but is also not optimally aligned with the native isopeptide bond, **Figure S1A**), whereas the role of the amide proton itself can be examined by replacing it with a methyl group in *N*-methylated propargyl derivative **10**. Finally, propylamide (**Prp**) was included as a control, as this compound lacks a reactive warhead and should be uncapable of forming covalent adducts.

Activity of Rho-Ub-ABPs with substituted alkyne warheads. To explore the reactivity of our panel of substituted alkyne ABPs we explored DUB adduct formation both in lysates and against recombinant DUBs. Whole HEK293 lysate was incubated with the panel of Rho-Ub-ABPs in order to identify DUBs that form covalent adducts with substituted

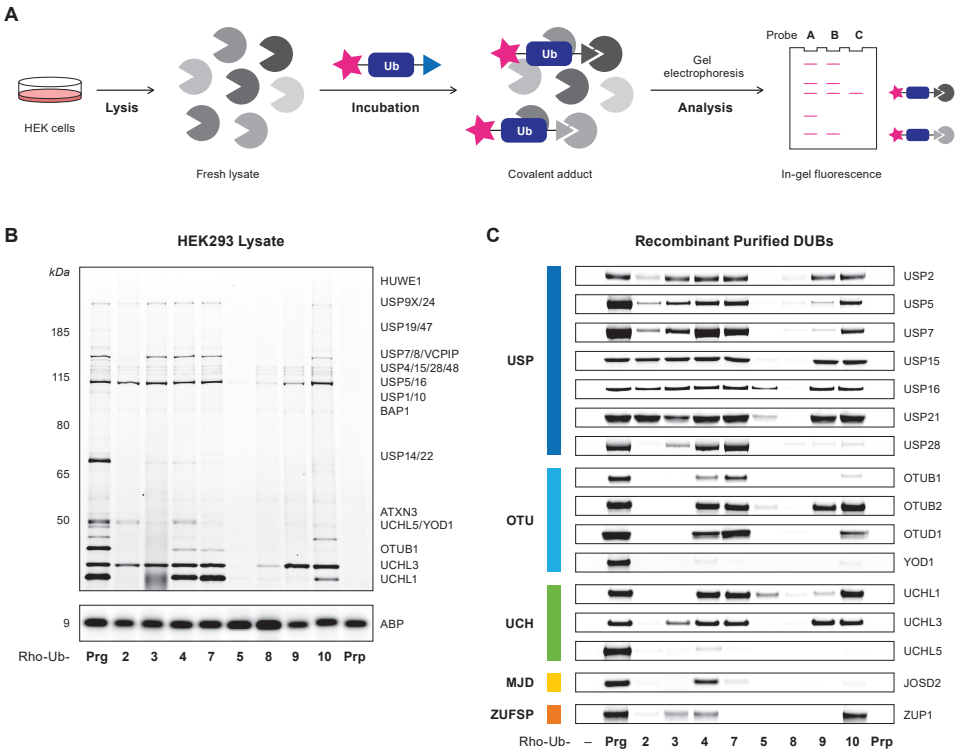

Figure 3 | Incubation of whole lysate and purified recombinant cysteine DUBs (CysDUBs) with Rho-Ub-alkyne ABPs. **(A)** Methodology. Incubation of whole lysate with Rho-Ub-ABPs to identify covalent DUB–ABP adducts. **(B)** Fluorescence scan of HEK293 lysate incubated with 10 µM Rho-Ub-ABP reveals that acceptance of alkyne substituents is CysDUB-specific. Assignment of labeled CysDUBs based on proteomic analysis by Altun *et al.*[14] Darker bands correlate with more covalent protein–ABP adduct, but the maximum intensity depends on total protein expression. Fluorescence scans of HEK293 and EL4 lysates incubated with 1 or 10 µM Rho-Ub-ABP are available in **Figure S2**. **(C)** Fluorescence scan of recombinant purified CysDUBs incubated with 10 µM Rho-Ub-ABP. Fluorescence intensity was adjusted to the signal of adduct with Rho-Ub-**Prg**. CysDUB conversion to covalent adduct is visualized by Coomassie protein stain (shown in **Figure S3**).

alkynes **2**-**10** (**Figure 3A**).[43] In-gel fluorescence shows the typical labeling pattern for Rho-Ub-**Prg**, and reveals that substituents on alkynes **2**-**10** do not fully mitigate covalent adduct formation (**Figure 3B**) as labeling, although to a lesser extent, can still be observed. A similar pattern was observed upon incubation of EL4 lysate (**Figure S2A**). Next, we validated the labeling observed in whole lysates by incubation of purified recombinant cysteine DUBs with Rho-Ub-ABPs (**Figure 3C**). Strikingly, substituted alkynes **2** and **5**, which were previously reported unreactive towards UCHL3,[27] showed reactivity towards other cysteine DUBs. A closer look into our data reveals that Rho-Ub-ABPs with terminally modified alkyne **2** or **3** generally do not form covalent adduct with our set of recombinant OTU, UCH, MJD and ZUFSP DUBs, but labeling is observed for several USP DUBs. Moreover, labeling patterns in lysate and

recombinant DUBs show that mono-substituted alkynes **4** (Ala mimic) and **7** are generally accepted, highlighting that variants at the Ub-ABP P1 position are acceptable. There are some controversies in the field on this matter as DUBs are believed to be sensitive to modifications at P1; available crystal structures show Gly76 occupies a restricted tunnel.[44] The most-described example here is mutant Ub^{G76A}, which renders poly-Ub chains resistant to DUB cleavage while still posing as a substrate for E1 ligases.[45-46] However, Wilkinson *et al.*[47] report that poly-Ub chains with Ub^{G76A} at the distal position, although processed slower than Ub^{WT} chains, are not resistant to USP5-mediated proteolysis. This is in agreement with our findings that Ala mimic **4** forms a covalent adduct with recombinant USP5 (**Figure 3C**). Furthermore, even double substituted alkynes **5** and **8** are accepted by some DUBs. Adduct formation of Rho-Ub-**5** with recombinant purified USP16 was evident (**Figure 3C**) but labeling of endogenous USP16 in HEK lysate was hard to observe (**Figure 3B**). However, adduct formation of Rho-Ub-**5** with USP16 in lysate could be detected when the fluorescence exposure was increased (**Figure S2C**), as well as by incubation of HeLa lysate overexpressing FLAG-HA-USP16 (**Figure S2D**). In addition, lysate treatment reveals that UCHL3 is one of the few DUBs that has enough flexibility at its active site to accommodate the longer linker of butargyl **9**. Even close family members, UCHL1 and UCHL5, do not accommodate the longer linker length, confirming the deciding role of the cysteine protease in adduct formation. Methylation of amide nitrogen in alkyne **10** is accepted by the majority of DUBs included in our panel. As expected, covalent adducts with Rho-Ub-**Prp** were not observed, since this compound lacks an electrophilic warhead.

Based on these results we can conclude that substituents on the alkyne warhead do not generally block covalent adduct formation. Mitigation of covalent adduct formation with the cysteine thiol by introduction of substituents is DUB-specific and could be the result of electronic or steric effects, or a combination thereof. Two alkyne ABPs were selected for validation of the covalent bond formation; terminal modified alkyne **2** to gain insight into the role of the terminal proton (or steric hindrance), and *gem*-dimethylated alkyne **5** as isomerization to a more reactive allene intermediate prior to nucleophilic thiol addition (**Scheme 1C**) is not possible for this substituted alkyne.

ABPs form covalent adducts with catalytic cysteine residue in recombinant USP16. USP16 (Ubp-M) was selected for validation of covalent adduct formation as it forms a covalent adduct with both Rho-Ub-**2** and Rho-Ub-**5** (**Figure 3C**, **Figure S2**). We selected catalytic USP domain rather than full length USP16 for validation because of its higher stability and compatibility with top-down mass spectrometry (MS). Firstly, covalent adduct formation with Rho-Ub-**Prg**, Rho-Ub-**2** and Rho-Ub-**5** was validated by incubation of recombinant $USP16CD^{WT}$, and resolved by SDS-PAGE under denaturing conditions (**Figure 4A**, *left*). As expected, a higher running band corresponding to the fluorescent covalent enzyme–ABP adduct (+ 8.9 kDa) was revealed by in-gel fluorescence scanning and protein staining. Preincubation of $USP16CD^{WT}$ with thiol-alkylating reagent *N*-ethylmaleimide (NEM) prior to incubation with ABPs abolishes adduct formation (**Figure 4A**, *middle*), indicative of adduct formation with a cysteine thiol. Catalytically inactive mutant $USP16CD^{C205A}$ was generated to validate modification of catalytic Cys205 rather than one of the thirteen noncatalytic cysteine residues present in USP16CD,[48-49] as covalent adduct formation of ABP Ub-**VS** (vinyl sulfone) with

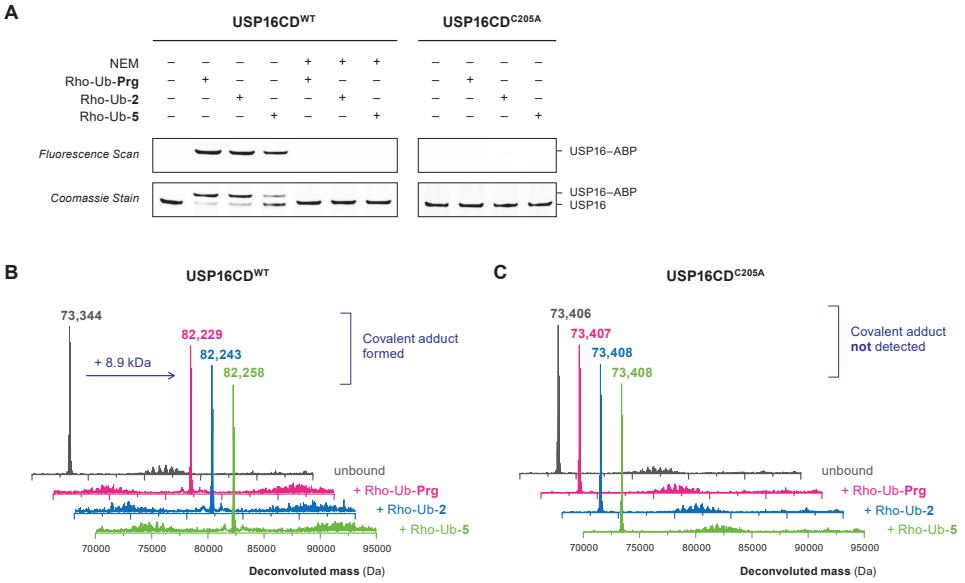

Figure 4 | Validation of covalent adduct between Rho-Ub-alkyne ABPs and catalytic Cys205 in recombinant purified USP16CD (catalytic domain). **(A)** In-gel fluorescence *(top)* and Coomassie stain *(bottom)* of purified recombinant USP16CD^{WT} and mutant USP16CD^{C205A} incubated with ABP (Rho-Ub-**Prg**, Rho-Ub-**2** or Rho-Ub-**5**). Adduct is formed with USP16CD^{WT} but preincubation with thiol-alkylating reagent *N*-ethylmaleimide (NEM) prior to incubation with ABPs blocks adduct formation, indicating cysteine thiol is required for adduct formation. Adduct is not observed with USP16CD^{C205A}, identifying catalytic Cys205 as the modified cysteine residue. **(B)** Deconvoluted mass from intact protein MS confirms covalent adduct (+8.9 kDa) of USP16CD^{WT} with Rho-Ub-**Prg**, Rho-Ub-**2**, and Rho-Ub-**5**. **(C)** Covalent adduct is not observed in deconvoluted mass from intact protein MS for catalytically inactive mutant USP16CD^{C205A} with Rho-Ub-**Prg**, Rho-Ub-**2** or Rho-Ub-**5**.

less nucleophilic noncatalytic cysteine residues has been reported for UCHL1 and OTUB1.[18] Covalent adduct formation was not observed upon incubation of USP16CD^{C205A} mutant (**Figure 4A**, *right*). Top-down MS analysis of intact protein (adducts)[50-51] confirms covalent CysDUB–ABP adduct formation with USP16CD^{WT} (**Figure 4B**), but covalent adducts are not observed with inactive mutant USP16CD^{C205A} (**Figure 4C**). Together, these findings confirm that USP16 is covalently modified by the Rho-Ub-alkyne ABPs on catalytic Cys205.

Bottom-up mass spectrometric analysis identifies alkyne not allene as the reactive group. Covalent adduct formation of *gem*-dimethylated alkyne **5** with USP16 does not only illustrate the important role of the cysteine DUB in the *in situ* thiol–alkyne addition; the retained ability to form a covalent adduct also has mechanistic implications. Adduct formation with Rho-Ub-**5** cannot occur through isomerization to an allene intermediate prior to nucleophilic addition (**Scheme 1C**); deprotonation of the quaternary C3 carbon atom to form the allene is not possible. To confirm our hypothesis we synthesized Rho-Ub-[$\mathbf{D_2}$]-**Prg** with deuterated propargylamine [$\mathbf{D_2}$]-**Prg** as warhead (**Figure 5A**). The covalent adduct of a recombinant DUB with Rho-Ub-[$\mathbf{D_2}$]-**Prg** will contain two deuterium atoms if the alkyne is indeed the reactive species (**Scheme 1B/D**) while isomerization to an allene intermediate (**Scheme 1C**)

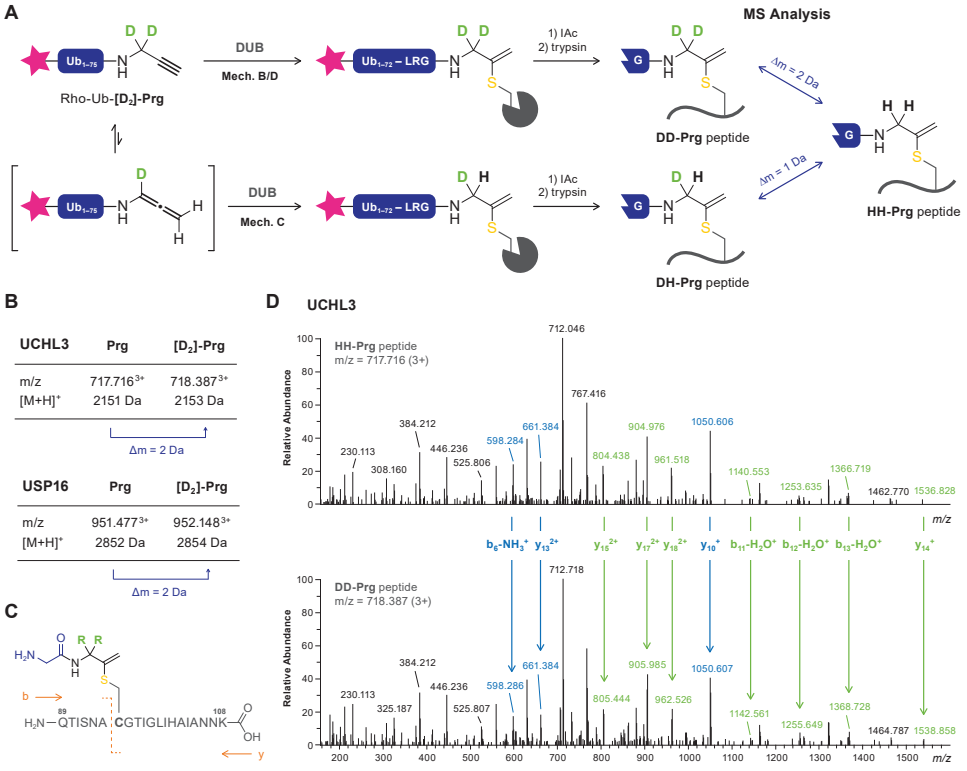

Figure 5 | Bottom-up mass spectrometric analysis of covalent adduct with Rho-Ub-**[D$_2$]-Prg** excludes allenic intermediate in mechanism of *in situ* thiol–alkyne addition. Details on chemical synthesis of deuterated propargylamine **[D$_2$]-Prg** can be found in **Scheme S1**. **(A)** Schematic overview of methodology. Incubation of recombinant DUB with Rho-Ub-**[D$_2$]-Prg** and Rho-Ub-**Prg** is followed by alkylation and trypsin digestion to generate modified peptides for mass spectrometric analysis. Isomerization to an allenic intermediate (*Mechanism C* in **Scheme 1C**) will result in replacement of one deuterium atom in the covalent adduct, whilst both deuterium atoms remain for *mechanisms B* and *D* (**Scheme 1B/D**). **(B)** Modified peptides detected for adducts of Rho-Ub-**[D$_2$]-Prg** and Rho-Ub-**Prg** with UCHL3^{WT} (QTISNACGTIGLIHAIANNK) or USP16CD^{WT} (GLSNLGNTCFFNAVM$^{(ox)}$QNLSQTPVLR) have a mass difference of 2 Da, corresponding with *mechanism B/D*. Details on detected tryptic peptides are provided in **Table S4** and **Table S5**. **(C)** Tandem MS fragmentation of trypsin-digested UCHL3 peptide QTISNAC*GTIGLIHAIANNK (residues 89-108). **(D)** Full MS2 spectrum for UCHL3 peptide QTISNAC*GTIGLIHAIANNK modified with Gly-HH-**Prg** *(top)* or Gly-DD-**Prg** *(bottom)*. Relevant fragment ions are assigned in green (contains cysteine residue) or blue (does not contain cysteine residue), confirming modification on the cysteine residue with 2 Da mass difference. The m/z values of expected and detected fragment ions are provided in **Table S6**.

would result in replacement of one deuterium atom by a hydrogen atom. Covalent adducts of Rho-Ub-[D$_2$]-**Prg** and Rho-Ub-**Prg** with UCHL3 (unreactive towards Rho-Ub-**5**) and USP16 (reactive towards Rho-Ub-**5**) were submitted to alkylation and trypsin digestion to generate peptides for bottom-up mass spectrometric analysis. Peptides of different lengths containing the QTISNACGTIGLIHAIANNK stretch were detected for UCHL3 adducts modified with **Prg** or [D$_2$]-**Prg**, with a mass difference of 2 Da between deuterated and protonated adducts (**Figure 5B**, **Table S4**). For both USP16 adducts, tryptic peptide GLSNLGNTCFFNAVM$^{(ox)}$QNLSQTPVLR

(with oxidized methionine) was detected with a mass difference of 2 Da between deuterated and protonated adducts (**Figure 5B**, **Table S5**). Peptides corresponding with isomerization were not detected for the **[D_2]-Prg** adducts. Furthermore, tandem mass spectrometric analysis of both modified UCHL3 peptides confirms that the 2 Da mass difference can be attributed to a modification on the catalytic cysteine residue (**Figure 5C-D**, **Table S6**).

Together, this clearly shows that the *in situ* thiol–alkyne addition to unsubstituted alkynes does not involve isomerization to an allene intermediate thereby excluding *mechanism C* (**Scheme 1C**). It is more challenging to conclude whether nucleophilic addition to the alkyne moiety is exclusively proximity-driven (**Scheme 1B**) or goes through enzyme-templated stabilization of a carbanion intermediate in the oxyanion hole (**Scheme 1D**). To our knowledge, all cysteine residues targeted by nonactivated alkynes are located at the active site of cysteine proteases (or ligases), which could stabilize a carbanion intermediate in an oxyanion hole (**Scheme 2**). We cannot exclude nor confirm this mechanism based on our current data, but we

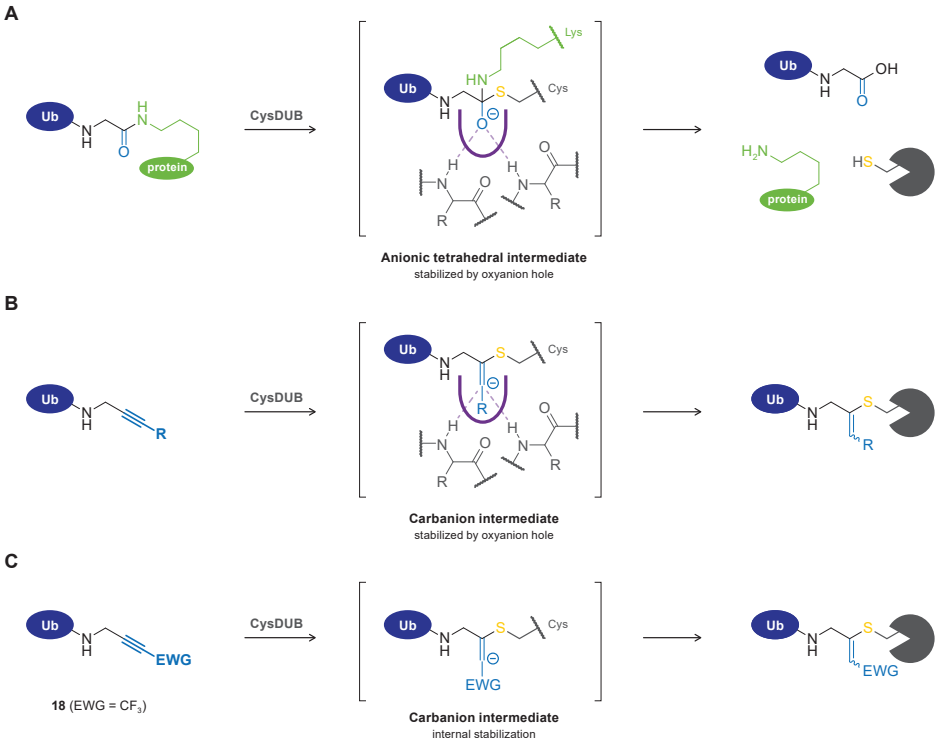

Scheme 2 | Stabilization of anionic intermediates for (enzymatic) reactions with cysteine DUBs. **(A)** CysDUB-mediated isopeptide bond proteolysis. Stabilization of anionic tetrahedral intermediate in the oxyanion hole. Release of ubiquitin, (ubiquitinated) substrate, and CysDUB. **(B)** Proposed enzyme-templated thiol–alkyne addition with stabilization of unfavored carbanion intermediate in the oxyanion hole. Terminal alkynes such as **Prg** would form a secondary carbanion, but internal alkynes such as terminally methylated alkyne **2** would form a tertiary carbanion intermediate that is internally destabilized if R is an electron-donating group (EDG). **(C)** Non-enzymatic internal stabilization of a carbanion intermediate by inductive effect of electron-withdrawing group. Details on chemical synthesis of trifluoromethylated alkyne **18** are provided in **Scheme S2**.[52]

would like to note that the inductive effect of the electron-donating methyl-group in alkyne **2** contributes negatively to the internal stabilization of the negative charge, thus reducing the stability of the tertiary carbanion compared to the already unfavored secondary carbanion intermediate that is formed with terminal alkynes (**Scheme 2B**). It is possible that enzyme oxyanion hole sufficiently stabilizes the tertiary carbanion to progress with covalent bond formation, but the proximity-driven reaction seems more likely for internal alkyne **2**.

Kinetic analysis of covalent adduct formation with USP16. Next, we examined whether introduction of bulky and/or electron-donating substituents on the alkyne terminal C1 or internal C3 carbon atom reduces the rate of covalent adduct formation. Incubation of USP16CD^{WT} with 10 μM Rho-Ub-ABP does indeed show time-dependent increase of the higher running covalent adduct and a decrease of the lower running noncovalent/unbound USP16 for Rho-Ub-**2** and Rho-Ub-**5** (**Figure 6A**). Adduct formation does not progress beyond the first timepoint for Rho-Ub-**Prg**, indicating that reaction completion was reached before the first sample was quenched (within 15 min). This finding is in agreement with exceptionally fast adduct formation reported for Ub(l)-**Prg** ABPs (reaction completion within minutes).[27-28] Covalent adduct formation of USP16 with Rho-Ub-ABPs is slower with substituted alkynes **2** and **5** than with **Prg**, requiring a longer incubation time to reach maximum covalent occupancy.

We performed a kinetic evaluation of covalent adduct formation to calculate the minimum incubation time to reach reaction completion at a specific ABP concentration (**Figure 6B**). Covalent adduct formation between ABP and cysteine protease is a two-step process; noncovalent enzyme–ABP complex is formed rapidly, followed by covalent adduct formation as the rate-determining step.[53-55] Time-dependent covalent occupancy of irreversible covalent ligands can be directly detected (in absence of competing substrate/ligand) by separation of covalent adduct from noncovalent complex and unbound enzyme on LC-MS or gel, and subsequent quantification of signals.[58-62] Here we incubated USP16CD^{WT} with excess Rho-Ub-ABPs, and quantified incubation time-dependent covalent occupancy by gel analysis (**Figure 6C**). Estimates for the rate of covalent adduct formation k_{obs}, reaction half-life t½ and incubation time to reach reaction completion were obtained assuming maximum covalent occupancy is shared among all ABPs. Adduct formation with all ABPs is concentration-dependent; reaction completion is reached faster at the high ABP concentration. However, covalent adduct formation with Rho-Ub-**Prg** is unusually fast; maximum covalent occupancy is reached within a few minutes at both concentrations, and the reaction rates might be even faster than what we reported here. The half-life and extrapolated incubation time to reach maximum covalent adduct formation provide valuable insights into the reduced reactivity of Rho-Ub-**5** in previous incubation experiments (**Figure 3**, **Figure S2**); reaction completion is reached after more than four hours, which well exceeds the common incubation time for ABPs with lysate or recombinant protein. Incomplete adduct formation is observed as a band with (significantly) lower intensity than the band with Rho-Ub-**Prg** that does reach maximum intensity. Overall, introduction of substituents on propargylamide decreases the rate of covalent adduct formation with USP16CD^{WT} by >30-fold for methylation of the terminal C1 carbon (Rho-Ub-**2**), and >100-fold for *gem*-dimethylation of the internal C3 carbon (Rho-Ub-**5**). This dramatic reduction in

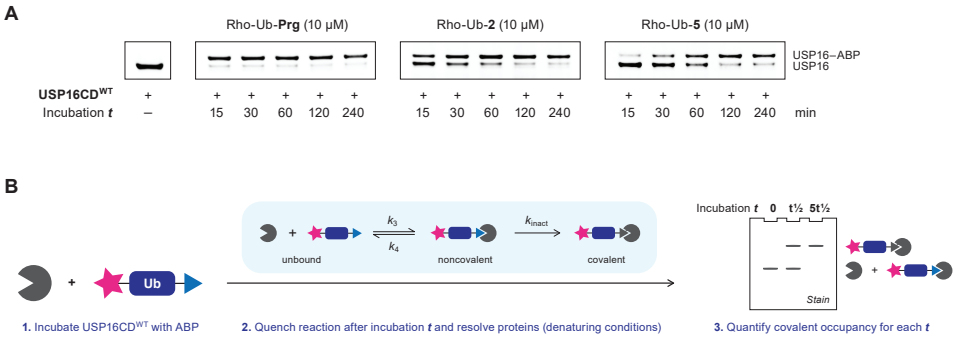

C

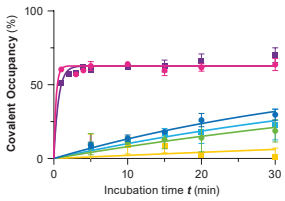

ABP	[ABP] (μM)	k_{obs} (min^{-1})	t½ (min)	Reaction completion	K_D (μM)
		USP16CD^{WT}			USP16CD^{C205S}
Rho-Ub-**Prg**	10	3.3 ± 2.3	< 1	< 2 min	2.4 ± 0.21
	1	1.6 ± 0.38	< 1	< 3 min	
Rho-Ub-**2**	10	0.024 ± 0.0021	29	2.4 h	5.2 ± 0.41
	1	0.018 ± 0.0018	39	3.3 h	
Rho-Ub-**5**	10	0.014 ± 0.0017	51	4.2 h	26 ± 1.8
	1	0.003 ± 0.0013	200	17 h	

Figure 6 | Kinetic analysis of covalent adduct formation with Rho-Ub-alkyne ABPs. **(A)** Incubation time-dependent covalent adduct formation of Rho-Ub-alkyne ABPs with USP16CD^{WT} visualized by Coomassie stain after gel electrophoresis (denaturing conditions). Intensity of covalent USP16–ABP adduct band increases upon longer incubation time for substituted alkyne ABPs Rho-Ub-**2** and Rho-Ub-**5**, but reaction completion is already reached before the first timepoint for Rho-Ub-**Prg**. **(B)** General method to obtain kinetic parameters for covalent ligands from incubation time-dependent covalent occupancy. **(C)** Kinetic analysis of covalent adduct formation between USP16CD and Rho-Ub-ABP. USP16CD^{WT} was incubated with excess ABP, and samples were quenched after various incubation times. Covalent occupancy was quantified from gel analysis (triplicate measurement) to obtain the rate of covalent adduct formation k_{obs}, reaction half-life t½ and reaction completion (details in *section 7.7*). The maximum occupancy is less than 100%, which can be attributed to commonly observed inactive subpopulations in (recombinant) enzyme.[56-57] Adduct formation with Rho-Ub-**Prg** was completed within 5 minutes, therefore the measurement was repeated with shorter intervals. Reliable estimates for the kinetic parameters could not be obtained because reaction completion was still reached too quickly. K_D-values for noncovalent binding were obtained in a binding assay based on fluorescence polarization (FP) of Rho-Ub-ABPs with excess USP16CD^{C205S} mutant (details in **Figure S4**, *section 7.8*).

reaction rate explains the low reactivity of substituted alkynes upon incubation of lysate or recombinant protein as adduct formation is not completed within the standard incubation time of 30-60 min. Rho-Ub-ABPs with slower covalent adduct formation than Rho-Ub-**Prg** could be desirable as they are more suited to study (ir)reversible inhibitor potency in kinetic competition assays.[12, 63-64]

Next, a binding assay based on fluorescence polarization (FP) of the Rho-Ub-ABPs with excess catalytic inactive USP16^{C205S} mutant was performed to determine K_D-values independent of electronic factors as covalent adduct formation with USP16^{C205S} does not occur (**Figure 6C**). Introduction of methyl substituents clearly reduced the noncovalent affinity (reflected in

higher K_D), indicative of disfavored steric interactions. However, electronic effects cannot be disregarded as the rate of adduct formation (k_{obs}) with Rho-Ub-**2** is more than 30-fold slower than with Rho-Ub-**Prg** where the noncovalent affinity (K_D) is less than 3-fold lower. This shows that disfavored steric interactions as well as electronic effects contribute to the reduced rate of covalent adduct formation with methylated alkynes.

Contribution of steric and electronic effects on DUB reactivity towards substituted alkynes. Substituents introduced on the alkyne C1 and C3 position (**Figure 2**) were designed to have a minimal electronic effect, but kinetic evaluation of covalent adduct formation (k_{obs}) and noncovalent affinity (reflected in the K_D) with USP16 revealed that the role of steric and electronic effects cannot be separated completely (**Figure 6C**). To further study the individual contribution of steric and electronic components we included electron-deficient alkyne **18**, with an electron-withdrawing $-CF_3$ group on the terminal alkyne carbon (**Scheme 2C**, **Figure 7A**). Introduction of an electron-withdrawing group (EWG) on the terminal position of an alkyne significantly increases the thiol reactivity as the inductive effect contributes positively to the stabilization of a negative charge, thereby enabling non-enzymatic internal stabilization of a carbanion intermediate (**Scheme 2C**). The increased electrophilicity was indeed reflected in the observation of significant adduct formation with nontargeted thiol glutathione (GSH) (**Figure 7B-C**). Incubation of HEK293T lysate (**Figure 7D**) showed that most DUBs form a covalent adduct with Rho-Ub-**18**, indicating an electronic rather than steric component driving the lack of reactivity with alkyne **2**. Faint covalent adduct formation with Rho-Ub-**18** was observed upon incubation of USP16CD^{C205A} mutant, indicating a preference for the catalytic cysteine residue over other (nontargeted) cysteine residues (**Figure 7E-F**). Altogether, we can conclude that (disfavored) steric as well as electronic properties of the substituent affect DUB reactivity with substituted alkynes.

Implications on the scope of the *in situ* thiol–alkyne addition. Introduction of bulky and/or electron-donating substituents can reduce the rate of covalent bond formation but it is DUB-dependent whether modifications are allowed. We foresee this might be used for the development of ABPs with improved selectivity for a specific DUB. Here, introduction of electron-donating and electron-withdrawing substituents on the C1 and C3 position would tune alkyne reactivity (electronic effect) while simultaneously modulating selectivity (steric effect). Another possibility would be to introduce primed site recognition peptide fragments on the terminal alkyne position to improve selectivity and/or affinity.[10, 65-66]

The reaction mechanism has extensive consequences for the scope of the *in situ* alkyne–thiol addition. Enzyme-templated stabilization of a carbanion intermediate (*Mechanism D*, **Scheme 1D**) would restrict the applicability in drug design to targeting catalytic cysteine residues with nonactivated alkynes, but it also mitigates the risk of covalent adduct formation with nontargeted thiols. A covalent adduct is not formed with noncatalytic cysteine residues because the carbanion intermediate cannot be stabilized as there is no oxyanion hole present in their vicinity, resulting in a mechanism-based selectivity for the targeted thiol. To date, only electron-deficient (activated) alkynes such as propiolamides, propiolonitriles and alkynylated heteroarenes have been reported to form covalent adducts with noncatalytic cysteine residues (in kinase targets).[25, 34, 62, 67-69] The inductive effect of (conjugated)

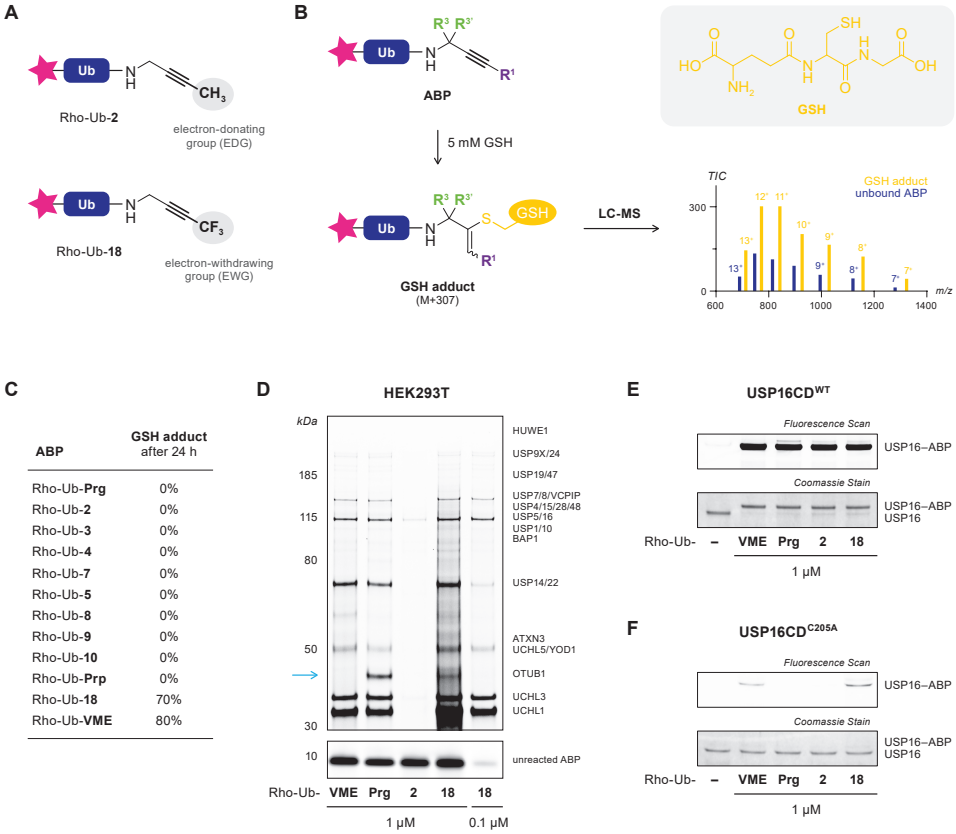

Figure 7 | Selectivity and reactivity of electron-deficient alkyne **18** as warhead in Rho-Ub-ABPs. **(A)** Mildly electron-donating methyl group on terminal C1 position of alkyne **2** and strongly electron-withdrawing trifluoromethyl group on terminal C1 position of alkyne **18**. Synthetic scheme for trifluoromethylation of terminal alkynes to obtain alkyne **18** is provided in **Scheme S2**.[52] Our design is based on the assumption that the terminal trifluoromethyl ($-CF_3$) in alkyne **18** is sterically similar to the terminal methyl ($-CH_3$) in alkyne **2**, while having the opposite electronic property. **(B)** Schematic overview of methodology for indiscriminate thiol reactivity. Rho-Ub-ABPs are incubated with 5 mM glutathione (GSH) in phosphate-buffered saline (PBS) for 24 h, after which the reaction mixture was submitted to LC-MS analysis. GSH adduct and unreacted ABP are quantified from the total ion count (TIC). **(C)** GSH adduct formed upon incubation with 5 mM GSH for 24 h as percentage of total. Charge states used for quantification are provided in **Table S7**. Adduct formation with GSH does not necessarily equal complete loss of selectivity, as is illustrated by established CysDUB-selective ABP Ub-**VME**.[39] **(D)** Fluorescence scan of HEK293T lysate incubated with Rho-Ub-ABPs reveals the importance of both steric and electronic effects of alkyne substituents. Most but not all CysDUBs that are unreactive with Rho-Ub-**2** do form covalent adducts with Rho-Ub-**18**, indicating an electronic rather than steric component driving the lack of reactivity with Rho-Ub-**2**. The blue arrow marks a CysDUB adduct – previously identified as OTUB1 [14] – that is reactive towards Rho-Ub-**Prg** but unreactive towards the more electrophilic Rho-Ub-**VME** and Rho-Ub-**18**. This suggests that lack of reactivity for this specific CysDUB could be driven by the available space at the active site to accommodate bulky substituents at the C1 position (disfavored steric interactions) rather than electronic effects. **(E)** In-gel fluorescence *(top)* and Coomassie protein stain *(bottom)* for adduct formation with recombinant USP16CD^{WT} upon incubation with Rho-Ub-ABPs for 1 h. **(F)** In-gel fluorescence *(top)* and Coomassie protein stain *(bottom)* for adduct formation with recombinant USP16CD^{C205A} upon incubation with Rho-Ub-ABPs for 1 h. Faint labeling can be observed for Rho-Ub-**VME** and Rho-Ub-**18** in the fluorescence scan, indicating that these ABPs are reactive towards noncatalytic cysteines, but CysDUB selectivity is retained: adduct formation with the catalytic cysteine residue is much faster than reaction with nontargeted thiols.

electron-withdrawing groups sufficiently stabilizes the carbanion intermediate to progress with covalent bond formation, with targeted as well as (undesired) nontargeted thiols (**Scheme 2C**). Unfortunately, electron-deficient alkyne **18** is not suited to study whether the *in situ* thiol addition to nonactivated alkynes involves enzymatic stabilization of a carbanion in the oxyanion hole (**Scheme 1D**, **Scheme 2B**) because thiol addition can progress through an alternative, non-enzymatic mechanism (**Scheme 2C**). We believe further research to elucidate the mechanism of thiol addition to nonactivated (internal) alkynes should be directed towards computational studies with enzymes for which structural data is available, or by successfully targeting noncatalytic cysteines with nonactivated alkynes.

3. Conclusion

To conclude, this work shows that the *in situ* thiol–alkyne reaction is more flexible and versatile than previously assumed. A panel of substituted propargylamide derivatives was incorporated into Rho-Ub-ABPs as the electrophilic warhead, and treatment of lysate or recombinant cysteine DUBs showed that covalent adducts can also be formed with internal alkynes and terminal alkynes with (double) substituents on the internal C3 carbon. Covalent adduct formation of terminally methylated alkyne **2** and *gem*-dimethylated alkyne **5** with catalytic Cys205 of USP16 was validated by gel analysis and mass spectrometry of intact covalent adducts. Adduct formation was mitigated by preincubation with thiol-alkylating reagent NEM or by C205A mutation, thus confirming catalytic Cys205 as the targeted amino acid residue. Mechanistically, acceptance of *gem*-dimethylated alkyne **5** together with mass spectrometric analysis of covalent adducts with deuterated ABP Rho-Ub-[$\mathbf{D_2}$]-**Prg** validates the alkyne moiety rather than an allenic isomer as the reactive species in the *in situ* thiol–alkyne addition. Kinetic analysis revealed reaction completion was reached within in a few minutes for Rho-Ub-**Prg**, while electron-donating/bulky methyl substituents on alkynes **2** and **5** significantly reduced the rate of covalent adduct formation resultant from a combination of (disfavored) steric interactions and electronic effects, reaching maximum covalent occupancy after (several) hours. Whether nucleophilic addition of the catalytic cysteine thiol to the alkyne moiety is solely proximity-driven or involves enzymatic stabilization of a carbanion intermediate could not be concluded definitively.

Altogether, we extended the scope of the *in situ* thiol–alkyne reaction from unmodified terminal alkynes to substituted (internal) alkynes, provided mechanistic insight, and discovered that acceptance of alkyne substituents is CysDUB-dependent. We anticipate substituted nonactivated alkynes not to be restricted to bioorthogonal handles but also to be of great value as electrophiles in future development of cysteine-targeting covalent inhibitors and activity-based probes with improved selectivity profiles.

Acknowledgements
In memory of prof. dr. Huib Ovaa. His passion for science will always be an inspiration to us. We thank Henk Hilkmann, Dris el Atmioui and Cami Talavera Ormeño for the chemical synthesis of Ubiquitin, and Dris el Atmioui for his support with ABP synthesis. Paul Brundel and Robin van Veen are thanked for their help with the chemical synthesis of building blocks. Angeliki

Moutsiopoulou, Patrick Celie, Ruud Wijdeven, Aysegul Sapmaz, Gabrielle van Tilburg, and Remco Merkx are thanked for expression and purification of recombinant DUBs. Recombinant YOD1 was kindly provided by Tycho Mevissen and David Komander, and recombinant ZUFSP was a gift from Kay Hofmann. Sabina van der Zanden, Yves Leestemaker, Merve Öyken and Lorina Gjonaj are thanked for culturing HEK293, EL4, HEK293T and HeLa cells respectively. We thank Annemarie Otte for mass spectrometric measurements. This work was supported by a VICI grant (no.724.013.002) from The Netherlands Organization for Scientific Research (NWO) to H.O.

Competing Interests

The authors declare the following competing financial interest: H.O. was founder and shareholder of the company UbiQ that markets reagents in the Ub field.

Author Contributions

E.M.: Conceptualization, Investigation *(Chemical Synthesis, Biochemical Assays)*, Formal Analysis, Writing – Original Draft, Writing – Review & Editing. R.Q.K.: Investigation *(Protein Expression)*, Supervision, Writing – Review & Editing. B.R.v.D.: Investigation *(Top-Down MS)*. P.A.v.V.: Investigation *(Bottom-Up MS/MS)*, Formal Analysis. M.P.C.M.: Supervision, Writing – Review & Editing. H.O.: Conceptualization, Supervision, Funding acquisition.

4. Materials and Methods: *Biochemistry*

General

Synthesis of Rho-Ub-ABPs is described in *section 5.1*. Incubations are performed in Protein Lobind Tubes (Eppendorf, #022431018) to reduce (time-dependent) loss of enzyme due to precipitation/aggregation. Recombinant purified DUBs used in this work: USP2 (Ubiquigent, #64-0014-050), USP5 (Ubiquigent, #64-0002-050), USP7 (*in-house*, see *section 4.1*), USP15 (*in-house*, see *section 4.1*), USP16FL (*in-house*, see *section 4.1*), USP16CD^{WT} (*in-house*, see *section 4.1*), USP16CD^{C205A} (*in-house*, see *section 4.1*), USP16CD^{C205S} (*in-house*, see *section 4.1*), USP21 (Ubiquigent, #64-0037-050), USP28 (*in-house*, see *section 4.1*), OTUB1 (*in-house*, [Wang, 2009][70]), OTUB2 (*in-house*, [Nanao, 2004][71]), OTUD1 (*in-house*, [Mevissen, 2013][72]), YOD1 (Gift from David Komander, [Mevissen, 2013][72]), UCHL1 (*in-house*, [Larsen, 1996][73]), UCHL3 (*in-house*, [Larsen, 1996][73]), UCHL5 (Novus biochemicals, #NBP1-72315), JOSD2 (Ubiquigent, #64-0032-050), and ZUP1 (Gift from Kay Hofmann, [Hermanns, 2018][74]).

4.1. Recombinant Protein Expression and Purification

Protein expression constructs. Expression constructs for USP7FL, USP15(D1D2) and OTUB1FL were kind gifts from Titia K. Sixma, Ingrid Dreveny and Frank Sicheri, respectively. Full-length USP16 (UniProtID: Q9Y5T5; isoform 3, Q141H, EY480DN) and USP16CD (residues 196-823; canonical numbering) were cloned into in-house baculovirus expression vector pCPF2.13 harboring an N-terminal His-tag and 3C protease site, using IVA cloning.[75] Point mutations C205A and C205S were introduced using overlapping primer mutagenesis.[76] USP28FL was cloned into pFastNKI-his3C-LIC using ligase-independent cloning.[77] OTUD1(CD+UIM) (residues 290-481) was cloned into pGEX-4T-1 with BamHI and HindIII. All expression constructs were sequence-verified.

Expression of USP16 (variants) and USP28FL

USP28FL and all USP16 constructs were expressed using baculovirus expression in *Spodoptera frugiperda* (Sf9) using an adapted Bac-to-Bac system (Invitrogen). Bacmids were generated using EmBacY cells (Geneva Biotech)

or DH10Bac (USP28) and isolated using isopropanol precipitation. 10 µg was transfected into 0.8×10^6 sedentary Sf9 cells using CellFectin (Invitrogen) in SFM-II medium (Gibco) in a 6-well plate at 28 °C. After 72 h cells were checked for fluorescence and the medium was harvested (P0) for infection of P1 cultures; 50 mL of 1×10^6 cells/mL in Insect-Express medium (Lonza). P1 cultures were incubated at 28 °C whilst shaking for 72 h and then harvested by spinning down at 500 G for 5 min. The supernatant was used to infect P2 cultures (like P1, but now 500 mL), whilst the pellet was used to check for expression and purification optimization. P2 cultures were infected with low MOI and harvested after 72 h shaking at 28 °C.

Purification of USP16 (variants). Insect cells from P2 expressing USP16 variants were resuspended in lysis buffer (50 mM HEPES pH7.4, 500 mM NaCl, 20 mM imidazole and 5% glycerol), sonicated and centrifuged at 21,000 G at 4 °C to isolate the soluble fraction. The supernatant was applied to charged Ni-NTA beads, which were washed twice extensively with lysis buffer with 20 mM and 50 mM imidazole respectively. The protein was eluted using elution buffer (50 mM HEPES pH7.4, 100 mM NaCl, 200 mM imidazole, 1 mM DTT) and subsequently applied to a HiTrap MonoQ column (GE Healthcare). Protein was eluted using a salt gradient (20 mM HEPES pH7.4, 1 mM DTT, 50 to 1000 mM NaCl) and protein-containing fractions were pooled, concentrated and aliquoted before being flash frozen.

Purification of USP28FL. P2 expression cells were lysed using sonication in lysis buffer (20 mM Tris pH8.0, 500 mM NaCl, 5 mM BME, 10 mM imidazole and protease inhibitor cocktail). The lysates were centrifuged at 20,000 rpm for 30 min at 4 °C. The supernatants were incubated with washed Talon metal affinity resin (Clontech Inc., Palo Alto, CA) for 20 min at 4 °C and the beads were then washed with lysis buffer. Protein was eluted with lysis buffer supplemented 250 mM imidazole. Proteins were dialyzed to remove imidazole and purified over a Superdex200 gel filtration column. USP28(FL) was concentrated, aliquoted and flash-frozen for storage at −80 °C. Purified protein was confirmed via immunoblotting using anti-USP28 antibody (GeneTex, #EPR42492).

Expression and purification of USP7FL

USP7FL was expressed in BL21 (DE3) Rosetta2 bacteria using overnight induction with 0.2 mM IPTG in Terrific Broth medium at 18 °C. Cells were spun down and resuspended in GST buffer (50 mM HEPES pH7.5, 250 mM NaCl, 1 mM EDTA, 1 mM DTT) before being lysed using sonication. After high-speed centrifugation at 21,000 G at 4 °C, the supernatant was applied to Glutathione Sepharose 4B beads (GE Healthcare), which were washed extensively using GST buffer before eluting the protein using GST buffer supplemented with 15 mM GSH. The eluted protein was dialyzed overnight against PorosXQ buffer (20 mM HEPES pH7.5, 50 mM NaCl, 1 mM DTT) after the addition of 3C protease to remove the GST tag. To remove breakdown products and cleaved GST, the sample was purified on a PorosXQ column, eluting the protein using a gradient of buffer B (20 mM HEPES pH7.5, 1M NaCl, 1 mM DTT). Appropriate fractions were concentrated and applied to a Superdex200 gel filtration column (GE Healthcare) using GF buffer (20 mM HEPES pH7.5, 100 mM NaCl, 1 mM DTT). The peak fractions were pooled, concentrated to ~1 mg/mL and flash frozen using LN2.[65]

Expression and purification of USP15(D1D2)

USP15(D1D2) was expressed in BL21 (DE3) Rosetta2 cells, grown in 2xYT medium. Cells were induced overnight at 25 °C using 0.5 mM IPTG and harvested the next day in His-buffer (50 mM Tris pH7.5, 300 mM NaCl, 20 mM imidazole, 1% glycerol). Cells were lysed using sonication and the insoluble fraction was removed by centrifugation at 21,000 G at 4 °C for 30 min. Supernatant was applied to Ni-charged NTA beads and beads were washed extensively with His-buffer. USP15(D1D2) was eluted with the same buffer supplemented with 200 mM imidazole before being concentrated and applied to a Superdex200 gel filtration column in SEC buffer (20 mM Tris pH7.5, 150 mM NaCl, 1% glycerol). Appropriate fractions were concentrated to ~20 mg/mL, aliquoted and frozen in liquid nitrogen.[78]

4.2. Lysate Preparation

Cell culturing. HEK293 cells (ATCC, Manassas, VA), HeLa cells and HEK293T cells were cultured in Dulbecco's Modified Eagle's medium (DMEM) supplemented with 8-10% FCS/FBS. EL4 cells were cultured in Gibco

RPMI 1640 medium (Life technologies) supplemented with 10% FCS. Cells were maintained in a humidified atmosphere of 5% CO_2 at 37 °C and regularly tested for the absence of mycoplasma. Transfection of HeLa cells with FLAG-HA-USP16 (Addgene, #22595) as reported previously.[79]

Harvesting and cell lysis. Cells were harvested by washing with PBS, trypsinization to dissociate adherent cells from surface, and centrifuged. Fresh cell pellets were resuspended in two pellet volumes of cold lysis buffer, sonicated (5 cycles, high. 30 sec on, 30 sec off) on a Bioruptor Pico (Diagenode), and solute was separated from insoluble fraction by centrifuge (10 min, 13,200 rpm, 4 °C). Supernatant was transferred to clean tube and protein concentration was determined on Nanodrop One spectrophotometer (Isogen Life Science). Subsequently, volume was adjusted by addition of lysis buffer to a protein concentration of 2 mg/mL. Harvesting and cell lysis of HeLa cells as reported previously.[79]

4.3. Gel-Based Activity-Based Probe (ABP) Reactivity

General. Purified Rho-Ub-ABPs are stored at −20 °C as powder or as 500 µM stock solutions in DMSO. The concentration of stock solutions is calculated from the molecular mass and the added amount of dry powder. The concentration of unbound Rho-Ub-ABP stock solutions is within 2-fold range, as validated in gel electrophoresis of unbound Rho-Ub-ABP (10 µM) by quantification of fluorescence intensity and protein intensity with ImageJ.[80-82] Rho-Ub-ABPs are added to whole lysate or recombinant DUBs as 2-5× solutions, prepared by careful addition of DMSO stock to reaction buffer. Incubations with Rho-Ub-ABPs are conducted under gentle agitation (300 rpm) with strict restriction of light. Final CysDUB or ABP concentrations listed correspond to the concentration during incubation (before sample buffer addition). Prior to reaction initiation, lysis buffer (50 mM Tris-HCl pH7.4, 5 mM $MgCl_2$, 250 mM sucrose, 2 mM DTT), HEPES reaction buffer (50 mM HEPES pH7.4, 150 mM NaCl, 5 mM DTT, 0.005% Tween20) or Tris reaction buffer (50 mM Tris pH7.5, 100 mM NaCl, 5 mM DTT) are prepared with fresh addition of DTT and surfactants. Single-use 1M aliquots of DTT (1,4-dithio-DL-threitol; Chem-Impex, #00127) are stored at −20 °C.

General Method I. ABP Labeling Quenching and SDS-PAGE Gel Electrophoresis
After indicated incubation time, the reaction was quenched by addition of 3× reducing sample buffer (150 µL 4× LDS-PAGE loading buffer (NuPAGE, Invitrogen) supplemented with 35 µL water and 15 µL β-mercaptoethanol (BME; Sigma-Aldrich, #M6250)) and boiling the samples for 10 min at 94 °C to abolish noncovalent interactions (denaturing conditions). Multiple timepoints; samples were stored on ice until the experiment was completed. Samples were loaded on precast Bis-Tris gels (Invitrogen) and resolved by SDS-PAGE gel electrophoresis with MES (NuPAGE MES SDS running buffer 20×, Novex by Life Technologies) or MOPS (NuPAGE MOPS SDS running buffer 20×, Novex by Life Technologies) as running buffer. Reference protein standard/ladder; PageRuler™ Plus Prestained Protein Ladder (Thermo Fisher Sci., #26619), PageRuler™ Prestained Protein Ladder (Thermo Fisher Sci., #26616) or SeeBlue™ Plus2 Pre-stained Protein Standard (Invitrogen, LC5925). Covalent enzyme–ABP adducts were visualized by in-gel fluorescence using Typhoon FLA 9500 imaging system (GE Healthcare Life Sciences) with blue LD laser and BPB1 emission filter (λ_{ex} = 473 nm, λ_{em} = 530 ± 10 nm), and protein marker was visualized with red LD laser and LPR emission filter (λ_{ex} = 635 nm, λ_{em} = 665 nm). Subsequently, covalent DUB–ABP adduct and unbound DUB were visualized by InstantBlue™ Ultrafast Protein Stain (Expedeon Protein Solutions, #ISB1L), and scanning stained gels using an Amersham Imager 600 (Trans-illumination).

Incubation of whole lysate
EL4/HEK293/HEK293T. 20 µL lysate (final conc. 2 mg/mL) was incubated with 5 µL Rho-Ub-ABP (final conc. 1-10 µM) for 1 h at 37 °C. Reaction was quenched as described in *General Method I*, and samples (10-15 µL) were loaded on 4-12% Bis-Tris gels (Invitrogen) and resolved by SDS-PAGE gel electrophoresis with MES as running buffer. Unreacted ABPs (loading control) were visualized by loading sample (3 µL) on 10% Bis-Tris gels (Invitrogen) and resolved by SDS-PAGE gel electrophoresis with MES as running buffer.

HeLa. 19 µL Lysate (WT or overexpressing FLAG-HA-USP16) was incubated with 1 µL Rho-Ub-ABP for 1 h at 37 °C. Reaction was quenched as described in *General Method I*, and samples (10 µL) were loaded on 4-12% Bis-Tris gels (Invitrogen) and resolved by SDS-PAGE gel electrophoresis with MOPS as running buffer. Gels were transferred to nitrocellulose membrane using a Trans-Blot Turbo Transfer System (Biorad) and subjected to standard Western Blotting protocols. Antibodies: mouse anti-HA (1:1,000; Covance, #MMS-101R) and goat anti-mouse HRP (1:5,000; Dako, #P0447). Blots with HRP secondary antibody were incubated with SuperSignal™ West Dura Extended Duration Substrate (Thermo Sci., #34076) according to manufacturer protocols and scanned on an Amersham Imager 600.

Incubation of recombinant DUBs

Recombinant purified cysteine DUB (final conc. 1 µM) was incubated with Rho-Ub-ABP (final conc. 10 µM) for 1 h at 37 °C. Reaction was quenched as described in *General Method I*. Bis-Tris gels and running buffer were adjusted to optimize separation of unbound enzyme and covalent CysDUB–ABP adduct.

Incubation of recombinant USP16CD^{WT} (+/– NEM) and USP16CD^{C205A}

Recombinant purified USP16CD^{WT} or USP16CD^{C205A} mutant (final conc. 0.1 µM) was incubated with Rho-Ub-ABP (final conc. 10 µM) for 1 h at 37 °C. Preincubation of USP16CD^{WT} with 10 mM *N*-ethylmaleimide (NEM; SigmaAldrich, #E3876) for 30 min at 37 °C was performed prior to incubation with ABPs to alkylate/block cysteine thiols. The reaction was quenched and resolved as described in *General Method I*. Fluorescence scans for resolved gels with USP16CD^{WT} and USP16CD^{C205A} were obtained with the same settings/sensitivity (PMT = 500), and images were processed simultaneously to ensure observed (lack of) fluorescent covalent adduct is independent of settings.

Time-dependent covalent USP16–ABP adduct formation

Rho-Ub-**Prg**, Rho-Ub-**2**, and Rho-Ub-**5** solutions were prepared from single-use aliquots of 500 µM stock solutions in DMSO. USP16CD^{WT} (final conc. 0.25 µM) was incubated with Rho-Ub-ABP (final conc. 10 µM) at 37 °C. Samples were removed after indicted incubation time (0.5-4 h), and adduct formation was quenched and resolved as described in *General Method I*.

4.4. MS Analysis

Intact protein MS

Recombinant USP16CD^{WT} or USP16CD^{C205A} (1 µM) in HEPES reaction buffer (20 µL) was incubated with Rho-Ub-**Prg**, Rho-Ub-**2** or Rho-Ub-**5** (10 µM) or buffer at 21 °C for at least 2 h prior to analysis. Chromatographic separation and MS analysis was carried out on a Waters ACQUITY UPLC-MS system equipped with a Waters ACQUITY Quaternary Solvent Manager (QSM), Waters ACQUITY FTN AutoSampler, Waters ACQUITY UPLC Protein BEH C4 Column (300 Å, 1.7 µm, 2.1×50 mm) and XEVO-G2 XS QTOF Mass Spectrometer (m/z = 200-2500) in ES+ mode. Samples were run with a 7 min gradient (run time 15 min) using 0.1% FA in MeCN and 0.1% FA in water as mobile phases (flow rate 0.6-0.8 mL/min). The first 4 min the flow was diverted to the waste to avoid contamination of the MS with high concentrations of buffer components. After 4 min, the elution flow was ionized with an electrospray ionization (ESI) source in positive ion mode. The data was analyzed using Waters MassLynx Mass Spectrometry Software V4.2. The total mass of the covalent USP16–ABP adducts was obtained by deconvolution of electrospray ionization mass spectrum envelope (m/z = 600-1600 Da) with the MaxEnt1 (average isotopes) function.

HRMS of unbound ABPs

Stock solutions of Rho-Ub-**Prg** and Rho-Ub-**[D_2]-Prg** in DMSO (500 µM) were diluted 500-fold in 2% MeCN in water (0.1% FA). MS analysis was carried out on a Waters ACQUITY UPLC-MS system in Resolution Mode, equipped with a Waters ACQUITY Quaternary Solvent Manager (QSM), Waters ACQUITY FTN AutoSampler, Waters ACQUITY UPLC Protein BEH C4 Column (300 Å, 1.7 µm, 2.1×50 mm) and XEVO-G2 XS QTOF Mass Spectrometer (m/z = 500-2000). Samples were run with a 1.6 min 2-100% gradient (run time 3 min) using

0.1% FA in MeCN and 0.1% FA in water as mobile phases (flow rate 0.6 mL/min). The elution flow was ionized with an electrospray ionization (ESI) source in positive ion mode. Data processing was performed using Waters MassLynx Mass Spectrometry Software 4.2. Theoretical mass was calculated with the isotope modelling function; Tools – Isotope model – Create charge state series. More details in *section 7.5*.

Bottom-up MS analysis

Recombinant purified USP16CD^{WT} (2.4 µM) or UCHL3FL^{WT} (7 µM) in HEPES reaction buffer was incubated with Rho-Ub-**Prg** or Rho-Ub-**[D_2]-Prg** (final conc. 10 µM) for 1 h at 37 °C. Reaction was quenched as described in *General Method I*. Samples (21 µL, corresponding to 2.5 µg protein/lane) were run on a 10% Bis-Tris gel, and stained with InstantBlue™ Ultrafast Protein Stain. The CysDUB–ABP adduct band was cut out, and the proteins subjected to reduction with DTT, alkylation with iodoacetamide and in-gel trypsin digestion using Proteineer DP digestion robot (Bruker). Tryptic peptides were extracted from the gel slices, lyophilized, dissolved in 95:3:0.1 water/MeCN/FA (v/v/v) and subsequently analyzed by on-line C18 nanoHPLC MS/MS with a system consisting of an Easy nLC 1200 gradient HPLC system (Thermo, Bremen, Germany), and a LUMOS mass spectrometer (Thermo). Digests were injected onto a homemade precolumn (100 µm×15 mm; Reprosil-Pur C18-AQ 3 µm, Dr. Maisch, Ammerbuch, Germany) and eluted via a homemade analytical nano-HPLC column (15 cm×75 µm; Reprosil-Pur C18-AQ 3 µm). The gradient was run from 0% to 50% solvent B (20:80:0.1 water/MeCN/FA (v/v/v)) in 20 min. The nano-HPLC column was drawn to a tip of ~5 µm and acted as the electrospray needle of the MS source. The LUMOS mass spectrometer was operated in data-dependent MS/MS (top-10 mode) with collision energy at 32 V and recording of the MS2 spectrum in the orbitrap. In the master scan (MS1) the resolution was 120,000, the scan range 400-1500, at an AGC target of 400,000 @maximum fill time of 50 ms. Dynamic exclusion after n = 1 with exclusion duration of 10 s. Charge states 2-5 were included. For MS2 precursors were isolated with the quadrupole with an isolation width of 1.2 Da. HCD collision energy was set to 32 V. The MS2 scan resolution was 30,000 with an AGC target of 50,000 @maximum fill time of 60 ms. In a post-analysis process, raw data were first converted to peak lists using Proteome Discoverer version 2.4 (Thermo Electron), and then submitted to the Homo sapiens database (71591 entries), using Mascot v. 2.2.07 (www.matrixscience.com) for protein identification. Mascot searches were with 10 ppm and 0.02 Da deviation for precursor and fragment mass, respectively, and trypsin as enzyme. Up to two missed cleavages were allowed. Methionine oxidation, carbamidomethyl on cysteine, and the Gly-Prg modification (also in mono and dideuterated form) on cysteine were set as a variable modification. More details in *section 7.6*.

4.5. Kinetic Evaluation of Covalent USP16 Occupancy

Rho-Ub-**Prg**, Rho-Ub-**2**, and Rho-Ub-**5** solutions were prepared from single-use aliquots of 500 µM stock solutions in DMSO. USP16CD^{WT} (final conc. 0.1 µM) was incubated with Rho-Ub-**Prg**, Rho-Ub-**2** or Rho-Ub-**5** (final conc. 1-10 µM) at 21 °C in a total volume of 98 µL. Samples (18 µL) were removed after indicated incubation time (5-30 min), and adduct formation was quenched as described in *General Method I*. Samples (24 µL/lane) were loaded on 10% Bis-Tris gels (Invitrogen) and resolved by SDS-PAGE gel electrophoresis with MES as running buffer. Measurements were performed in triplicate (n = 3). Details on equations and pseudo-first order reaction conditions are provided in *section 7.7*.

Intensity of signals corresponding to unbound USP16 and covalent USP16–ABP adduct were quantified with ImageJ v1.52a,[80-82] and the gel-specific background was subtracted. Incubation time-dependent covalent occupancy (Covalent occupancy)$_t$ (in %) was calculated from background-subtracted intensity of bands corresponding to unbound USP16 and covalent adduct after each incubation time *t*.

$$\left(\text{Covalent Occupancy}\right)_t = 100\% \frac{\left(\text{adduct}\right)_t}{\left(\text{adduct}\right)_t + \left(\text{unbound}\right)_t}$$

Triplicate values of time-dependent covalent occupancy (Covalent occupancy)$_t$ (in %) were plotted against incubation time *t* (in min) and fitted to one-phase exponential association (GraphPad Prism 8.1.1, Exponential – One-phase association) with constrained value of Y0 = 0 (covalent occupancy at reaction initiation) and a globally shared value (for all ABPs) for Plateau (maximum covalent occupancy) to obtain the rate of covalent bond formation k_{obs} (in min^{-1}).

$$\left(\text{Covalent Occupancy}\right)_t = \text{Y}_0 + \left(\text{Plateau} - \text{Y}_0\right)\left(1 - e^{-k_{obs}\,t}\right) = \text{Max}\left(1 - e^{-k_{obs}\,t}\right)$$

Reaction half-life t½ (in min) – corresponding to the incubation time to reach 50% of maximum covalent occupancy – was calculated from the pseudo-first order rate of covalent bond formation k_{obs} (in min^{-1}) for each ABP concentration.

$$\text{t½} = \frac{\text{LN}\,(2)}{k_{obs}}$$

Reaction completion (in min) – the incubation time to reach a covalent occupancy corresponding to 97% of the maximum covalent occupancy – is reached after five half-lives (5t½).

4.6. Fluorescence Polarization (FP) Binding Assay

Binding assays of Rho-Ub-ABPs with catalytically inactive USP16^{C205S} mutant were performed in triplicate using HEPES reaction buffer (50 mM HEPES pH7.4, 150 mM NaCl, 2 mM DTT) supplemented with 0.005% Tween20. Rho-Ub-ABPs (20 nL of 5 µM dilution in 1% DMSO, final conc. 5 nM) were dispensed using an ECHO 550 Liquid Handler (Labcyte Inc.) acoustic dispenser, followed by manual addition of serially diluted purified recombinant USP16CD^{C205S} (20 µL, final conc. 0-64 µM). Fluorescence polarization (FP) of the Rhodamine fluorophore was measured every 3 min for 120 min on a PHERAstar plate reader (BMG LABTECH GmbH, Germany) with 485-520-520 FP module (λ_{ex} = 485 nm with detection of polarization at λ_{em} = 520 nm). Change in fluorescence polarization (in mP) upon USP16 interaction was calculated using MARS data analysis software (BMG LABTECH GmbH, Germany). The concentration-dependent fluorescence polarization FP (in mP) after sufficient incubation to reach noncovalent equilibrium (60 min) was plotted against USP16CD^{C205S} concentration (in M) for each Rho-Ub-ABP and fitted using nonlinear regression (GraphPad Prism 8.4.2, Binding – Saturation, One site – Total) with globally shared values for nonspecific binding NS (in mP/M), background signal in absence of enzyme (in mP), and maximum specific binding B_{max} (in mP) to obtain the noncovalent dissociation constant K_D (in M) for each Rho-Ub-ABP. More details in *section 7.8*.

$$\text{FP} = \frac{\text{B}_{max}\,[\text{E}]}{\text{K}_\text{D} + [\text{E}]} + \text{NS} \times [\text{E}] + \text{background}$$

4.7. Thiol Reactivity Assay

Stock solutions of Rho-Ub-ABPs in DMSO (500 µM) were diluted in PBS (10 mM phosphate buffer pH7.45, 140 mM NaCl, 2.7 mM KCl, Gibco PBS tablets) freshly supplemented with GSH (Chem-Impex, #00159) to a final concentration of 5 µM Rho-Ub-ABP and 5 mM GSH. Immediately a 30 µL sample was removed, quenched by 2-fold dilution in 0.1% FA in water and submitted to LC-MS analysis. The remaining material was incubated at 37 °C under gentle agitation (600 rpm) for 24 h, after which the reaction was quenched by 2-fold dilution in 0.1% FA in water, and submitted to LC-MS analysis. LC-MS analysis was performed on a Waters ACQUITY UPLC H-class System equipped with Waters ACQUITY Quaternary Solvent Manager (QSM), Waters ACQUITY UPLC Photodiode Array (PDA) eλ Detector (λ = 210-800 nm), Waters ACQUITY UPLC Protein BEH C4 Column (300 Å, 1.7 µm, 2.1×50 mm) and LCT Premier Orthogonal Acceleration Time of Flight Mass Spectrometer (m/z = 100-1600) in ES+ mode. Samples were run with a 7 min 2-100% gradient (run time 10 min) using 96% water and 96% MeCN mixed with 2.5% FA in water/MeCN as mobile phases (flow rate = 0.5 mL/min). Data processing was performed using Waters MassLynx Mass Spectrometry Software V4.2. Adduct formation was

quantified from the total ion count (TIC) detected for GSH–ABP adduct, remaining unreacted ABP or hydrolysis product; the intensity of the naturally most abundant isotope peak in seven charge states (z = 7-13) of the ionization envelope was combined to calculate the ratio of GSH adduct over total ABP content for each sample. More details in *section 7.9*.

$$\text{GSH Adduct} = 100\% \frac{\text{TIC}_{\text{adduct}}}{\left(\text{TIC}_{\text{adduct}} + \text{TIC}_{\text{inhibitor}}\right)}$$

5. Materials and Methods: *Chemical Synthesis*

5.1. Synthesis of Rho-Ub-ABPs

Reagents and solvents were purchased from various suppliers and are used as received. Linear solid phase synthesis of Ub was performed according to established method reported by our group.[83] Data processing of LC-MS analysis was performed using Waters MassLynx Mass Spectrometry Software V4.2. Deconvoluted mass was obtained from the electrospray ionization mass spectrum envelope (average isotopes) with the MaxEnt1 function. The calculated mass of Ub (derivatives) is obtained with ChemDraw Professional 16.0.1.4 (PerkinElmer Informatics, Inc.) by calculating the molecular weight of the complete structure. Rho-M20-**Prg** was obtained by reported *in-house* synthesis.[79]

General Method II. Trial Cleavage and LC-MS Analysis of Crude Mixtures

Trial Cleavage. An aliquot is incubated with Trial Cleavage Mix (92.5:2.5:2.5:2.5 TFA/water/iPr_3SiH/DODt) for 30 min at 38 °C under gentle agitation. Resin-bound samples are then transferred to a filter tip and filtered prior to continuation. The reaction mixture or filtrate is treated with cold 1:1 Et_2O/pentane (v/v) to precipitate the product, centrifuged and the soluble material is removed by suction. The precipitate is washed twice with cold Et_2O, and remaining Et_2O is removed by submitting to a gentle air flow. The solid material is dissolved in DMSO, and reaction progress is analyzed by LC-MS.

LC-MS Analysis. LC-MS analysis of crude reaction mixtures and purification fractions was performed on a Waters Alliance 2795 Separation Module system equipped with Waters 2996 Photodiode Array Detector (λ = 190-750 nm), Waters Xbridge C18 column (130 Å, 3.5 µm, 2.1×30 mm) and LCT Premier Orthogonal Acceleration Time of Flight Mass Spectrometer (m/z = 300-2000). Samples were run with a 3 min 5-95% gradient (run time 6 min) using two mobile phases; 1% MeCN + 0.1% FA in water and 1% water + 0.1% FA in MeCN (flow rate = 0.8 mL/min).

Step I. **SPPS**

UbiquitinΔG on trityl-resin was prepared by linear solid phase peptide synthesis on a Syro II Automated Peptide Synthesizer (MultiSynTech GmbH, Germany) as described previously.[83] Met1 (methionine) was replaced by its close isostere Nle (norleucine) to prevent oxidation, which typically does not affect recognition by DUBs but can reduce cleavage efficiency of linear diUb chains.[84-85] Briefly, Glycine-loaded trityl resin (Rapp Polymere, Germany, #RA1213) was incubated twice for 25 min with Fmoc-protected amino acids (4 eq; Novabiochem), DIPEA (8 eq; Biosolve, #041533), and PyBOP (4 eq; SigmaAldrich, #851009) in NMP (Biosolve, #13563202), followed by Fmoc removal by incubating three times for 2 min with 20% piperidine/NMP (v/v). This procedure was repeated for each amino acid coupling cycle, with a total of 68 cycles. Coupling sequence has previously been optimized for incorporation of Fmoc-protected dipeptides.[83]

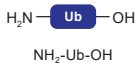

NH_2-Ub-OH

Reaction monitoring. An aliquot of protected NH_2-Ub_{1-75}-OH on resin was submitted to trial cleavage conditions, and the crude material was submitted to LC-MS analysis as described in *General Method II*. LC-MS Rt = 1.85 min, M = 8490 Da (Calc. 8489.78 Da).

Step II. **Rhodamine coupling**

Rhodamine coupling to the N-terminus was performed as described previously.[86] Briefly, *N*,*N'*-Boc$_2$-5-carboxy-Rhodamine **11** (4 eq; *in-house synthesis*),[86] PyBOP (4 eq; SigmaAldrich, #851009), and DIPEA (8 eq; Biosolve, #041533) were dissolved in NMP, and the preactivated mixture was added to NH$_2$-Ub$_{1–75}$(PG)-resin (1 eq), and incubated overnight. The resin was washed with NMP and DCM, after which trial cleavage was performed on a small aliquot to evaluate reaction progress. The resin-bound material was either resubmitted to reach reaction completion or used in the next step.

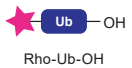

Rho-Ub-OH

Reaction monitoring. An aliquot of protected Rho-Ub$_{1–75}$-OH on resin is submitted to trial cleavage conditions, and the crude material was submitted to LC-MS analysis as described in *General Method II*. LC-MS Rt = 2.37 min, M = 8845 Da (Calc. 8846.12 Da).

Step III. **Cleavage from resin**

Resin cleavage was performed as described previously: treatment with 1,1,1,3,3,3-hexafluoroisopropylalcohol (HFIP; Chem-Impex, #00080) in DCM cleaves bond between glycine and the trityl resin, while protecting groups on the amino acid side chains remain intact.[83] Briefly, (Boc)$_2$Rho-Ub$_{1–75}$(PG)-resin was washed with DCM to remove all NMP, and then twice incubated for 30 min at room temperature with 20% HFIP/DCM (v/v). The combined filtrate was collected, and the solvent was removed by rotary evaporation. Residual HFIP was removed by co-evaporation 2-3 times with 1,2-dichloroethane (DCE; Acros Organics, #406820025) – to prevent formation of HFIP ester in next steps – and dried to use in the next step.

Step IV. **Amine coupling**

Amine coupling was performed as described previously.[83] Amines were obtained from commercial sources or by chemical synthesis. Briefly, (Boc)$_2$Rho-Ub$_{1–75}$(PG)-OH was dissolved in DCM (Biosolve, #13790502) or DMF (Biosolve, #4190501), and incubated overnight with amine (4 eq), DIPEA (8 eq) and PyBOP (4 eq). DCM was removed by rotary evaporation or N_2 (g) shower. DMF was removed by dilution of the reaction mixture in 1:1 MeCN/water and subsequently lyophilized. Trial cleavage was performed to evaluate reaction progress by LC-MS. The residue was either resubmitted to coupling conditions until reaction completion was reached or submitted to global deprotection conditions.

Step V. **Global deprotection and purification**

Global deprotection was performed as described previously.[79] Briefly, (Boc)$_2$Rho-Ub$_{1–75}$(PG)-warhead was incubated for 2.5-3 hours with freshly prepared Cleavemix (90:5:2.5:2.5 TFA/water/iPr$_3$SiH/PhOH) under gentle agitation at room temperature to remove protecting groups from all amino acid sidechains. Then, cold 3:1 Et$_2$O/pentane (v/v) was added to precipitate the product. The reaction mixture was spun down in the centrifuge (2000 rpm, 5 min, 4 °C), supernatant was removed, and the pellet was washed twice with cold Et$_2$O. The remaining solvent was removed by a N_2 shower. The solid crude material was dissolved in DMSO and carefully diluted 10-fold in (warm) water (containing 0.05% TFA if required), filtered and submitted to preparative RP-HPLC purification (methods below, determined by synthesis scale).

prepRP-HPLC method A. RP-HPLC purifications (max. 0.5 mL/run) were performed on a Waters AutoPurification HPLC/MS System equipped with a 2767 Sample Manager, 2545 Binary Gradient Module, two 515 HPLC pumps, SFO Fluid Organizer, 2998 Photodiode Array Detector (λ = 210-650 nm), 3100 Mass Detector (m/z = 100-1500), and a Waters Xbridge BEH C18 OBD Prep. Column (130 Å, 5 µm, 19×150 mm). Column was pre-equilibrated depending on the gradient (prerun time 8 min), and samples (0.45 mL/run) were run with a 15 min 10-40% *(A1)* or 18-48% *(A2)* gradient (run time 21 min) using water and MeCN as mobile phases (flow rate = 30 mL/min), with additional at column dilution (ACD) of 1.5% TFA in MeCN (flow rate = 1 mL/min). Fraction collection was triggered by mass detection; after column separation, 0.02% of the sample was diverted and sent to the mass detector. Fractions containing the correct mass were collected, pooled and lyophilized to obtain product as a pink powder.

prepRP-HPLC method B. RP-HPLC purifications (max. 5 mL/run) were performed on a Shimadzu LC-20AT HPLC system equipped with an SPD-20A UV/Vis detector, RF-20A Fluorescence Detector (λ_{ex} = 507 nm, λ_{em} = 529 nm), FRC-10A fraction collector and a Waters XBridge BEH C18 Prep. Column (130 Å, 5 µm, 10×150 mm). Samples were run with a 15 min 10-70% gradient (run time 22.1 min) using 0.05% TFA in water (v/v) and 0.05% TFA in MeCN (v/v) as mobile phases (flow rate = 6.5 mL/min). Sample collection was triggered by UV/Vis intensity. Pure fractions (checked by LC-MS) were pooled and lyophilized to obtain products as a pink powder.

prepRP-HPLC method C. RP-HPLC purifications (max. 20 mL/run) were performed on a Waters HPLC equipped with a Waters 2489 UV/Vis detector, Waters fraction collector III and a Waters XBridge BEH C18 OBD Prep. Column (130 Å, 5 µm, 30×150 mm). Samples were run with a 13 min 5-20% gradient (run time 25 min) using water, MeCN and 1% TFA in water (v/v) as mobile phases (flow rate = 37.5 mL/min). Fraction collection was triggered by UV intensity (λ = 210 nm). Pure fractions (checked by LC-MS) were pooled and lyophilized to obtain products as a pink powder.

LC-MS evaluation of purified ABPs

Stock solutions of pure ABP (500 µM in DMSO) were diluted 100-fold in 0.1% FA in water, and 10 µL was injected for LC-MS analysis. LC-MS analysis of pure ABPs was performed on a Waters ACQUITY UPLC H-class System equipped with Waters ACQUITY Quaternary Solvent Manager (QSM), Waters ACQUITY UPLC Photodiode Array (PDA) eλ Detector (λ = 210-800 nm), Waters ACQUITY UPLC Protein BEH C4 Column (300 Å, 1.7 µm, 2.1×50 mm) and LCT Premier Orthogonal Acceleration Time of Flight Mass Spectrometer (m/z = 100-1600) in ES+ mode. Samples were run with a 7 min 2-100% gradient (run time 10 min) using 96% water and 96% MeCN mixed with 2.5% FA in water/MeCN as mobile phases (flow rate = 0.5 mL/min).

Rho-Ub-**Prg**

$(Boc)_2$Rho-$Ub_{1–75}$(PG)-OH (10 µmol) was incubated with propargylamine (SigmaAldrich, #P50900) in DCM, and purified by *prepRP-HPLC method C* to yield Rho-$Ub_{1–75}$-**Prg** as a solid pink powder. LC-MS Rt = 3.42 min, M = 8883 Da (Calc. 8883.18 Da).

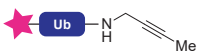

Rho-Ub-**2**

$(Boc)_2$Rho-$Ub_{1–75}$(PG)-OH (2 µmol) was incubated with 1-amino-2-butyne hydrochloride (*in-house synthesis*)[87] in DCM, and purified by *prepRP-HPLC method B* to yield Rho-$Ub_{1–75}$-**2** as a solid pink powder. LC-MS Rt = 3.46 min, M = 8897 Da (Calc. 8897.21 Da).

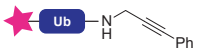

Rho-Ub-**3**

$(Boc)_2$Rho-$Ub_{1–75}$(PG)-OH (2 µmol) was incubated with 3-phenylprop-2-yn-1-amine hydrochloride (Enamine, #EN300-26681) in DCM, and purified by *prepRP-HPLC method B* to yield a 7:10 mixture of Rho-$Ub_{1–75}$-**3** and hydrolyzed Rho-$Ub_{1–75}$-**3b** as a solid pink powder. Rho-Ub-**3** is prone to hydrolysis or possibly (acid-catalyzed) hydration resulting in hydrolyzed Rho-Ub-**3b** (M+18) and could thus only be obtained as a mixture. LC-MS Rt = 3.51 min, M = 8959 & 8977 Da (Calc. 8959.28 Da).

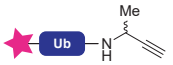

Rho-Ub-**4**

$(Boc)_2$Rho-$Ub_{1–75}$(PG)-OH (2 µmol) was incubated with 1-methyl-prop-2-ynylamine hydrochloride (Chem-Impex, #18527) in DMF, and purified by *prepRP-HPLC method A2* to yield Rho-$Ub_{1–75}$-**4** as a solid pink powder. LC-MS Rt = 3.44 min, M = 8897 Da (Calc. 8897.21 Da).

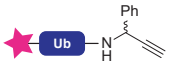

Rho-Ub-**7**

$(Boc)_2$Rho-$Ub_{1–75}$(PG)-OH (2 µmol) was incubated with 1-phenylprop-2-yn-1-amine hydrochloride (Enamine, #EN300-190354) in DMF, and purified by *prepRP-HPLC method A2* to yield Rho-$Ub_{1–75}$-**7** as a solid pink powder. LC-MS Rt = 3.49 min, M = 8959 Da (Calc. 8959.28 Da).

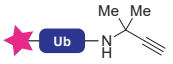

Rho-Ub-**5**

$(Boc)_2$Rho-$Ub_{1–75}$(PG)-OH (10 µmol) was incubated with 2-methyl-3-butyn-2-amine (SigmaAldrich, #687189) in DCM, and purified by *prepRP-HPLC method C* to yield Rho-$Ub_{1–75}$-**5** as a solid pink powder. LC-MS Rt = 3.44 min, M = 8912 Da (Calc. 8911.24 Da).

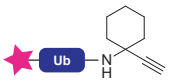

Rho-Ub-**8**

$(Boc)_2$Rho-$Ub_{1–75}$(PG)-OH (2 µmol) was incubated with 1-ethynylcyclohexylamine (SigmaAldrich, #177024) in DMF, and purified by *prepRP-HPLC method A2* to yield Rho-$Ub_{1–75}$-**8** as a solid pink powder. LC-MS Rt = 3.49 min, M = 8951 Da (Calc. 8951.30 Da).

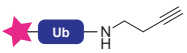

Rho-Ub-**9**

$(Boc)_2$Rho-$Ub_{1–75}$(PG)-OH (2 µmol) was incubated with 1-amino-3-butyne (SigmaAldrich, #715190) in DMF, and purified by *prepRP-HPLC method A1* to yield Rho-$Ub_{1–75}$-**9** as a solid pink powder. LC-MS Rt = 3.42 min, M = 8897 Da (Calc. 8897.21 Da).

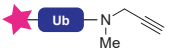

Rho-Ub-**10**

$(Boc)_2$Rho-$Ub_{1–75}$(PG)-OH (2 µmol) was incubated with *N*-methylpropargylamine (SigmaAldrich, #150223) in DMF, and purified by *prepRP-HPLC method A2* to yield Rho-$Ub_{1–75}$-**10** as a solid pink powder. LC-MS Rt = 3.44 min, M = 8897 Da (Calc. 8897.21 Da).

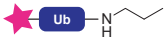

Rho-Ub-**Prp**

$(Boc)_2$Rho-$Ub_{1–75}$(PG)-OH (2 µmol) was incubated with propylamine (Fluka Analytical, #82100) in DMF, and purified by *prepRP-HPLC method A1* to yield Rho-$Ub_{1–75}$-**Prp** as a solid pink powder. LC-MS Rt = 3.44 min, M = 8887 Da (Calc. 8887.22 Da).

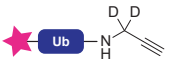

Rho-Ub-**[D_2]-Prg**

$(Boc)_2$Rho-$Ub_{1–75}$(PG)-OH (2 µmol) was incubated with prop-2-yn-1,1-d_2-1-amine hydrochloride (*in-house synthesis*, see *section 5.2.1*) in DCM, and purified by *prepRP-HPLC method B* to yield Rho-$Ub_{1–75}$-**[D_2]-Prg** as a solid pink powder. LC-MS Rt = 3.39 min, M = 8885 Da (Calc. 8885.20 Da).

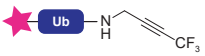

Rho-Ub-**18**

$(Boc)_2$Rho-$Ub_{1–75}$(PG)-OH (2 µmol) was incubated with 4,4,4-trifluorobut-2-yn-1-amine hydrochloride (*in-house synthesis*, see *section 5.2.2*) in DCM, and purified by *prepRP-HPLC method B* to yield Rho-$Ub_{1–75}$-**18** as a solid pink powder. LC-MS Rt = 3.46 min, M = 8951 Da (Calc. 8951.18 Da).

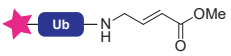

Rho-Ub-**VME**

$(Boc)_2$Rho-$Ub_{1–75}$(PG)-OH (4 µmol) was incubated with methyl (*E*)-4-aminobut-2-enoate hydrochloride (*in-house synthesis*)[48] in DCM, and purified by *prepRP-HPLC method C* to yield Rho-$Ub_{1–75}$-**VME** as a solid pink powder. LC-MS Rt = 3.40 min, M = 8942 Da (Calc. 8943.24 Da).

5.2. Synthesis of Building Blocks

Synthetic schemes can be found in *section 7.2* for deuterated propargylamine **[D_2]-Prg** (**Scheme S1**), trifluoromethylated alkyne **18** (**Scheme S2**), 2-butynylamine **2** (**Scheme S3**), and vinyl methyl ester warhead **VME** (**Scheme S4**).

General. All commercially available reagents and solvents were used as purchased. Reported yields are not optimized. Nuclear magnetic resonance (NMR) spectra were recorded on a Bruker Avance 300 (300 MHz for ^{1}H, 75.00 MHz for ^{13}C) using the residual solvent as internal standard (^{1}H: 7.26 ppm for $CDCl_3$, 2.50 ppm for DMSO-d_6, and 3.31 ppm for MeOD. ^{13}C: 77.16 ppm for $CDCl_3$, 39.52 ppm for DMSO-d_6, and 49.00 ppm for MeOD). Chemical shifts (δ) are given in ppm and coupling constants (*J*) are quoted in hertz (Hz). Resonances are described as s (singlet), d (doublet), t (triplet), q (quartet), p (quintet), b (broad) and m (multiplet) or combinations thereof. The quaternary CD_2 carbon in ^{13}C NMR of deuterated compounds is detected/reported as quintet (p) due to J_{CD}-coupling with ^{2}D (n = 2, splitting pattern 2n+1). Carbons in vicinity of trifluoromethyl group in ^{13}C NMR are detected/reported as quartet due to J_{CF}-coupling with ^{19}F (n = 3, splitting pattern n+1, up to $^4J_{CF}$). Thin Layer Chromatography (TLC) was performed using TLC plates from Merck (SiO_2, Kieselgel 60 F254 neutral, on aluminum with fluorescence indicator) and compounds were visualized by $KMnO_4$ or ninhydrin staining. Flash

Column Chromatography (FCC) purifications were performed using Grace Davisil Silica Gel (particle size 40-63 µm, pore diameter 60 Å) and the indicated eluent.

5.2.1. Synthesis of Amine [D_2]-Prg

3-(trimethylsilyl)prop-2-yn-1,1-d_2-1-ol **12**

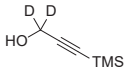

A 1M solution of lithium aluminum deuteride in Et_2O (2.2 mL, 2.2 mmol) was cooled to −78 °C and diluted with anhydrous Et_2O (8 mL). After stirring for 1 hour, a solution of ethyl 3-(trimethylsilyl)propiolate (1.0 gr, 5.9 mmol) in anhydrous Et_2O (2 mL) was added in portions. The mixture was allowed to stir at room temperature for 18 hours after which the reaction was quenched by addition of 1N HCl solution (aq, 10 mL) and the layers were separated. The aqueous layer was extracted with Et_2O and the combined organic layers were dried over Na_2SO_4, filtered and carefully concentrated on a rotary evaporator (850 mbar, 42 °C) to avoid loss of the product. Intermediate **12** was obtained as a pale yellow oil (832 mg, quantitative) with some remnant Et_2O, and used crude in the next step. Spectral data was in agreement with structure and reported data.[88] TLC Rf = 0.67 (1:1 EtOAc/heptane). ^{1}H NMR (300 MHz, $CDCl_3$) δ 0.17 (s, 9H). ^{13}C NMR (75 MHz, $CDCl_3$) δ 104.0, 90.8, 51.3 (p, *J* = 22.6 Hz), −0.1.

tert-butyl (diethoxyphosphoryl)(3-(trimethylsilyl)prop-2-yn-1-yl-1,1-d_2)carbamate **13**

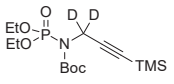

Adjustment of reported procedure for conversion of alcohols into amines under Mitsunobu conditions.[89] Crude deuterated 3-(trimethylsilyl)propargyl alcohol **12** (5.87 mmol), triphenylphosphine (1.77 gr, 6.74 mmol) and diethyl *N*-(*tert*-butoxycarbonyl) phosphoramidate (1.49 gr, 5.87 mmol, 1 eq) were dissolved in anhydrous THF (30 mL). The reaction mixture was flushed with argon and subsequently cooled to 0 °C. Diisopropyl azodicarboxylate (1.33 mL, 6.74 mmol) was added dropwise to the reaction over 10 min. Cooling was removed and the reaction mixture was stirred at room temperature for 18 hours. The solvent was removed *in vacuo* and the crude reaction mixture containing intermediate **13** was directly submitted to the next step.

3-(trimethylsilyl)prop-2-yn-1,1-d_2-1-amine hydrochloride **14**

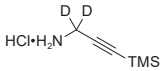

Adjustment of reported procedure.[27] Crude *tert*-butyl (diethoxyphosphoryl)(3-(trimethylsilyl) prop-2-yn-1-yl-1,1-d_2)carbamate **13** was dissolved in anhydrous toluene (40 mL) in a two-neck flask equipped with an inlet for gaseous hydrogen chloride and an outlet toward a strong alkaline solution to neutralize the acidic gas. HCl (g) was generated continuously *(in situ)* by slow dropwise addition of 37% HCl (aq) onto powdered $CaCl_2$ in a separate sealed flask, and bubbled through the reaction mixture for 2 hours. The reaction mixture was sealed and left to stir overnight. The reaction mixture was filtered, triturated with Et_2O (3X) and dried *in vacuo* to give product **14**. Additional product was obtained by removal of solvent from the filtrate *in vacuo*, followed by trituration with Et_2O and toluene. Intermediate **14** was obtained as a white solid (426 mg, 2.57 mmol, 44% over 3 steps). TLC Rf = 0.21 (5% MeOH/DCM). ^{1}H NMR (300 MHz, DMSO-d_6) δ 8.45 (s, 3H), 0.17 (s, 9H). ^{13}C NMR (75 MHz, DMSO-d_6) δ 99.0, 91.2, 28.5 (p, *J* = 22.3 Hz), −0.4.

tert-butyl (3-(trimethylsilyl)prop-2-yn-1-yl-1,1-d_2)carbamate **15**

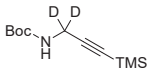

To 3-(trimethylsilyl)prop-2-yn-1,1-d_2-1-amine hydrochloride **14** (42.9 mg, 0.26 mmol) were added DCM (0.8 mL) and triethylamine (72 µL, 0.52 mmol, 2 eq). The suspension was stirred at room temperature for 10 min prior to addition of di-*tert*-butyl dicarbonate (56.5 mg, 0.26 mmol, 1 eq), and additional triethylamine (72 µL, 0.52 mmol, 2 eq) in DCM (2 mL). The clear solution was stirred for 60 min (until full conversion of the starting material was detected by TLC) and concentrated by rotary evaporation to give a white solid. The material was treated with ethyl acetate, water and 1N $KHSO_4$ (aq). The organic layer was extracted with saturated $NaHCO_3$ solution (aq), dried over Na_2SO_4, filtered and concentrated to give a colorless oil (63.4 mg) containing a 2:1 mixture of intermediate **15** with unreacted Boc anhydride. The material was used in the next step without further purification. TLC Rf = 0.87 (5% MeOH/DCM), Rf = 0.72 (1:1 EtOAc/heptane). ^{1}H NMR (300 MHz, $CDCl_3$) δ 4.64 (s, 1H), 1.45 (s, 9H), 0.15 (s, 9H).

tert-butyl (prop-2-yn-1-yl-1,1-d_2)carbamate **16**

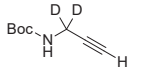

Crude tert-butyl (3-(trimethylsilyl)prop-2-yn-1-yl-1,1-d_2)carbamate **15** (63.4 mg, *max.* 0.26 mmol) was dissolved in methanol (3 mL), to which potassium carbonate (184 mg, 1.3 mmol, 5 eq) was added. The suspension was stirred at room temperature for 30 min, when full conversion was detected by TLC analysis. The reaction mixture was diluted with EtOAc and water, and layers were separated. The organic layer was extracted with water and brine, dried over Na_2SO_4, filtered and carefully concentrated in vacuo to give intermediate **16** as a colorless oil (26.4 mg, 0.17 mmol, 65% over 2 steps). *Note:* Exposure of intermediate **16** to high vacuum for a few minutes can result in significant loss of material. TLC Rf = 0.74 (5% MeOH/DCM), Rf = 0.64 (1:1 EtOAc/heptane). ^{1}H NMR (300 MHz, $CDCl_3$) δ 4.73 (s, 1H), 2.20 (s, 1H), 1.44 (s, 9H).

prop-2-yn-1,1-d_2-1-amine hydrochloride **[D_2]-Prg**

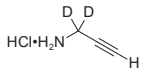

To a mixture of 3-(trimethylsilyl)prop-2-yn-1,1-d_2-1-amine hydrochloride **14** (20 mg, 0.12 mmol), di-*tert*-butyl dicarbonate (29 mg, 0.13 mmol) and potassium carbonate (83 mg, 0.60 mmol) were added MeOH (0.5 mL) and water (0.5 mL). The reaction mixture was stirred at room temperature for 18 hours, and volatiles (methanol) were removed by rotary evaporation upon reaction completion (as detected by TLC. Analytical details for deuterated Boc-propargylamine **16** described above). The reaction mixture was resuspended in ethyl acetate and extracted with water. The organic layer was dried over Na_2SO_4, filtered and carefully concentrated by rotary evaporation. Crude Boc-protected propargylamine **16** was dissolved in methanol (1.5 mL) to which was added 4N hydrogen chloride in dioxane (1 mL, 4 mmol), and the reaction mixture was left to stir 18 hours. Then the solvent was removed in vacuo, and the precipitate was triturated with Et_2O to obtain hydrochloride salt of deuterated propargylamine **[D_2]-Prg** as a white solid (10 mg, 0.064 mmol, 53%). TLC Rf = 0.02 (5% MeOH/DCM). ^{1}H NMR (300 MHz, DMSO-d_6) δ 8.37 (s, 3H), 3.58 (s, 1H). ^{13}C NMR (75 MHz, DMSO-d_6) δ 77.8, 76.9, 27.7 (p, *J* = 22.4 Hz).

5.2.2. Synthesis of Amine 18

tert-butyl (4,4,4-trifluorobut-2-yn-1-yl)carbamate **17**

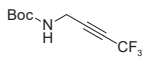

Adjustment of reported procedure for copper(I)-catalyzed trifluoromethylation of terminal alkynes.[52] A flask was charged with copper(I) iodide (1.43 gr, 7.5 mmol), potassium carbonate (2.07 gr, 15 mmol), tetramethylethyleendiamine (1.12 mL, 7.5 mmol) in DMF (23 mL). The dark blue reaction mixture was stirred vigorously under an atmosphere of air at room temperature for 15 min. trimethyl(trifluoromethyl)silane (1.5 mL, 10 mmol) was added and the resulting dark green reaction mixture was stirred for 5 min under air atmosphere prior to cooling to 0 °C. A solution of *N-tert*-butoxycarbonyl-1-amino-3-propyne (776 mg, 5 mmol) and trimethyl(trifluoromethyl)silane (1.5 mL, 10 mmol) in DMF (23 mL), already cooled to 0 °C, was added dropwise in 10 min. The reaction mixture was stirred at 0 °C for 30 min under air atmosphere after which the cooling was removed and the dark blue reaction mixture was left to stir at room temperature for 18 hours. The dark green solution was diluted with water and extracted with Et_2O (2X). The combined organic layers were extracted with water (2X) and brine, dried over $MgSO_4$ and filtered. The solution was diluted with DCM and transferred to a pad of Hyflo which was washed with Et_2O. The mixture was concentrated to give a crude 2:1 mixture of desired product **17** and undesired dimer **19**, which could be separated by FCC (1:4 EtOAc/heptane) to give intermediate **17** as a yellow oil (260.3 mg, 1.2 mmol, 23%). TLC Rf = 0.76 (1:1 EtOAc/heptane). ^{1}H NMR (300 MHz, $CDCl_3$) δ 4.80 (s, 1H), 4.06 (s, 2H), 1.46 (s, 9H). ^{13}C NMR (75 MHz, $CDCl_3$) δ 155.1, 114.0 (q, *J* = 257 Hz), 84.3 (q, *J* = 6.3 Hz), 80.9, 70.4 (q, *J* = 52.6 Hz), 30.1, 28.4.

4,4,4-trifluorobut-2-yn-1-amine hydrochloride **18**

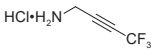

To *tert*-butyl (4,4,4-trifluorobut-2-yn-1-yl)carbamate **17** (120 mg, 0.54 mmol) was added 4N HCl in dioxane (2 mL, 8 mmol) and the reaction mixture was stirred for 90 min at room temperature. After 5 min a precipitate started to form. Volatiles were removed by rotary evaporation and the material was triturated with Et_2O to give amine **18** as a white solid (78.1 mg, 0.49 mmol, 91%). TLC Rf = 0.00 (1:1 EtOAc/heptane). ^{1}H NMR (300 MHz, DMSO-d_6) δ 8.85 (s, 3H), 4.05 (q, *J* = 3.4 Hz, 2H). ^{13}C NMR (75 MHz, DMSO-d_6) δ 113.4 (q, *J* = 257 Hz), 84.2 (q, *J* = 7.3 Hz), 70.9 (q, *J* = 52.3 Hz), 27.7. *Note:* product decomposition was observed within a few hours at high concentration in DMSO-d_6, therefore NMR measurements of the electrophilic hydrochloride salt is preferably conducted in deuterated methanol. ^{1}H NMR (300 MHz, MeOD) δ 4.08 (q, *J* = 3.2 Hz, 2H). ^{13}C NMR (75 MHz, MeOD) δ 115.1 (q, *J* = 257 Hz), 81.9 (q, *J* = 6.3 Hz), 73.8 (q, *J* = 53.5 Hz), 29.4.

di-tert-butyl hexa-2,4-diyne-1,6-diyldicarbamate **19**

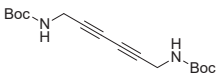

Dimer **19** is formed as undesired Glaser-Hay product in the copper(I)-catalyzed synthesis of trifluoromethylated alkyne **17** in presence of TMEDA. Dimer **19** was isolated as a colorless oil after separation by FCC (1:4 EtOAc/heptane). TLC Rf = 0.62 (1:1 EtOAc/heptane). ^{1}H NMR (300 MHz, $CDCl_3$) δ 4.69 (s, 2H), 3.99 (d, *J* = 5.4 Hz, 4H), 1.44 (s, 18H). ^{13}C NMR (75 MHz, $CDCl_3$) δ 155.2, 80.4, 74.9, 67.5, 31.2, 28.5.

6. References

1. Clague, M.J.; Urbé, S.; Komander, D. Breaking the Chains: Deubiquitylating Enzyme Specificity Begets Function. *Nat. Rev. Mol. Cell Biol.* **2019**, *20*, 338-352. doi: 10.1038/s41580-019-0099-1.
2. Ebner, P.; Versteeg, G.A.; Ikeda, F. Ubiquitin Enzymes in the Regulation of Immune Responses. *Crit. Rev. Biochem. Mol. Biol.* **2017**, *52*, 425-460. doi: 10.1080/10409238.2017.1325829.
3. Deng, L.; Meng, T.; Chen, L.; Wei, W.; Wang, P. The Role of Ubiquitination in Tumorigenesis and Targeted Drug Discovery. *Sig. Transduct. Target. Ther.* **2020**, *5*, 11. doi: 10.1038/s41392-020-0107-0.
4. Popovic, D.; Vucic, D.; Dikic, I. Ubiquitination in Disease Pathogenesis and Treatment. *Nat. Med.* **2014**, *20*, 1242-1253. doi: 10.1038/nm.3739.
5. Huang, X.; Dixit, V.M. Drugging the Undruggables: Exploring the Ubiquitin System for Drug Development. *Cell Res.* **2016**, *26*, 484-498. doi: 10.1038/cr.2016.31.
6. Veggiani, G.; Gerpe, M.C.R.; Sidhu, S.S.; Zhang, W. Emerging Drug Development Technologies Targeting Ubiquitination for Cancer Therapeutics. *Pharmacol. Ther.* **2019**, *199*, 139-154. doi: 10.1016/j.pharmthera.2019.03.003.
7. Wertz, I.E.; Wang, X. From Discovery to Bedside: Targeting the Ubiquitin System. *Cell Chem. Biol.* **2019**, *26*, 156-177. doi: 10.1016/j.chembiol.2018.10.022.
8. Kemp, M. Chapter Three - Recent Advances in the Discovery of Deubiquitinating Enzyme Inhibitors. *Prog. Med. Chem.* **2016**, *55*, 149-192. doi: 10.1016/bs.pmch.2015.10.002.
9. Zhao, B.; Tsai, Y.C.; Jin, B.; Wang, B.; Wang, Y.; Zhou, H.; Carpenter, T.; Weissman, A.M.; Yin, J. Protein Engineering in the Ubiquitin System: Tools for Discovery and Beyond. *Pharmacol. Rev.* **2020**, *72*, 380. doi: 10.1124/pr.118.015651.
10. Taylor, N.C.; McGouran, J.F. Strategies to Target Specific Components of the Ubiquitin Conjugation/Deconjugation Machinery. *Front. Chem.* **2020**, *7*, 914. doi: 10.3389/fchem.2019.00914.
11. Hewings, D.S.; Flygare, J.A.; Bogyo, M.; Wertz, I.E. Activity-Based Probes for the Ubiquitin Conjugation–Deconjugation Machinery: New Chemistries, New Tools, and New Insights. *FEBS J.* **2017**, *284*, 1555-1576. doi: 10.1111/febs.14039.
12. Deng, H.; Lei, Q.; Wu, Y.; He, Y.; Li, W. Activity-Based Protein Profiling: Recent Advances in Medicinal Chemistry. *Eur. J. Med. Chem.* **2020**, *191*, 112151. doi: 10.1016/j.ejmech.2020.112151.
13. Chakrabarty, S.; Kahler, J.P.; van de Plassche, M.A.T.; Vanhoutte, R.; Verhelst, S.H.L. Recent Advances in Activity-Based Protein Profiling of Proteases. *Curr. Top. Microbiol. Immunol.* **2019**, *420*, 253-281. doi: 10.1007/82_2018_138.
14. Altun, M.; Kramer, H.B.; Willems, L.I.; McDermott, J.L.; Leach, C.A.; Goldenberg, S.J.; Kumar, K.G.S.; Konietzny, R.; Fischer, R.; Kogan, E.; Mackeen, M.M.; McGouran, J.; Khoronenkova, S.V.; Parsons, J.L.; Dianov, G.L.; Nicholson, B.; Kessler, B.M. Activity-Based Chemical Proteomics Accelerates Inhibitor Development for Deubiquitylating Enzymes. *Chem. Biol.* **2011**, *18*, 1401-1412. doi: 10.1016/j.chembiol.2011.08.018.
15. Love, K.R.; Pandya, R.K.; Spooner, E.; Ploegh, H.L. Ubiquitin C-Terminal Electrophiles Are Activity-Based Probes for Identification and Mechanistic Study of Ubiquitin Conjugating Machinery. *ACS Chem. Biol.* **2009**, *4*, 275-287. doi: 10.1021/cb9000348.
16. Resnick, E.; Bradley, A.; Gan, J.; Douangamath, A.; Krojer, T.; Sethi, R.; Geurink, P.P.; Aimon, A.; Amitai, G.; Bellini, D., et al. Rapid Covalent-Probe Discovery by Electrophile-Fragment Screening. *J. Am. Chem. Soc.* **2019**, *141*, 8951-8968. doi: 10.1021/jacs.9b02822.
17. Pinto-Fernández, A.; Davis, S.; Schofield, A.B.; Scott, H.C.; Zhang, P.; Salah, E.; Mathea, S.; Charles, P.D.; Damianou, A.; Bond, G.; Fischer, R.; Kessler, B.M. Comprehensive Landscape of Active Deubiquitinating Enzymes Profiled by Advanced Chemoproteomics. *Front. Chem.* **2019**, *7*, 592. doi: 10.3389/fchem.2019.00592.
18. Hewings, D.S.; Heideker, J.; Ma, T.P.; AhYoung, A.P.; El Oualid, F.; Amore, A.; Costakes, G.T.; Kirchhofer, D.; Brasher, B.; Pillow, T.; Popovych, N.; Maurer, T.; Schwerdtfeger, C.; Forrest, W.F.; Yu, K.; Flygare, J.; Bogyo, M.; Wertz, I.E. Reactive-Site-Centric Chemoproteomics Identifies a Distinct Class of Deubiquitinase Enzymes. *Nat. Commun.* **2018**, *9*, 1162. doi: 10.1038/s41467-018-03511-6.

19. Borodovsky, A.; Ovaa, H.; Kolli, N.; Gan-Erdene, T.; Wilkinson, K.D.; Ploegh, H.L.; Kessler, B.M. Chemistry-Based Functional Proteomics Reveals Novel Members of the Deubiquitinating Enzyme Family. *Chem. Biol.* **2002**, *9*, 1149-1159. doi: 10.1016/S1074-5521(02)00248-X.
20. Rehman, S.A.A.; Kristariyanto, Y. A.; Choi, S.-Y.; Nkosi, P. J.; Weidlich, S.; Labib, K.; Hofmann, K.; Kulathu, Y. MINDY-1 Is a Member of an Evolutionarily Conserved and Structurally Distinct New Family of Deubiquitinating Enzymes. *Mol. Cell* **2016**, *63*, 146-155. doi: 10.1016/j.molcel.2016.05.009.
21. Hermanns, T.; Woiwode, I.; Guerreiro, R.F.M.; Vogt, R.; Lammers, M.; Hofmann, K. An Evolutionary Approach to Systematic Discovery of Novel Deubiquitinases, Applied to *Legionella*. *Life Sci. Alliance* **2020**, *3*, e202000838. doi: 10.26508/lsa.202000838.
22. Schubert, A.F.; Nguyen, J.V.; Franklin, T.G.; Geurink, P.P.; Roberts, C.G.; Sanderson, D.J.; Miller, L.N.; Ovaa, H.; Hofmann, K.; Pruneda, J.N.; Komander, D. Identification and Characterization of Diverse OTU Deubiquitinases in Bacteria. *EMBO J.* **2020**, *39*, e105127. doi: 10.15252/embj.2020105127.
23. Hausman, J.M.; Kenny, S.; Iyer, S.; Babar, A.; Qiu, J.; Fu, J.; Luo, Z.-Q.; Das, C. The Two Deubiquitinating Enzymes from *Chlamydia trachomatis* Have Distinct Ubiquitin Recognition Properties. *Biochemistry* **2020**, *59*, 1604-1617. doi: 10.1021/acs.biochem.9b01107.
24. Parker, C.G.; Pratt, M.R. Click Chemistry in Proteomic Investigations. *Cell* **2020**, *180*, 605-632. doi: 10.1016/j.cell.2020.01.025.
25. Talele, T.T. Acetylene Group, Friend or Foe in Medicinal Chemistry. *J. Med. Chem.* **2020**, *63*, 5625-5663. doi: 10.1021/acs.jmedchem.9b01617.
26. Wright, M.H.; Sieber, S.A. Chemical Proteomics Approaches for Identifying the Cellular Targets of Natural Products. *Nat. Prod. Rep.* **2016**, *33*, 681-708. doi: 10.1039/C6NP00001K.
27. Ekkebus, R.; van Kasteren, S.I.; Kulathu, Y.; Scholten, A.; Berlin, I.; Geurink, P.P.; de Jong, A.; Goerdayal, S.; Neefjes, J.; Heck, A.J.R.; Komander, D.; Ovaa, H. On Terminal Alkynes That Can React with Active-Site Cysteine Nucleophiles in Proteases. *J. Am. Chem. Soc.* **2013**, *135*, 2867-2870. doi: 10.1021/ja309802n.
28. Sommer, S.; Weikart, N.D.; Linne, U.; Mootz, H.D. Covalent Inhibition of SUMO and Ubiquitin-Specific Cysteine Proteases by an In Situ Thiol–Alkyne Addition. *Bioorg. Med. Chem.* **2013**, *21*, 2511-2517. doi: 10.1016/j.bmc.2013.02.039.
29. Jia, Y.; Claessens, L.A.; Vertegaal, A.C.O.; Ovaa, H. Chemical Tools and Biochemical Assays for SUMO Specific Proteases (SENPs). *ACS Chem. Biol.* **2019**, *14*, 2389-2395. doi: 10.1021/acschembio.9b00402.
30. Mons, E.; Jansen, I.D.C.; Loboda, J.; van Doodewaerd, B.R.; Hermans, J.; Verdoes, M.; van Boeckel, C.A.A.; van Veelen, P.A.; Turk, B.; Turk, D.; Ovaa, H. The Alkyne Moiety as a Latent Electrophile in Irreversible Covalent Small Molecule Inhibitors of Cathepsin K. *J. Am. Chem. Soc.* **2019**, *141*, 3507-3514. doi: 10.1021/jacs.8b11027.
31. Fairbanks, B.D.; Sims, E.A.; Anseth, K.S.; Bowman, C.N. Reaction Rates and Mechanisms for Radical, Photoinitated Addition of Thiols to Alkynes, and Implications for Thiol–Yne Photopolymerizations and Click Reactions. *Macromolecules* **2010**, *43*, 4113-4119. doi: 10.1021/ma1002968.
32. Jayasree, E.G.; Reshma, S. A Computational Study on the Reaction Mechanism and Energetics of Markovnikov and Anti-Markovnikov Addition in Alkyne Hydrothiolation Reactions. *Comput. Theor. Chem.* **2016**, *1098*, 13-21. doi: 10.1016/j.comptc.2016.10.012.
33. Hashmi, A.S.K. Synthesis of Allenes by Isomerization Reactions. *Mod. Allene Chem.* **2004**, 2-50. doi: 10.1002/9783527619573.ch1.
34. Gehringer, M.; Laufer, S.A. Emerging and Re-Emerging Warheads for Targeted Covalent Inhibitors: Applications in Medicinal Chemistry and Chemical Biology. *J. Med. Chem.* **2019**, *62*, 5673-5724. doi: 10.1021/acs.jmedchem.8b01153.
35. Arkona, C.; Rademann, J. Propargyl Amides as Irreversible Inhibitors of Cysteine Proteases—A Lesson on the Biological Reactivity of Alkynes. *Angew. Chem. Int. Ed.* **2013**, *52*, 8210-8212. doi: 10.1002/anie.201303544.
36. Ménard, R.; Storer, A.C. Oxyanion Hole Interactions in Serine and Cysteine Proteases. *Biol. Chem.* **1992**, *373*, 393-400. doi: 10.1515/bchm3.1992.373.2.393.
37. Shokhen, M.; Traube, T.; Vijayakumar, S.; Hirsch, M.; Uritsky, N.; Albeck, A. Differentiating Serine and Cysteine Protease Mechanisms by New Covalent QSAR Descriptors. *ChemBioChem* **2011**, *12*, 1023-1026. doi: 10.1002/cbic.201000459.
38. Heal, W.P.; Dang, T.H.T.; Tate, E.W. Activity-Based Probes: Discovering New Biology and New Drug Targets. *Chem. Soc. Rev.* **2011**, *40*, 246-257. doi: 10.1039/C0CS00004C.
39. de Jong, A.; Merkx, R.; Berlin, I.; Rodenko, B.; Wijdeven, R.H.M.; El Atmioui, D.; Yalçin, Z.; Robson, C.N.; Neefjes, J.J.; Ovaa, H. Ubiquitin-Based Probes Prepared by Total Synthesis To Profile the Activity of Deubiquitinating Enzymes. *ChemBioChem* **2012**, *13*, 2251-2258. doi: 10.1002/cbic.201200497.
40. Sui, X.; Wang, Y.; Du, Y.-X.; Liang, L.-J.; Zheng, Q.; Li, Y.-M.; Liu, L. Development and Application of Ubiquitin-Based Chemical Probes. *Chem. Sci.* **2020**, *11*, 12633-12646. doi: 10.1039/D0SC03295F.
41. Hameed, D.S.; Sapmaz, A.; Ovaa, H. How Chemical Synthesis of Ubiquitin Conjugates Helps To Understand Ubiquitin Signal Transduction. *Bioconjug. Chem.* **2017**, *28*, 805-815. doi: 10.1021/acs.bioconjchem.6b00140.
42. Rut, W.; Zmudzinski, M.; Snipas, S.J.; Bekes, M.; Huang, T.T.; Drag, M. Engineered Unnatural Ubiquitin for Optimal Detection of Deubiquitinating Enzymes. *Chem. Sci.* **2020**, *11*, 6058-6069. doi: 10.1039/D0SC01347A.
43. Leestemaker, Y.; de Jong, A.; Ovaa, H. Profiling the Activity of Deubiquitinating Enzymes Using Chemically Synthesized Ubiquitin-Based Probes. *Methods Mol. Biol.* **2017**, *1491*, 113-130. doi: 10.1007/978-1-4939-6439-0_9.
44. Drag, M.; Mikolajczyk, J.; Bekes, M.; Reyes-Turcu, F.E.; Ellman, J.A.; Wilkinson, K.D.; Salvesen, G.S. Positional-Scanning Fluorigenic Substrate Libraries Reveal Unexpected Specificity Determinants of DUBs (Deubiquitinating Enzymes). *Biochem. J.* **2008**, *415*, 367-375. doi: 10.1042/BJ20080779.
45. Hodgins, R.R.; Ellison, K.S.; Ellison, M.J. Expression of a Ubiquitin Derivative that Conjugates to Protein Irreversibly Produces Phenotypes Consistent with a Ubiquitin Deficiency. *J. Biol. Chem.* **1992**, *267*, 8807-8812. doi: 10.1016/S0021-9258(19)50351-9.
46. Pickart, C.M.; Kasperek, E.M.; Beal, R.; Kim, A. Substrate Properties of Site-Specific Mutant Ubiquitin Protein (G76A) Reveal Unexpected Mechanistic Features of Ubiquitin-Activating Enzyme (E1). *J. Biol. Chem.* **1994**, *269*, 7115-7123. doi: 10.1016/S0021-9258(17)37255-1.
47. Wilkinson, K.D.; Tashayev, V.L.; O'Connor, L.B.; Larsen, C.N.; Kasperek, E.; Pickart, C.M. Metabolism of the Polyubiquitin Degradation Signal: Structure, Mechanism, and Role of Isopeptidase T. *Biochemistry* **1995**, *34*, 14535-14546. doi: 10.1021/bi00044a032.
48. Kathman, S.G.; Span, I.; Smith, A.T.; Xu, Z.; Zhan, J.; Rosenzweig, A.C.; Statsyuk, A.V. A Small Molecule That Switches a Ubiquitin Ligase From a Processive to a Distributive Enzymatic Mechanism. *J. Am. Chem. Soc.* **2015**, *137*, 12442-12445. doi: 10.1021/jacs.5b06839.
49. Li, Y.-J.; Du, L.; Wang, J.; Vega, R.; Lee, T.D.; Miao, Y.; Aldana-Masangkay, G.; Samuels, E.R.; Li, B.; Ouyang, S.X.; Colayco, S.A.; Bobkova, E.V.; Divlianska, D.B.; Sergienko, E.; Chung, T.D.Y.; Fakih, M.; Chen, Y. Allosteric Inhibition of Ubiquitin-like Modifications by a Class of Inhibitor of SUMO-Activating Enzyme. *Cell Chem. Biol.* **2019**, *26*, 278-288.e6. doi: 10.1016/j.chembiol.2018.10.026.
50. Tailor, A.; Waddington, J.C.; Meng, X.; Park, B.K. Mass Spectrometric and Functional Aspects of Drug–Protein Conjugation. *Chem. Res. Toxicol.* **2016**, *29*, 1912-1935. doi: 10.1021/acs.chemrestox.6b00147.
51. Backus, K.M. Applications of Reactive Cysteine Profiling. *Curr. Top. Microbiol. Immunol.* **2019**, *420*, 375-417. doi: 10.1007/82_2018_120.

52. Tresse, C.; Guissart, C.; Schweizer, S.; Bouhoute, Y.; Chany, A.-C.; Goddard, M.-L.; Blanchard, N.; Evano, G. Practical Methods for the Synthesis of Trifluoromethylated Alkynes: Oxidative Trifluoromethylation of Copper Acetylides and Alkynes. *Adv. Synth. Catal.* **2014**, *356*, 2051-2060. doi: 10.1002/adsc.201400057.
53. Copeland, R.A. Chapter 9. Irreversible Enzyme Inactivators. In *Evaluation of Enzyme Inhibitors in Drug Discovery: A Guide for Medicinal Chemists and Pharmacologists*, Second ed.; John Wiley & Sons, Inc.: Hoboken, New Jersey, 2013; pp 345-382. doi: 10.1002/9781118540398.
54. Tuley, A.; Fast, W. The Taxonomy of Covalent Inhibitors. *Biochemistry* **2018**, *57*, 3326-3337. doi: 10.1021/acs.biochem.8b00315.
55. Singh, J.; Petter, R.C.; Baillie, T.A.; Whitty, A. The Resurgence of Covalent Drugs. *Nat. Rev. Drug Discov.* **2011**, *10*, 307-317. doi: 10.1038/nrd3410.
56. Bovet, C.; Zenobi, R. Determination of Active Enzyme Concentration using Activity-Based Probes and Direct Mass Spectrometric Readout. *Anal. Biochem.* **2008**, *373*, 380-382. doi: 10.1016/j.ab.2007.11.003.
57. Brocklehurst, K.; Resmini, M.; Topham, C.M. Kinetic and Titration Methods for Determination of Active Site Contents of Enzyme and Catalytic Antibody Preparations. *Methods* **2001**, *24*, 153-167. doi: 10.1006/meth.2001.1176.
58. Johansson, H.; Isabella Tsai, Y.-C.; Fantom, K.; Chung, C.-W.; Kümper, S.; Martino, L.; Thomas, D.A.; Eberl, H.C.; Muelbaier, M.; House, D.; Rittinger, K. Fragment-Based Covalent Ligand Screening Enables Rapid Discovery of Inhibitors for the RBR E3 Ubiquitin Ligase HOIP. *J. Am. Chem. Soc.* **2019**, *141*, 2703-2712. doi: 10.1021/jacs.8b13193.
59. Wan, X.; Yang, T.; Cuesta, A.; Pang, X.; Balius, T.E.; Irwin, J.J.; Shoichet, B.K.; Taunton, J. Discovery of Lysine-Targeted eIF4E Inhibitors through Covalent Docking. *J. Am. Chem. Soc.* **2020**, *142*, 4960-4964. doi: 10.1021/jacs.9b10377.
60. Klüter, S.; Simard, J.R.; Rode, H.B.; Grütter, C.; Pawar, V.; Raaijmakers, H.C.A.; Barf, T.A.; Rabiller, M.; van Otterlo, W.A.L.; Rauh, D. Characterization of Irreversible Kinase Inhibitors by Directly Detecting Covalent Bond Formation: A Tool for Dissecting Kinase Drug Resistance. *ChemBioChem* **2010**, *11*, 2557-2566. doi: 10.1002/cbic.201000352.
61. Hansen, R.; Firdaus, S.J.; Li, S.; Janes, M.R.; Zhang, J.; Liu, Y.; Zarrinkar, P.P. An Internally Controlled Quantitative Target Occupancy Assay for Covalent Inhibitors. *Sci. Rep.* **2018**, *8*, 14312. doi: 10.1038/s41598-018-32683-w.
62. Watterson, S.H.; Liu, Q.; Beaudoin Bertrand, M.; Batt, D.G.; Li, L.; Pattoli, M.A.; Skala, S.; Cheng, L.; Obermeier, M.T.; Moore, R., et al. Discovery of Branebrutinib (BMS-986195): A Strategy for Identifying a Highly Potent and Selective Covalent Inhibitor Providing Rapid In Vivo Inactivation of Bruton's Tyrosine Kinase (BTK). *J. Med. Chem.* **2019**, *62*, 3228-3250. doi: 10.1021/acs.jmedchem.9b00167.
63. Miyahisa, I.; Sameshima, T.; Hixon, M.S. Rapid Determination of the Specificity Constant of Irreversible Inhibitors (k_{inact}/K_I) by Means of an Endpoint Competition Assay. *Angew. Chem. Int. Ed.* **2015**, *54*, 14099-14102. doi: 10.1002/anie.201505800.
64. Sameshima, T.; Tanaka, Y.; Miyahisa, I. Universal and Quantitative Method To Evaluate Inhibitor Potency for Cysteinome Proteins Using a Nonspecific Activity-Based Protein Profiling Probe. *Biochemistry* **2017**, *56*, 2921-2927. doi: 10.1021/acs.biochem.7b00190.
65. Kim, R.Q.; Geurink, P. .; Mulder, M.P.C.; Fish, A.; Ekkebus, R.; El Oualid, F.; van Dijk, W.J.; van Dalen, D.; Ovaa, H.; van Ingen, H.; Sixma, T.K. Kinetic Analysis of Multistep USP7 Mechanism Shows Critical Role for Target Protein in Activity. *Nat. Commun.* **2019**, *10*, 231. doi: 10.1038/s41467-018-08231-5.
66. Hocek, M.; Fojta, M. Cross-Coupling Reactions of Nucleoside Triphosphates Followed by Polymerase Incorporation. Construction and Applications of Base-functionalized Nucleic Acids. *Org. Biomol. Chem.* **2008**, *6*, 2233-2241. doi: 10.1039/B803664K.
67. Wood, E.R.; Shewchuk, L.M.; Ellis, B.; Brignola, P.; Brashear, R.L.; Caferro, T.R.; Dickerson, S.H.; Dickson, H.D.; Donaldson, K.H.; Gaul, M., et al. 6-Ethynylthieno[3,2-d]- and 6-Ethynylthieno[2,3-d]pyrimidin-4-anilines as Tunable Covalent Modifiers of ErbB Kinases. *Proc. Natl. Acad. Sci.* **2008**, *105*, 2773. doi: 10.1073/pnas.0708281105.
68. McAulay, K.; Hoyt, E.A.; Thomas, M.; Schimpl, M.; Bodnarchuk, M.S.; Lewis, H.J.; Barratt, D.; Bhavsar, D.; Robinson, D.M.; Deery, M.J.; Ogg, D.J.; Bernardes, G.J.L.; Ward, R.A.; Waring, M.J.; Kettle, J.G. Alkynyl Benzoxazines and Dihydroquinazolines as Cysteine Targeting Covalent Warheads and Their Application in Identification of Selective Irreversible Kinase Inhibitors. *J. Am. Chem. Soc.* **2020**, *142*, 10358-10372. doi: 10.1021/jacs.9b13391.
69. Barf, T.; Covey, T.; Izumi, R.; van de Kar, B.; Gulrajani, M.; van Lith, B.; van Hoek, M.; de Zwart, E.; Mittag, D.; Demont, D.; Verkaik, S.; Krantz, F.; Pearson, P.G.; Ulrich, R.; Kaptein, A. Acalabrutinib (ACP-196): A Covalent Bruton Tyrosine Kinase Inhibitor with a Differentiated Selectivity and In Vivo Potency Profile. *J. Pharmacol. Exp. Ther.* **2017**, *363*, 240. doi: 10.1124/jpet.117.242909.
70. Wang, T.; Yin, L.; Cooper, E.M.; Lai, M.-Y.; Dickey, S.; Pickart, C.M.; Fushman, D.; Wilkinson, K.D.; Cohen, R.E.; Wolberger, C. Evidence for Bidentate Substrate Binding as the Basis for the K48 Linkage Specificity of Otubain 1. *J. Mol. Biol.* **2009**, *386*, 1011-1023. doi: 10.1016/j.jmb.2008.12.085.
71. Nanao, M.H.; Tcherniuk, S.O.; Chroboczek, J.; Dideberg, O.; Dessen, A.; Balakirev, M.Y. Crystal Structure of Human Otubain 2. *EMBO Rep.* **2004**, *5*, 783-788. doi: 10.1038/sj.embor.7400201.
72. Mevissen, T.E.T.; Hospenthal, M.K.; Geurink, P.P.; Elliott, P.R.; Akutsu, M.; Arnaudo, N.; Ekkebus, R.; Kulathu, Y.; Wauer, T.; El Oualid, F.; Freund, S.M.V.; Ovaa, H.; Komander, D. OTU Deubiquitinases Reveal Mechanisms of Linkage Specificity and Enable Ubiquitin Chain Restriction Analysis. *Cell* **2013**, *154*, 169-184. doi: 10.1016/j.cell.2013.05.046.
73. Larsen, C.N.; Price, J.S.; Wilkinson, K.D. Substrate Binding and Catalysis by Ubiquitin C-Terminal Hydrolases: Identification of Two Active Site Residues. *Biochemistry* **1996**, *35*, 6735-6744. doi: 10.1021/bi960099f.
74. Hermanns, T.; Pichlo, C.; Woiwode, I.; Klopffleisch, K.; Witting, K.F.; Ovaa, H.; Baumann, U.; Hofmann, K. A Family of Unconventional Deubiquitinases with Modular Chain Specificity Determinants. *Nat. Commun.* **2018**, *9*, 799. doi: 10.1038/s41467-018-03148-5.
75. García-Nafría, J.; Watson, J.F.; Greger, I.H. IVA Cloning: A Single-Tube Universal Cloning System Exploiting Bacterial *In Vivo* Assembly. *Sci. Rep.* **2016**, *6*, 27459. doi: 10.1038/srep27459.
76. Liu, H.; Naismith, J.H. An Efficient One-Step Site-Directed Deletion, Insertion, Single and Multiple-Site Plasmid Mutagenesis Protocol. *BMC Biotechnol.* **2008**, *8*, 91. doi: 10.1186/1472-6750-8-91.
77. Luna-Vargas, M.P.A.; Christodoulou, E.; Alfieri, A.; van Dijk, W.J.; Stadnik, M.; Hibbert, R.G.; Sahtoe, D.D.; Clerici, M.; Marco, V.D.; Littler, D.; Celie, P.H.N.; Sixma, T.K.; Perrakis, A. Enabling High-Throughput Ligation-independent Cloning and Protein Expression for the Family of Ubiquitin Specific Proteases. *J. Struct. Biol.* **2011**, *175*, 113-119. doi: 10.1016/j.jsb.2011.03.017.
78. Ward, S.J.; Gratton, H.E.; Indrayudha, P.; Michavila, C.; Mukhopadhyay, R.; Maurer, S.K.; Caulton, S.G.; Emsley, J.; Dreveny, I. The Structure of the Deubiquitinase USP15 Reveals a Misaligned Catalytic Triad and an Open Ubiquitin-Binding Channel. *J. Biol. Chem.* **2018**, *293*, 17362-17374. doi: 10.1074/jbc.ra118.003857.
79. Gjonaj, L.; Sapmaz, A.; Flierman, D.; Janssen, G.M.C.; van Veelen, P.A.; Ovaa, H. Development of a DUB-Selective Fluorogenic Substrate. *Chem. Sci.* **2019**, *10*, 10290-10296. doi: 10.1039/C9SC02226K.
80. Abramoff, M.; Magalhães, P.; Ram, S.J. Image Processing with ImageJ. *Biophotonics Intern.* **2003**, *11*, 36-42.
81. Rasband, W.S. *ImageJ*, U. S. National Institutes of Health, Bethesda, Maryland, USA: 1997-2018. https://imagej.nih.gov/ij/.

82. Schneider, C.A.; Rasband, W.S.; Eliceiri, K.W. NIH Image to ImageJ: 25 Years of Image Analysis. *Nat. Meth.* **2012**, *9*, 671-675. doi: 10.1038/nmeth.2089.

83. El Oualid, F.; Merkx, R.; Ekkebus, R.; Hameed, D.S.; Smit, J.J.; de Jong, A.; Hilkmann, H.; Sixma, T.K.; Ovaa, H. Chemical Synthesis of Ubiquitin, Ubiquitin-Based Probes, and Diubiquitin. *Angew. Chem. Int. Ed.* **2010**, *49*, 10149-10153. doi: 10.1002/anie.201005995.

84. Moroder, L. Isosteric Replacement of Sulfur with Other Chalcogens in Peptides and Proteins. *J. Pept. Sci.* **2005**, *11*, 187-214. doi: 10.1002/psc.654.

85. Xin, B.-T.; van Tol, B.D.M.; Ovaa, H.; Geurink, P.P. Native Chemical Ligation at Methionine Bioisostere Norleucine Allows for N-Terminal Chemical Protein Ligation. *Org. Biomol. Chem.* **2018**, *16*, 6306-6315. doi: 10.1039/C8OB01627E.

86. Geurink, P.P.; van Tol, B.D.M.; van Dalen, D.; Brundel, P.J.G.; Mevissen, T.E.T.; Pruneda, J.N.; Elliott, P.R.; van Tilburg, G.B.A.; Komander, D.; Ovaa, H. Development of Diubiquitin-Based FRET Probes To Quantify Ubiquitin Linkage Specificity of Deubiquitinating Enzymes. *ChemBioChem* **2016**, *17*, 816-820. doi: 10.1002/cbic.201600017.

87. Nishizawa, R.; Nishiyama, T.; Hisaichi, K.; Hirai, K.; Habashita, H.; Takaoka, Y.; Tada, H.; Sagawa, K.; Shibayama, S.; Maeda, K.; Mitsuya, H.; Nakai, H.; Fukushima, D.; Toda, M. Discovery of Orally Available Spirodiketopiperazine-Based CCR5 Antagonists. *Bioorg. Med. Chem.* **2010**, *18*, 5208-5223. doi: 10.1016/j.bmc.2010.05.057.

88. Roşca, D.-A.; Radkowski, K.; Wolf, L.M.; Wagh, M.; Goddard, R.; Thiel, W.; Fürstner, A. Ruthenium-Catalyzed Alkyne *trans*-Hydrometalation: Mechanistic Insights and Preparative Implications. *J. Am. Chem. Soc.* **2017**, *139*, 2443-2455. doi: 10.1021/jacs.6b12517.

89. Klepacz, A.; Zwierzak, A. New Protocol for Converting Alcohols into Amines. *Synth. Commun.* **2001**, *31*, 1683-1689. doi: 10.1081/SCC-100103987.

90. Rennie, M.L.; Arkinson, C.; Chaugule, V.K.; Toth, R.; Walden, H. Structural Basis of FANCD2 Deubiquitination by USP1–UAF1. *Nat. Struct. Mol. Biol.* **2021**, *28*, 356-364. doi: 10.1038/s41594-021-00576-8.

91. Dharadhar, S.; Clerici, M.; van Dijk, W.J.; Fish, A.; Sixma, T.K. A Conserved Two-step Binding for the UAF1 Regulator to the USP12 Deubiquitinating Enzyme. *J. Struct. Biol.* **2016**, *196*, 437-447. doi: 10.1016/j.jsb.2016.09.011.

92. Gersch, M.; Wagstaff, J.L.; Toms, A.V.; Graves, B.; Freund, S.M.V.; Komander, D. Distinct USP25 and USP28 Oligomerization States Regulate Deubiquitinating Activity. *Mol. Cell* **2019**, *74*, 436-451.e7. doi: 10.1016/j.molcel.2019.02.030.

93. Sauer, F.; Klemm, T.; Kollampally, R.B.; Tessmer, I.; Nair, R.K.; Popov, N.; Kisker, C. Differential Oligomerization of the Deubiquitinases USP25 and USP28 Regulates Their Activities. *Mol. Cell* **2019**, *74*, 421-435.e10. doi: 10.1016/j.molcel.2019.02.029.

94. Gersch, M.; Gladkova, C.; Schubert, A.F.; Michel, M.A.; Maslen, S.; Komander, D. Mechanism and Regulation of the Lys6-Selective Deubiquitinase USP30. *Nat. Struct. Mol. Biol.* **2017**, *24*, 920-930. doi: 10.1038/nsmb.3475.

95. Xu, G.; Su, H.; Lu, L.; Liu, X.; Zhao, L.; Tang, B.; Ming, Z. Structural Insights into the Catalytic Mechanism and Ubiquitin Recognition of USP34. *J. Mol. Biol.* **2022**, *434*, 167634. doi: 10.1016/j.jmb.2022.167634.

96. O'Dea, R.; Kazi, N.; Hoffmann-Benito, A.; Zhao, Z.; Recknagel, S.; Wendrich, K.; Janning, P.; Gersch, M. Molecular Basis for Ubiquitin/Fubi Cross-Reactivity in USP16 and USP36. *Nat. Chem. Biol.* **2023**. doi: 10.1038/s41589-023-01388-1.

97. Sahtoe, D.D.; van Dijk, W.J.; El Oualid, F.; Ekkebus, R.; Ovaa, H.; Sixma, T.K. Mechanism of UCH-L5 Activation and Inhibition by DEUBAD Domains in RPN13 and INO80G. *Mol. Cell* **2015**, *57*, 887-900. doi: 10.1016/j.molcel.2014.12.039.

98. Mevissen, T.E.T.; Kulathu, Y.; Mulder, M.P.C.; Geurink, P.P.; Maslen, S.L.; Gersch, M.; Elliott, P.R.; Burke, J.E.; van Tol, B.D.M.; Akutsu, M.; El Oualid, F.; Kawasaki, M.; Freund, S.M.V.; Ovaa, H.; Komander, D. Molecular Basis of Lys11-Polyubiquitin Specificity in the Deubiquitinase Cezanne. *Nature* **2016**, *538*, 402-405. doi: 10.1038/nature19836.

99. Kwasna, D.; Rehman, S.A.A.; Natarajan, J.; Matthews, S.; Madden, R.; De Cesare, V.; Weidlich, S.; Virdee, S.; Ahel, I.; Gibbs-Seymour, I.; Kulathu, Y. Discovery and Characterization of ZUFSP/ZUP1, a Distinct Deubiquitinase Class Important for Genome Stability. *Mol. Cell* **2018**, *70*, 150-164.e6. doi: 10.1016/j.molcel.2018.02.023.

100. Li, Y.; De Bolòs, A.; Amador, V.; Reverter, D. Structural Basis for the SUMO2 Isoform Specificity of SENP7. *J. Mol. Biol.* **2022**, *434*, 167875. doi: 10.1016/j.jmb.2022.167875.

101. Nair, R.M.; Seenivasan, A.; Liu, B.; Chen, D.; Lowe, E.D.; Lorenz, S. Reconstitution and Structural Analysis of a HECT Ligase-Ubiquitin Complex via an Activity-Based Probe. *ACS Chem. Biol.* **2021**, *16*, 1615-1621. doi: 10.1021/acschembio.1c00433.

102. Hermanns, T.; Pichlo, C.; Baumann, U.; Hofmann, K. A Structural Basis for the Diverse Linkage Specificities Within the ZUFSP Deubiquitinase Family. *Nat. Commun.* **2022**, *13*, 401. doi: 10.1038/s41467-022-28049-6.

103. Dzimianski, J.V.; Mace, S.L.; Williams, I.L.; Freitas, B.T.; Pegan, S.D. Flipping the Substrate Preference of Hazara Virus Ovarian Tumour Domain Protease Through Structure-Based Mutagenesis. *Acta Crystallogr., Sect. D* **2020**, *76*, 1114-1123. doi: 10.1107/S2059798320012875.

104. Deaton, M.K.; Dzimianski, J.V.; Daczkowski, C.M.; Whitney, G.K.; Mank, N.J.; Parham, M.M.; Bergeron, E.; Pegan, S.D. Biochemical and Structural Insights into the Preference of Nairoviral DeISGylases for Interferon-Stimulated Gene Product 15 Originating from Certain Species. *J. Virol.* **2016**, *90*, 8314. doi: 10.1128/JVI.00975-16.

105. Dzimianski, J.V.; Scholte, F.E.M.; Williams, I.L.; Langley, C.; Freitas, B.T.; Spengler, J.R.; Bergeron, É.; Pegan, S.D. Determining the Molecular Drivers of Species-Specific Interferon-Stimulated Gene Product 15 Interactions with Nairovirus Ovarian Tumor Domain Proteases. *PLoS ONE* **2019**, *14*, e0226415. doi: 10.1371/journal.pone.0226415.

106. Békés, M.; van der Heden van Noort, G.J.; Ekkebus, R.; Ovaa, H.; Huang, T.T.; Lima, C.D. Recognition of Lys48-Linked Di-Ubiquitin and Deubiquitinating Activities of the SARS Coronavirus Papain-like Protease. *Mol. Cell* **2016**, *62*, 572-585. doi: 10.1016/j.molcel.2016.04.016.

107. Daczkowski, C.M.; Dzimianski, J.V.; Clasman, J.R.; Goodwin, O.; Mesecar, A.D.; Pegan, S.D. Structural Insights into the Interaction of Coronavirus Papain-Like Proteases and Interferon-Stimulated Gene Product 15 from Different Species. *J. Mol. Biol.* **2017**, *429*, 1661-1683. doi: 10.1016/j.jmb.2017.04.011.

108. Klemm, T.; Ebert, G.; Calleja, D.J.; Allison, C.C.; Richardson, L.W.; Bernardini, J.P.; Lu, B.G.C.; Kuchel, N.W.; Grohmann, C.; Shibata, Y., et al. Mechanism and Inhibition of the Papain-like Protease, PLpro, of SARS-CoV-2. *EMBO J.* **2020**, *39*, e106275. doi: 10.15252/embj.2020106275.

109. Daczkowski, C.M.; Goodwin, O.Y.; Dzimianski, J.V.; Farhat, J.J.; Pegan, S.D. Structurally Guided Removal of DeISGylase Biochemical Activity from Papain-Like Protease Originating from Middle East Respiratory Syndrome Coronavirus. *J. Virol.* **2017**, *91*, e01067-17. doi: 10.1128/JVI.01067-17.

110. Clasman, J.R.; Everett, R.K.; Srinivasan, K.; Mesecar, A.D. Decoupling DeISGylating and Deubiquitinating Activities of the MERS Virus Papain-Like Protease. *Antiviral Res.* **2020**, *174*, 104661. doi: 10.1016/j.antiviral.2019.104661.

111. Durie, I.A.; Dzimianski, J.V.; Daczkowski, C.M.; McGuire, J.; Faaberg, K.; Pegan, S.D. Structural Insights into the Interaction of Papain-Like Protease 2 from the Alphacoronavirus Porcine Epidemic Diarrhea Virus and Ubiquitin. *Acta Crystallogr., Sect. D* **2021**, *77*, 943-953. doi: 10.1107/S205979832100509X.

112. Swatek, K.N.; Aumayr, M.; Pruneda, J.N.; Visser, L.J.; Berryman, S.; Kueck, A.F.; Geurink, P.P.; Ovaa, H.; van Kuppeveld, F.J.M.; Tuthill, T.J.; Skern, T.; Komander, D. Irreversible Inactivation of ISG15 by a Viral Leader Protease Enables Alternative Infection Detection Strategies. *Proc. Natl. Acad. Sci.* **2018**, *115*, 2371. doi: 10.1073/pnas.1710617115.

113. Ramirez, Y.A.; Adler, T.B.; Altmann, E.; Klemm, T.; Tiesmeyer, C.; Sauer, F.; Kathman, S.G.; Statsyuk, A.V.; Sotriffer, C.; Kisker, C. Structural Basis of Substrate Recognition and Covalent Inhibition of Cdu1 from *Chlamydia trachomatis*. *ChemMedChem* **2018**, *13*, 2014-2023. doi: 10.1002/cmdc.201800364.
114. Pruneda, J.N.; Bastidas, R.J.; Bertsoulaki, E.; Swatek, K.N.; Santhanam, B.; Clague, M.J.; Valdivia, R.H.; Urbé, S.; Komander, D. A *Chlamydia* Effector Combining Deubiquitination and Acetylation Activities Induces Golgi Fragmentation. *Nat. Microbiol.* **2018**, *3*, 1377-1384. doi: 10.1038/s41564-018-0271-y.
115. Liu, S.; Luo, J.; Zhen, X.; Qiu, J.; Ouyang, S.; Luo, Z.-Q. Interplay Between Bacterial Deubiquitinase and Ubiquitin E3 Ligase Regulates Ubiquitin Dynamics on Legionella Phagosomes. *eLife* **2020**, *9*, e58114. doi: 10.7554/eLife.58114.
116. Luo, J.; Ruan, X.; Huang, Z.; Li, Z.; Ye, L.; Wu, Y.; Zhen, X.; Ouyang, S. Structural Basis for the Dual Catalytic Activity of the *Legionella pneumophila* Ovarian Tumor (OTU) Domain Deubiquitinase LotA. *J. Biol. Chem.* **2022**, *298*, 102414. doi: 10.1016/j.jbc.2022.102414.
117. Erven, I.; Abraham, E.; Hermanns, T.; Baumann, U.; Hofmann, K. A Widely Distributed Family of Eukaryotic and Bacterial Deubiquitinases Related to Herpesviral Large Tegument Proteins. *Nat. Commun.* **2022**, *13*, 7643. doi: 10.1038/s41467-022-35244-y.
118. Pruneda, J.N.; Durkin, C.H.; Geurink, P.P.; Ovaa, H.; Santhanam, B.; Holden, D.W.; Komander, D. The Molecular Basis for Ubiquitin and Ubiquitin-like Specificities in Bacterial Effector Proteases. *Mol. Cell* **2016**, *63*, 261-276. doi: 10.1016/j.molcel.2016.06.015.
119. Franklin, T.G.; Brzovic, P.S.; Pruneda, J.N. Bacterial Mimicry of Eukaryotic HECT Ubiquitin Ligation. *bioRxiv* **2023**. doi: 10.1101/2023.06.05.543783.
120. Bogyo, M.; Shin, S.; McMaster, J.S.; Ploegh, H.L. Substrate Binding and Sequence Preference of the Proteasome Revealed by Active-Site-Directed Affinity Probes. *Chem. Biol.* **1998**, *5*, 307-320. doi: 10.1016/S1074-5521(98)90169-7.
121. Thompson, S.K.; Heathcock, C.H. Effect of Cation, Temperature, and Solvent on the Stereoselectivity of the Horner-Emmons Reaction of Trimethyl Phosphonoacetate with Aldehydes. *J. Org. Chem.* **1990**, *55*, 3386-3388. doi: 10.1021/jo00297a076.
122. Mons, E.; Roet, S.; Kim, R.Q.; Mulder, M.P.C. A Comprehensive Guide for Assessing Covalent Inhibition in Enzymatic Assays Illustrated with Kinetic Simulations. *Curr. Protoc.* **2022**, *2*, e419. doi: 10.1002/cpz1.419.
123. Copeland, R.A. Chapter 2. Chemical Bonds and Reactions in Biochemistry. In *ENZYMES: A Practical Introduction to Structure, Mechanism, and Data Analysis*, Second ed.; John Wiley & Sons, Inc.: New York, NY, 2000; pp 11-41. doi: 10.1002/0471220639.ch2.
124. Copeland, R.A. Chapter 4. Protein–Ligand Binding Equilibria. In *ENZYMES: A Practical Introduction to Structure, Mechanism, and Data Analysis*, Second ed.; John Wiley & Sons, Inc.: New York, NY, 2000; pp 76-108. doi: 10.1002/0471220639.ch4.
125. Hameed, D.S.; Sapmaz, A.; Burggraaff, L.; Amore, A.; Slingerland, C.J.; van Westen, G.J.P.; Ovaa, H. Development of Ubiquitin-Based Probe for Metalloprotease Deubiquitinases. *Angew. Chem. Int. Ed.* **2019**, *58*, 14477-14482. doi: 10.1002/anie.201906790.
126. Morrow, M.E.; Morgan, M.T.; Clerici, M.; Growkova, K.; Yan, M.; Komander, D.; Sixma, T.K.; Simicek, M.; Wolberger, C. Active Site Alanine Mutations Convert Deubiquitinases into High-Affinity Ubiquitin-Binding Proteins. *EMBO Rep.* **2018**, *19*, e45680. doi: 10.15252/embr.201745680.
127. Moerke, N.J. Fluorescence Polarization (FP) Assays for Monitoring Peptide-Protein or Nucleic Acid-Protein Binding. *Curr. Protoc. Chem. Biol.* **2009**, *1*, 1-15. doi: 10.1002/9780470559277.ch090102.
128. Lonsdale, R.; Burgess, J.; Colclough, N.; Davies, N.L.; Lenz, E.M.; Orton, A.L.; Ward, R.A. Expanding the Armory: Predicting and Tuning Covalent Warhead Reactivity. *J. Chem. Inf. Model.* **2017**, *57*, 3124-3137. doi: 10.1021/acs.jcim.7b00553.
129. Crowe, S.O.; Rana, A.S.J.B.; Deol, K.K.; Ge, Y.; Strieter, E.R. Ubiquitin Chain Enrichment Middle-Down Mass Spectrometry Enables Characterization of Branched Ubiquitin Chains *in Cellulo*. *Anal. Chem.* **2017**, *89*, 4428-4434. doi: 10.1021/acs.analchem.6b03675.
130. Xu, P.; Peng, J. Characterization of Polyubiquitin Chain Structure by Middle-Down Mass Spectrometry. *Anal. Chem.* **2008**, *80*, 3438-3444. doi: 10.1021/ac800016w.

7. Supporting Information

7.1. Crystal Structures

Table S1 | Crystal structures of Ub(l)-**Prg** ABPs covalently bound to a catalytic cysteine thiol.

Species	Protein	ABP	PDB	Reference
Human	USP1 + UAF1 (truncated)	Ub-**Prg**	7AY2	[Rennie, 2021] [90]
	USP12 + UAF1	Ub-**Prg**	5L8W	[Dharadhar, 2016] [91]
	USP28 USP28 (insertion deleted)	Ub-**Prg** Ub-**Prg**	6HEK 6HEI	[Gersch, 2019] [92]
	USP28CD^{E593D}	Ub-**Prg**	6H4H	[Sauer, 2019] [93]
	USP30	Ub-**Prg** Ub-**Prg**	5OHK 5OHN	[Gersch, 2017] [94]
	USP34CD	Ub-**Prg**	7W3U	[Xu, 2022] [95]
	USP36	Fubi-**Prg** Ub-**Prg**	8BS3 8BS9	[O'Dea, 2023] [96]
	UCHL5 + INO80G UCHL5 + RPN13 DEUBAD	Ub-**Prg** Ub-**Prg**	4UF6 4UEL	[Sahtoe, 2015] [97]
	A20 OTU	Ub-**Prg**	5LRX	[Mevissen, 2016] [98]
	MINDY-1	Ub-**Prg**	5JQS	[Rehman, 2016] [20]
	ZUP1 (232-578)	Ub-**Prg**	6EI1	[Hermanns, 2018] [74]
	ZUP1	Ub-**Prg**	6FGE	[Kwasna, 2018] [99]
	SENP7	SUMO2-**Prg**	7R2E	[Li, 2022] [100]
	HUWE1 (HECT domain) [a]	Ub-**Prg**	6XZ1	[Nair, 2021] [101]
Mouse	mUSP18	mISG15-**Prg**	5CHV	[Basters, 2017] [18]
Insect	*Tribolium castaneum* TcZUP	Ub-**Prg**	7OJE	[Hermanns, 2022] [102]
Virus	CCHFV OTU	Ub-**Prg**	3ZNH	[Ekkebus, 2013] [27]
	HAZV OTU	Ub-**Prg**	7JMS	[Dzimianski, 2020] [103]
	ERVV OTU	mISG15(CTD)-**Prg**	5JZE	[Deaton, 2016] [104]
	KUPEV OTU GANV OTU	sheepISG15(CTD)-**Prg** sheepISG15(CTD)-**Prg**	6OAR 6OAT	[Dzimianski, 2019] [105]
	SARS CoV PL^{pro}	K48 diUb-**Prg**	5E6J	[Békés, 2016] [106]
	SARS CoV PL^{pro}	hISG15(CTD)-**Prg** mISG15(CTD)-**Prg**	5TL6 5TL7	[Daczkowski, 2017] [107]
	SARS CoV-2 PL^{pro}	Ub-**Prg** ISG15(CTD)-**Prg**	6XAA 6XA9	[Klemm, 2020] [108]
	MERS CoV PL^{pro}	hISG15(CTD)-**Prg** hISG15(CTD)-**Prg**	5W8U 5W8T	[Daczkowski, 2017] [109]
	MERS CoV PL^{pro}	ISG15-**Prg**	6BI8	[Clasman, 2020] [110]
	PEDV PL^{pro} 2	Ub-**Prg**	7MC9	[Durie, 2021] [111]
	FMDV LB^{pro}	ISG15-**Prg**	6FFA	[Swatek, 2018] [112]

Table S1 continues on the next page

Table S1 | Crystal structures of Ub(l)-**Prg** ABPs covalently bound to a catalytic cysteine thiol. *(continued)*

Species	Protein	ABP	PDB	Reference
Bacteria	*C. trachomatis* ChlaDUB1	Ub-**Prg**	6FDK	[Ramirez, 2018] [113]
	C. trachomatis ChlaDUB1	Ub-**Prg**	6GZS	[Pruneda, 2018] [114]
	C. trachomatis ChlaDUB2 (93-339)	Ub-**Prg**	6OAM	[Hausman, 2020] [23]
	L. pneumophila Lem27 (1-417)	Ub-**Prg**	7BU0	[Liu, 2020] [115]
	L. pneumophila LotA (1-542)	Ub-**Prg**	7W54	[Luo, 2022] [116]
	W. chrondophila Wc-VTD1	Ub-**Prg**	8ADB	[Erven, 2022] [117]
	X. campestris XopD	Ub-**Prg** tSUMO-**Prg**	5JP3 5JP1	[Pruneda, 2016] [118]
	Verrucomicrobia VsHECT (639-847) [a]	Ub-**Prg**	8ST7	[Franklin, 2023] [119]
	S. enterica SopA (603-782) [a]	Ub-**Prg**	8ST8	[Franklin, 2023] [119]
	E. coli NleL (606-782) [a]	Ub-**Prg**	8ST9	[Franklin, 2023] [119]

Structures in PDB (Protein Data Bank) containing ligand AYE (prop-2-en-1-amine) updated until August 2023. [a] E3 ligase. **Prg** = propargylamide (warhead). Ub = ubiquitin. ISG15 = interferon-stimulated gene 15 protein. SUMO2 = small ubiquitin-like modifier isoform 2. h = human. m = mouse. t = tomato. CTD = C-terminal domain. PL^{pro} = papain-like protease. LB^{pro} = leader protease. CCHFV = Crimean Congo Hemorrhagic fever virus. HAZV = Hazara virus. ERVV = Erve virus. KUPEV = Kupe virus. GANV = Ganjam virus. SARS CoV = Severe acute respiratory syndrome coronavirus. MERS CoV = Middle East respiratory syndrome coronavirus. PEDV = porcine epidemic diarrhea virus. FMDV = Foot-and-mouth disease virus.

7.2. Chemical Synthesis

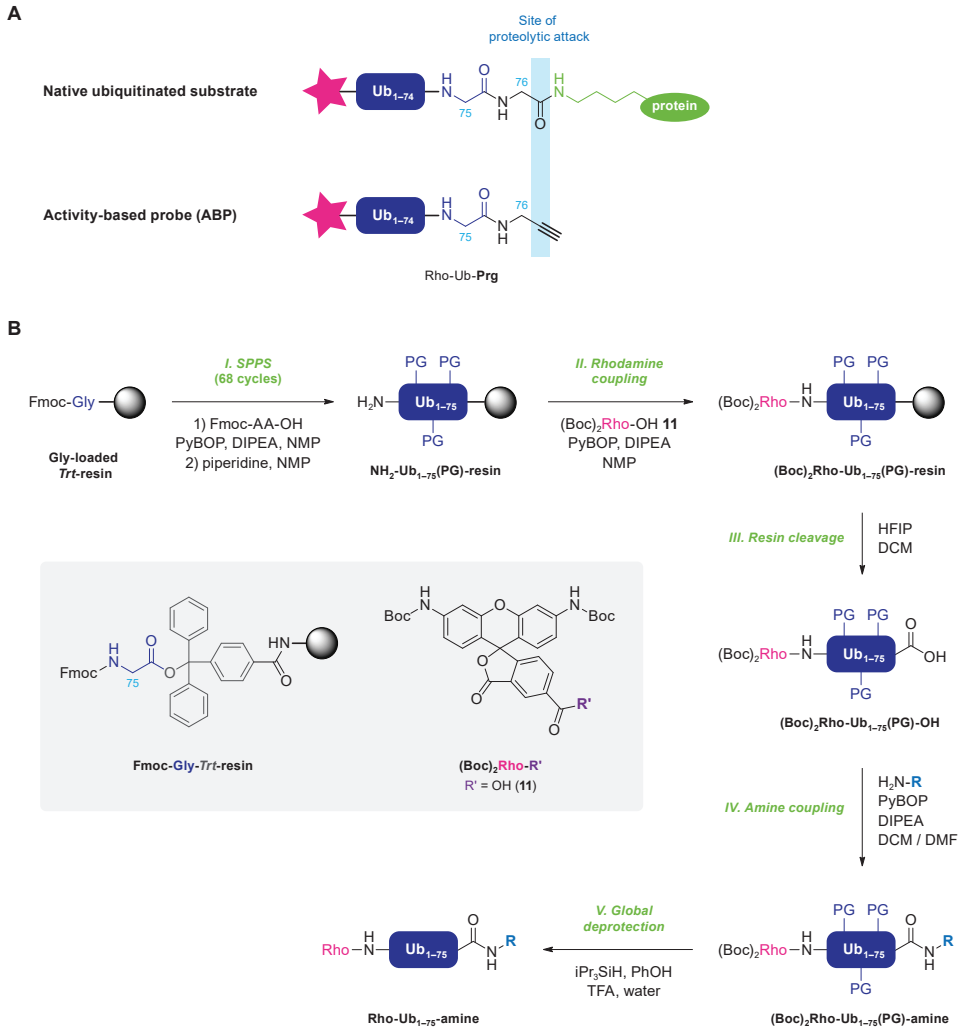

Figure S1 | Design and chemical synthesis of Rho-Ub-ABPs. **(A)** Alignment of warhead with native isopeptide bond. *Top:* nucleophilic attack of catalytic Cys on isopeptide carbonyl between C-terminal Gly76 in Ub and Lys residue in substrate or distal Ub. *Bottom:* nucleophilic attack of catalytic Cys on reactive carbon C2 in alkyne warhead. **(B)** Synthetic scheme for cysteine DUB ABPs with N-terminal 5-carboxy-Rhodamine110 as fluorescent reporter and C-terminal alkyne derivatives as warheads. ***Step I.*** Linear chemical synthesis of protected UbiquitinΔG ($Ub_{1–75}$) on Trt resin *via* solid phase synthesis (SPPS) as described before.[83] ***Step II.*** Coupling of $(Boc)_2$Rho-OH **11** to the N-terminus. ***Step III.*** Cleavage from resin while retaining side chain protecting groups. ***Step IV.*** Coupling of propargylamine (**Prg**) or derivatives (**2**-**10**) to C-terminus. ***Step V.*** TFA-mediated global deprotection to remove all protecting groups, followed by purification by RP-HPLC to obtain pure Rho-$Ub_{1–75}$-ABPs. PG = acid-labile protecting group. Rho = 5-carboxy-Rhodamine110. DIPEA = *N,N*-diisopropylethylamine. NMP = *N*-methyl-2-pyrrolidone. HFIP = hexafluoroisopropanol. DCM = dichloromethane. DMF = dimethylformamide. TFA = trifluoroacetic acid.

Sequence Rho-$Ub_{1–75}$-ABP:
Rho-(Nle)QIFVKTLTGKTITLEVEPSDTIENVKAKIQDKEGIPPDQQRLIFAGKQLEDGRTLSDYNIQKESTLHLVLRLRG-amine

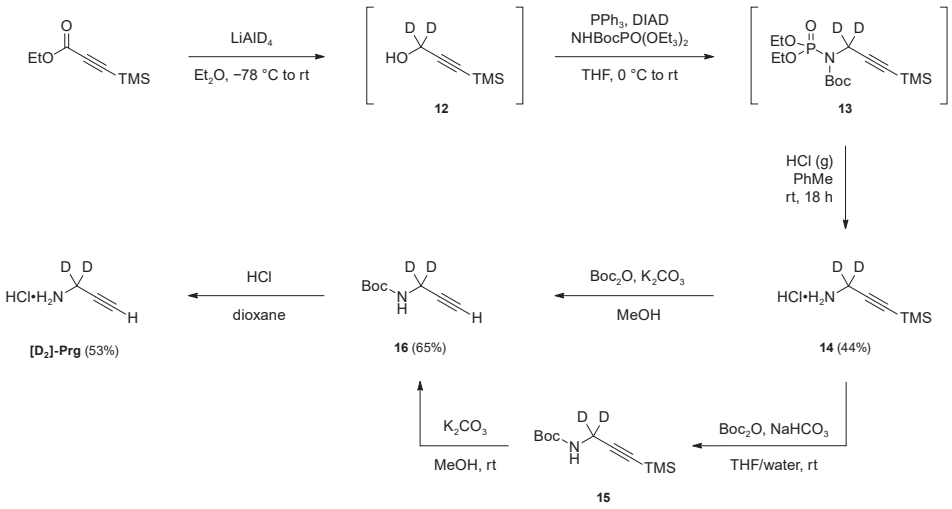

Scheme S1 | Chemical synthesis of deuterated propargylamine **[D_2]-Prg**. [D_2]-propargyl alcohol **12** was formed by reduction of ethyl propiolate with lithium aluminum deuteride, and subsequently converted into protected amine **13** under Mitsunobu conditions.[89] Acid-mediated deprotection generated hydrochloride [D_2]-propargylamine **14** bearing an acid-stable terminal TMS protecting group. Base-mediated TMS removal had to be performed after, or simultaneous with, Boc protection as the free amine [D_2]-propargylamine is very volatile and cannot be separated from reagents and solvents without loss of the product. The resulting Boc-[D_2]-Prg **16** is soluble in organic solvents and can be isolated by simple extraction. Stepwise Boc protection and TMS deprotection was performed to generate intermediates Boc-1-TMS-[D_2]-Prg **15** and Boc-[D_2]-Prg **16** as reference compounds for reaction progress detection by TLC. Finally, hydrochloride salt of deuterated propargylamine **[D_2]-Prg** could be obtained after acid-mediated Boc deprotection.

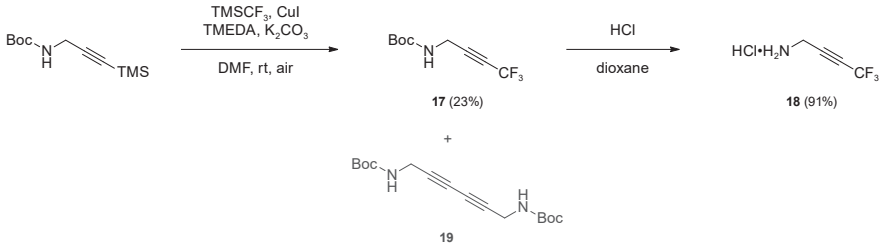

Scheme S2 | Chemical synthesis of electron-deficient propargylamine derivative **18**. Direct trifluoromethylation of Boc-propargylamine with Ruppert-Prakash reagent ($TMSCF_3$)[52] gave desired trifluoromethylated acetylene **17**, which could be separated by FCC from homocoupling product **19** (an undesired side product generated *via* a copper-catalyzed Glaser-Hay dimerization). Hydrochloride salt of amine **18** was obtained by treatment of Boc-protected alkyne **17** with hydrochloric acid.

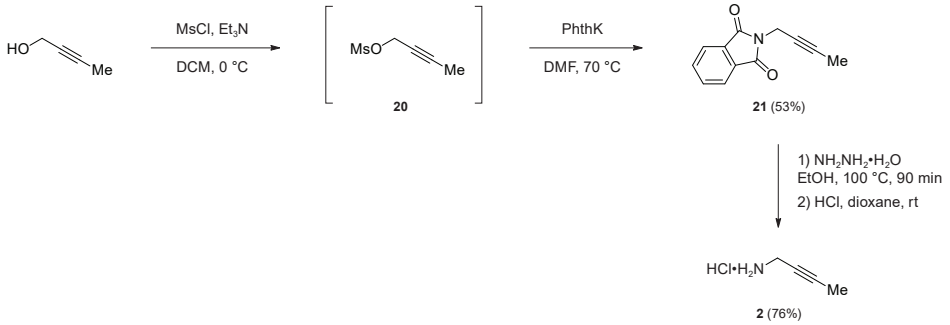

Scheme S3 | Chemical synthesis of methylated propargylamine derivative **2** following reported procedure.[87] The 2-butynylalcohol starting material was treated with methanesulfonyl chloride to form *O*-mesylated 2-butynyl **20**, which has a mesylate leaving group that is compatible with the subsequent Gabriel amine synthesis. Treatment with potassium phthalimide gave phthalimide **21**, and the amine was deprotected with hydrazine hydrate to form 2-butynylamine **2**. The crude reaction mixture was treated with HCl to form the corresponding hydrochloride salt that could be isolated by trituration with diethyl ether.

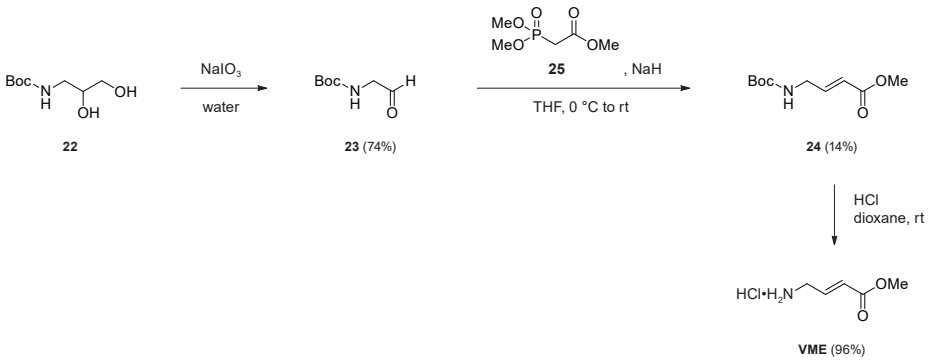

Scheme S4 | Chemical synthesis of vinyl methyl ester building block **VME** following reported procedure.[48] Aldehyde **23** was obtained from Boc-protected isoserinol **22** by oxidative cleavage of the vicinal diol in a Malaprade oxidation with sodium periodate. Horner-Wadsworth-Emmons (HWE) reaction of Boc-glycinal **23** with phosphonate **25** resulted in a mixture of desired (E)-olefin **24** and the undesired (Z)-olefin, which were separable by flash column chromatography. Of note is that the stereoselectivity for (E)-olefin **24** is expected to be lower than for HWE reactions forming olefins derived from other amino acids, which can be attributed to the lack of sidechain substituents on glycine:[120] bulky α-substituents on the aldehyde are known to sterically hinder formation of (Z)-olefins.[121] Finally, the hydrochloride salt of methyl (E)-4-aminobut-2-enoate (**VME**) was obtained by treatment of Boc-protected amine **24** with hydrochloric acid.

7.3. Gel Electrophoresis

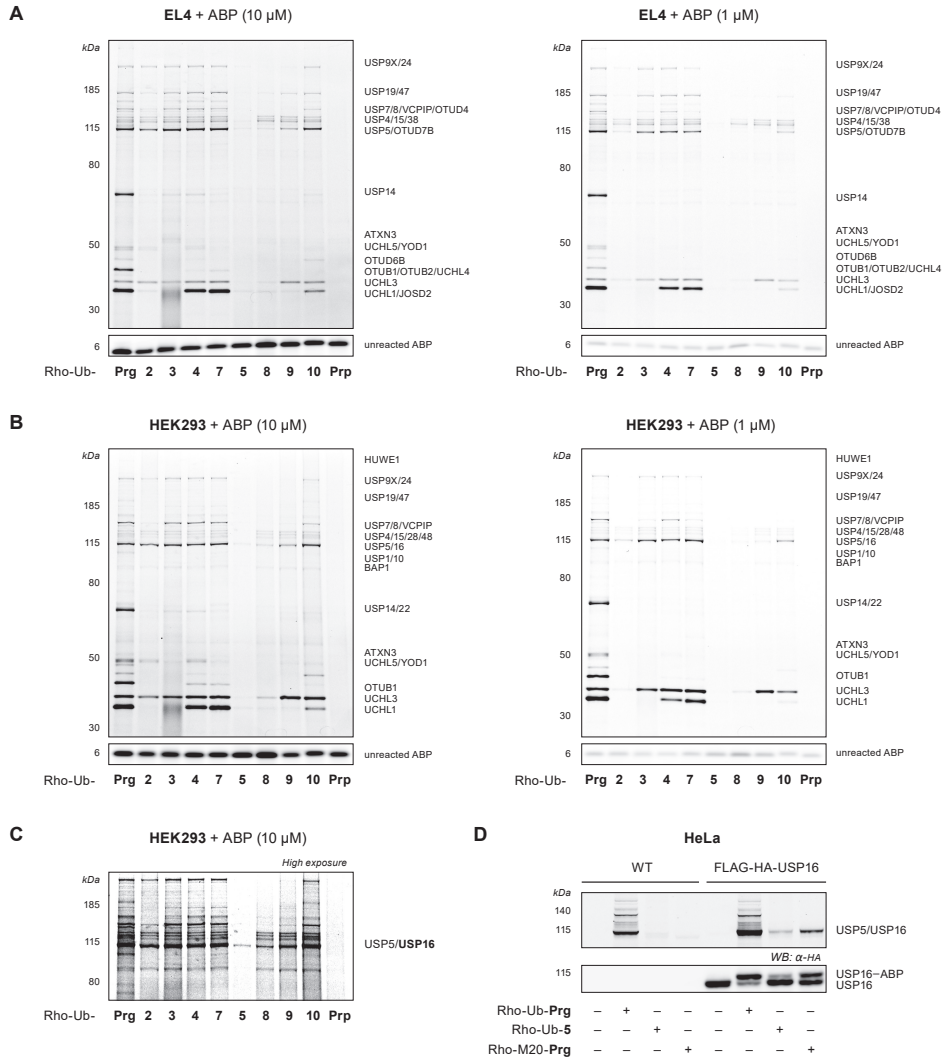

Figure S2 | Lysate incubation with 1-10 µM Rho-Ub-ABPs. **(A)** In-gel fluorescence scan of EL4 lysate incubated with 10 µM *(left)* or 1 µM *(right)* Rho-Ub-ABP. Assignment of labeled DUBs based on proteomic analysis with biotin-Ub-**Prg** by Ekkebus *et al*.[27] Cell lysates of the mouse lymphoma cell line (EL4) are commonly used as benchmark cell line for DUB activity,[19] but do not express (detectable levels of) endogenous USP16.[27] **(B)** In-gel fluorescence scan of HEK293 lysate incubated with 10 µM (*left*, also shown in **Figure 3B**) or 1 µM Rho-Ub-ABP *(right)*. Assignment of labeled DUBs based on proteomic analysis by Altun *et al*.[14] **(C)** Alternative image processing (increased exposure, contrast and adjusted levels) of the fluorescence scan shown in panel B *(left)* to visualize adduct formation between 10 µM Rho-Ub-**5** and endogenous USP16 in HEK293 lysate. Endogenous USP16 levels in HEK293 lysate are low (see panel D), and adduct formation with Rho-Ub-**5** is relatively slow (see **Figure 6C**). **(D)** Incubation of HeLa cell lysate expressing endogenous levels of USP16 *(left)* or expressing HA-FLAG-USP16 *(right)* with Rho-Ub-**Prg** (1 µM), Rho-Ub-**5** (10 µM) or USP16-selective ABP Rho-M20-**Prg** (0.5 µM).[79] Adduct formation of Rho-Ub-**5** with overexpressed HA-FLAG-USP16 is visualized by in-gel fluorescence *(top)* and western blotting for HA *(bottom)*.

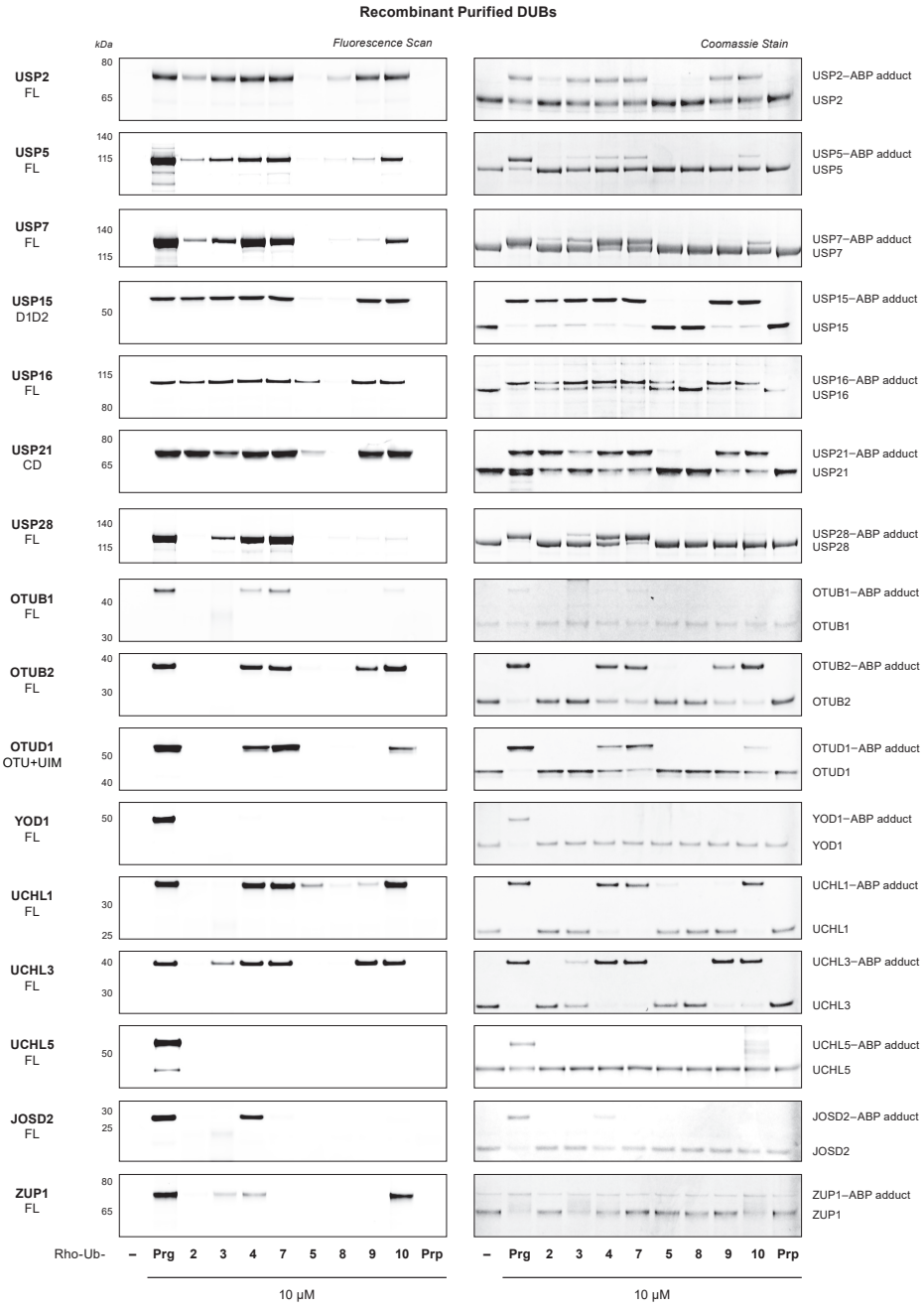

Figure S3 | Gel analysis of covalent DUB–ABP adduct formation between recombinant purified cysteine DUBs (1 µM) and Rho-Ub-ABPs (10 µM) related to **Figure 3C**. Unbound DUB and covalent DUB–ABP adduct (+8.9 kDa) are resolved by SDS-PAGE electrophoresis. *Left:* in-gel fluorescence (λ_{ex} = 473 nm, λ_{em} = 530 ± 10 nm). *Right:* Coomassie protein stain.

7.4. Intact Protein MS

Table S2 | Calculated and deconvoluted mass of intact USP16CD^{WT} and USP16CD^{C205A} (adducts)

		Deconvoluted mass (Da)		
Enzyme	**ABP**	*Calc.* [a]	*Found*	**Covalent adduct**
–	Rho-Ub-**Prg**	8,883.12	8,884	N.A.
	Rho-Ub-**2**	8,897.21	8,898	N.A.
	Rho-Ub-**5**	8,911.24	8,912	N.A.
USP16CD^{WT}	-	N.A.	73,344 & 73,426	N.A.
	Rho-Ub-**Prg**	82,228 & 82,310	82,229 & 82,309	+
	Rho-Ub-**2**	82,243 & 82,324	82,242 & 82,324	+
	Rho-Ub-**5**	82,258 & 82,339	82,256 & 82,338	+
USP16CD^{C205A}	-	N.A.	73,406 & 73,488	N.A.
	Rho-Ub-**Prg**	82,290 & 82,372	73,407 & 73,489	–
	Rho-Ub-**2**	82,304 & 82,386	73,408 & 73,490	–
		82,318 & 82,400	73,408 & 73,489	–

Data related to **Figure 4B-C**. [a] Mass of USP16–ABP adduct calculated based on deconvoluted mass of unbound ABP and unbound USP16.

7.5. HRMS

Table S3 | Calculated and detected m/z of naturally most abundant peak for each charge state.

		z					
Rho-Ub-	**m/z** (Da)	13	12	11	10	9	8
Prg	*Calc.* [a]	684.2974	741.2384	808.5319	889.2842	987.9816	1111.3534
	Found	684.3000	741.2388	808.5306	889.2878	987.9859	1111.3591
[D_2]-Prg	*Calc.* [b]	684.4522	741.4059	808.7148	889.4855	988.2053	1111.6050
	Found	684.4553	741.4115	808.7168	889.4891	988.2110	1111.6116

[a] Isotope model $C_{401}H_{643}N_{107}O_{120}$. [b] Isotope model $C_{401}H_{641}D_2N_{107}O_{120}$ with D = 2.0141017779 u.

7.6. Bottom-Up MS/MS Analysis

Sequence **UCHL3^{WT}** (Uniprot; P15374) with underlined proteolytic peptide containing catalytic residue (Cys95) after trypsin digestion:

MEGQRWLPLE ANPEVTNQFL KQLGLHPNWQ FVDVYGMDPE LLSMVPRPVC AVLLLFPITE KYEVFRTEEE EKIKSQGQDV
TSSVYFMKQT ISNACGTIGL IHAIANNKDK MHFESGSTLK KFLEESVSMS PEERARYLEN YDAIRVTHET SAHEGQTEAP
SIDEKVDLHF IALVHVDGHL YELDGRKPFP INHGETSDET LLEDAIEVCK KFMERDPDEL RFNAIALSAA

Table S4 | Tryptic peptides identified with Mascot (v1.36) after alkylation and tryptic digestion of covalent adducts of Rho-Ub-ABPs with recombinant UCHL3. Bottom-up MS analysis related to **Figure 5**.

	UCHL3^{WT}	
	Rho-Ub-**Prg**	Rho-Ub-**[D_2]-Prg**
Peptide sequence	QTISNACGTIGLIHAIANNK C7-Gly-HH-Prg (112.06366 Da)	QTISNACGTIGLIHAIANNK C7-Gly-DD-Prg (114.07622 Da)
Charge	+3	+3
Monoisotopic m/z	717.71631 Da (+0.16 mmu/+0.22 ppm)	718.38696 Da (−0.04 mmu/−0.05 ppm)
MH$^+$	2151.13437 Da	2153.14634 Da
Rt	32.4201 min	32.5055 min

Peptides with DH-Prg (113.06994 Da) modification were not found for the adduct with Rho-Ub-**[D_2]-Prg**.

Sequence **USP16CD^{WT}** (Uniprot; Q9Y5T5) with underlined proteolytic peptide containing catalytic residue (Cys205) after trypsin digestion:

*MAHHHHHHSA ALEVLFQGP*K GLSNLGNTCF FNAVMQNLSQ TPVLRELLKE VKMSGTIVKI EPPDLALTEP LEINLEPPGP
LTLAMSQFLN EMQETKKGVV TPKELFSQVC KKAVRFKGYQ QQDSQELLRY LLDGMRAEEH QRVSKGILKA FGNSTEKLDE
ELKNKVKDYE KKKSMPSFVD RIFGGELTSM IMCDQCRTVS LVHESFLDLS LPVLDDQSGK KSVNDKNLKK TVEDEDQDSE
EEKDNDSYIK ERSDIPSGTS KHLQKKAKKQ AKKQAKNQRR QQKIQGKVLH LNDICTIDHP EDSDNEAEMS LQGEVNIKSN
HISQEGVMHK EYCVNQKDLN GQAKMIESVT DNQKSTEEVD MKNINMDNDL EVLTSSPTRN LNGAYLTEGS NGEVDISNGF
KNLNLNAALH PDEINIEILN DSHTPGTKVY EVVNEDPETA FCTLANREVF NTDECSIQHC LYQFTRNEKL RDANKLLCEV
CTRRQCNGPK ANIKGERKHV YTNAKKQMLI SLAPPVLTLH LKRFQQAGFN LRKVNKHIKF PEILDLAPFC TLKCKNVAEE
NTRVLYSLYG VVEHSGTMRS GHYTAYAKAR TANSHLSNLV LHGDIPQDFE MESKGQWFHI SDTHVQAVPT TKVLNSQAYL
LFYERIL

Table S5 | Tryptic peptides identified with Mascot (v1.36) after alkylation and tryptic digestion of covalent adducts of Rho-Ub-ABPs with recombinant USP16. Bottom-up MS analysis related to **Figure 5**.

	USP16CD^{WT}	
	Rho-Ub-**Prg**	Rho-Ub-**[D_2]-Prg**
Peptide sequence	GLSNLGNTCFFNAVMQNLSQTPVLR M15-Oxidation (15.99492 Da) C9-Gly-HH-Prg (112.06366 Da)	GLSNLGNTCFFNAVMQNLSQTPVLR M15-Oxidation (15.99492 Da) C9-Gly-DD-Prg (114.07622 Da)
Charge	+3	+3
Monoisotopic m/z	951.47675 Da (−0.84 mmu/−0.88 ppm)	952.14832 Da (−0.12 mmu/−0.12 ppm)
MH$^+$	2852.41568 Da	2854.43039 Da
Rt	41.8239 min	41.9013 min

Peptides with DH-Prg (113.06994 Da) modification were not found for the adduct with Rho-Ub-**[D_2]-Prg**.

Table S6 | Tandem MS analysis. Expected and detected fragment ions of modified tryptic UCHL3 peptide QTISNACGTIGLIHAIANNK.

	b-H_2O^+		b-NH_3^+			y^+		y^{2+}		
$b_{\#}$	**HH-Prg**	**DD-Prg**	**HH-Prg**	**DD-Prg**	*Sequence*	**HH-Prg**	**DD-Prg**	**HH-Prg**	**DD-Prg**	$y_{\#}$
1			*112.03930*		Q					20
2	**212.10297**		*213.08698*		T	*2023.07532*	*2025.08787*	**1012.04130**	*1013.04757*	19
3	**325.18703**		**326.17105**		I	*1922.02764*	*1924.04019*	**961.51746**	**962.52374**	18
4	*412.21906*	**412.21906**	**413.20308**		S	*1808.94358*	*1810.95613*	**904.97543**	**905.98170**	17
5	*526.26199*		*527.24600*		N	*1721.91155*	*1723.92410*	**861.45941**	*862.46569*	16
6	**597.29910**	*597.29910*	**598.28312**		A	*1607.86862*	*1609.88117*	**804.43795**	**805.44423**	15
7	*812.37195*	*814.38450*	*813.35596*	*815.36852*	C*	**1536.83151**	**1538.84406**	*768.91939*	*769.92567*	14
8	*869.39341*	*871.40597*	*870.37743*	*972.38998*	G	**1321.75866**		**661.38297**		13
9	*970.44109*	*972.45364*	*971.42511*	*973.43766*	T	**1264.73720**		*632.87224*		12
10	*1083.55252*	*1085.53771*	*1084.50917*	*1086.52172*	I	**1163.68952**		**582.34840**	*582.34840*	11
11	**1140.54662**	**1142.55917**	**1141.53063**	*1143.54319*	G	**1050.60545**		**525.80637**		10
12	**1253.63068**	**1255.64324**	**1254.61470**	**1256.62725**	L	**993.58399**	*993.58399*	*497.29563*	*497.29563*	9
13	**1366.71475**	**1368.72730**	**1367.69876**	**1369.71131**	I	**880.49993**		**440.75360**		8
14	*1503.77366*	*1505.78621*	*1504.75767*	*1506.77023*	H	*767.41586*	**767.41586**	**384.21157**		7
15	*1574.81077*	*1576.82332*	*1575.79479*	*1577.80734*	A	**630.35695**		*315.68211*		6
16	*1687.89484*	*1689.90739*	*1688.87885*	*1690.89140*	I	**559.31984**		*280.16356*		5
17	*1758.93195*	*1760.94450*	*1759.91597*	*1761.92852*	A	**446.23577**		*223.62152*		4
18	*1872.97488*	*1874.98743*	*1873.95889*	*1875.97145*	N	*375.19866*		*188.10297*		3
19	*1987.01780*	*1989.03036*	*1988.00182*	*1990.01437*	N	**261.15573**		*131.08150*		2
20					K	*147.11280*		*74.06004*		1

Tandem MS analysis for QTISNAC*GTIGLIHAIANNK peptide modified with Gly-HH-Prg (m/z = 717.716 $^{3+}$ Da) or Gly-DD-Prg (m/z = 718.387 $^{3+}$ Da) related to **Figure 5D** and **Table S4**. Obtained by alkylation and trypsin digestion of covalent UCHL3–Rho-Ub-**Prg** adduct (HH-Prg) and UCHL3–Rho-Ub-**[D_2]-Prg** adduct (DD-Prg). **Bold** = detected fragment ions. *Italic* = expected fragment ion (not detected).

7.7. Kinetic Analysis of Covalent USP16 Occupancy

Kinetic evaluation of incubation time-dependent covalent occupancy was performed by quantification of unbound USP16 and covalent USP16–ABP adduct on gel for recombinant USP16CD^{WT} incubated with Rho-Ub-**Prg**, Rho-Ub-**2**, and Rho-Ub-**5** (**Figure 6B**). Each assay condition was conducted three individual times (biological triplicate, n = 3), thus there are three values for covalent occupancy for each ABP concentration/incubation time. Samples were exposed to denaturing conditions to promote disintegration of noncovalent USP16–ABP complexes into unbound USP16 and unbound ABP, while covalent adducts remain intact. To improve the standard deviation for Rho-Ub-**Prg**, 1-5 minute measurements were performed (n = 1) but these still showed reaction completion within the first minute. Lowering incubation temperature to 21 °C also resulted in maximum adduct formation with Rho-Ub-**Prg** before the first timepoint. In our experiments, we ensured that ABP is present in large excess at reaction initiation (t = 0): $[ABP]_0 \geq 10[USP16]_0$. We selected ABP rather than USP16 to be present in excess because unbound USP16 and covalent adduct can be quantified in the same gel, while quantification of unbound ABP and covalent adduct in a single gel is challenging: either unbound ABP signals overlap with the loading front, or the covalent adduct has run off the gel.

Kinetic analysis is performed under pseudo-first order reaction conditions ($[ABP]_0 \geq 10[USP16]_0$) to enable algebraic analysis: the unbound ABP concentration should not decrease significantly upon USP16 binding. It is essential not to violate this assumption to obtain reliable estimates for the rate of covalent adduct formation k_{obs}. Under pseudo-first order conditions, covalent adduct formation can be fitted to a one-phase exponential increase, with covalent occupancy increasing by 50% every half-life. 97% covalent adduct formation is reached after five half-lives, which generally is considered 'close enough' to reaction completion: detection of changes beyond this point will be affected by error margins.

Irreversible ligand binding kinetics. Covalent adduct formation between enzyme and ABP is a two-step ligand binding reaction. We normally assume that the noncovalent equilibrium is reached almost instantly *(rapid equilibrium approximation)* [122] and that this reaction is much faster than covalent adduct formation.[53] The reaction will slow down as the reaction progresses, because the concentration of both ABP and enzyme decreases when neither enzyme nor ABP is present in large excess *(second order reaction conditions)*.[122] Second order reaction conditions complicate algebraic analysis, and Morrisons quadratic equation – used to correct for the shift in equilibrium caused by inhibitor depletion – is limited to reversible ligands. Therefore, reaction kinetics of irreversible ligand binding are studied under pseudo-first order reaction conditions: [123-124] one of the reactants is present in excess ($[A]_0 \geq 10[B]_0$), so we can assume that the concentration of unbound reactant A (present in excess) will not change significantly upon protein binding ($[A]_t = [A]_0$).

7.8. Fluorescence Polarization (FP) Binding Assay

FP Binding assays of catalytic inactive DUBs with fluorophore-labeled ubiquitin as ligand are commonly performed to determine the noncovalent affinity.[65, 125] FP binding assays of reporter/ligand Rho-Ub-ABPs (9 kDa) with catalytically inactive USP16CD^{C205S} mutant (73 kDa) were performed to determine K_D-values that are independent of electronic factors as covalent adduct formation with USP16CD^{C205S} does not occur. Catalytic inactive mutant USP16CD^{C205S} rather than USP16CD^{C205A} was used because active site alanine mutations in cysteine DUBs increase the affinity for ubiquitin.[126] The concentration of Rho-Ub-ABP (5 nM) was kept constant and excess USP16 (>50 nM) was varied, as is common for FP binding assays to maximize the assay window.[65, 127] The assay was performed under pseudo-first order reaction conditions ($[E]_0 >> [ABP]_0$): no significant change in unbound enzyme concentration ($[E] = [E]_0$), and equilibrium has been reached. Fluorescence polarization was measured every 3 minutes for 120 minutes (**Figure S4A**), and values after sufficient incubation (60 minutes) were plotted against USP16 concentration (**Figure S4B**). High protein concentrations are prone to exhibit nonspecific binding due to hydrophobic interactions and crowding effects, which was observable as the inability to reach a plateau despite supplementing the buffer with 0.005% Tween20 or additional 0.1 mg/mL bovine serum albumin (BSA; Chemcruz, #sc-2323A).[127] All USP16 concentrations were fitted with a shared value for nonspecific binding (NS > 0, **Figure S4B**, *left*) or only USP16 concentrations below 20 µM, without taking nonspecific binding into account (NS = 0, **Figure S4B**, *right*). These restraints affect the absolute K_D-values, but regardless of the settings we observe the same trend; K_D for **Prg** < **2** < **5**.

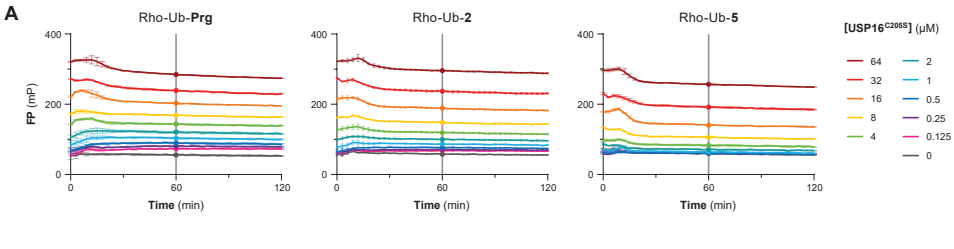

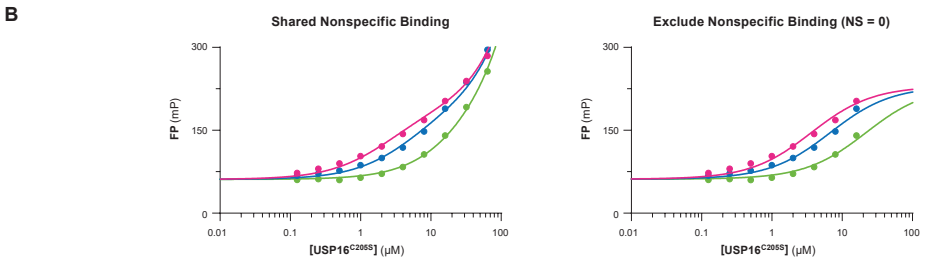

	Rho-Ub-**Prg**	Rho-Ub-**2**	Rho-Ub-**5**	Rho-Ub-**Prg**	Rho-Ub-**2**	Rho-Ub-**5**
K_D (µM)	2.446 ± 0.215	5.200 ± 0.415	25.83 ± 1.80	3.639 ± 0.323	6.762 ± 0.570	21.83 ± 1.92
Background (mP)		61.19 ± 0.85			61.55 ± 0.98	
B_{max} (mP)		129.6 ± 4.15			168.4 ± 5.29	
NS (mP/µM)		1.695 ± 0.069			0	

Figure S4 | Fluorescence polarization (FP) binding assay related to **Figure 6C**. **(A)** Progress curve for fluorescence polarization signal over time for Rho-Ub-ABPs (5 nM) with USP16CD^{C205S} (0-64 µM). Noncovalent equilibrium between ABP and enzyme is reached after ~30 min. **(B)** Direct binding curve. Fluorescence polarization after incubation for 60 min as a function of USP16CD^{C205S} concentration. Fitted with shared values for NS, B_{max} and background to obtain K_D-value for each Rho-Ub-ABP. *Left:* All USP16 concentrations were fitted with a shared value for nonspecific binding. *Right:* [USP16] < 20 µM was fitted with nonspecific binding NS = 0. Graphical data represents the mean ± standard deviation for a single representative experiment.

7.9. Thiol Reactivity Assay

Adduct formation with biological thiols such as cysteine and glutathione (GSH) is an established method to assess intrinsic chemical reactivity of electrophilic warheads towards thiols.[128] The mass difference of unbound ABP and GSH adduct was clearly detected, but it was not possible to separate the unbound ABP from the GSH adduct for quantification of the LC-MS UV trace. Instead, quantification was performed based on the intensity of the naturally most abundant peak for the most common charge states (z = 7-13) in the ionization envelope of ubiquitin (**Table S7**), as is more often used for quantification in top- and middle-down mass spectrometry of ubiquitin.[129-130]

Table S7 | Charge states used for quantification of unbound ABP and GSH adduct in thiol reactivity assay.

			m/z (Da)						
ABP	**State**	**M** (Da)	z = 13	z = 12	z = 11	z = 10	z = 9	z = 8	z = 7
Rho-Ub-**Prg**	unbound	8883	684.2	741.2	808.5	889.2	987.9	1111.3	1270.0
	GSH adduct	9190	*707.9*	*766.8*	*836.5*	*920.0*	*1022.1*	*1149.8*	*1313.9*
Rho-Ub-**2**	unbound	8897	685.4	742.3	809.7	890.6	989.4	1113.0	1271.9
	GSH adduct	9204	*709.0*	*768.0*	*837.7*	*921.4*	*1023.7*	*1151.5*	*1315.9*
Rho-Ub-**3**	unbound	8959	690.1	747.5	815.4	896.8	996.3	1120.9	1280.7
	GSH adduct	9266	*713.8*	*773.2*	*843.4*	*927.6*	*1030.6*	*1159.3*	*1324.7*
	hydrolysis	8977	691.5	749.0	817.0	898.7	998.4	1123.1	1283.3
Rho-Ub-**4**	unbound	8897	685.3	742.4	809.7	890.6	989.5	1113.0	1271.9
	GSH adduct	9204	*709.0*	*768.0*	*837.7*	*921.4*	*1023.7*	*1151.5*	*1315.9*
Rho-Ub-**7**	unbound	8959	690.1	747.5	815.3	896.8	996.4	1120.8	1280.7
	GSH adduct	9266	*713.8*	*773.2*	*843.4*	*927.6*	*1030.6*	*1159.3*	*1324.7*
Rho-Ub-**5**	unbound	8912	686.4	743.5	811.0	892.0	991.0	1114.9	1273.9
	GSH adduct	9219	*710.2*	*769.3*	*839.1*	*922.9*	*1025.3*	*1153.4*	*1318.0*
Rho-Ub-**8**	unbound	8951	689.4	746.8	814.6	896.0	995.5	1119.7	1279.7
	GSH adduct	9258	*713.2*	*772.5*	*842.6*	*926.8*	*1029.7*	*1158.3*	*1323.6*
Rho-Ub-**9**	unbound	8897	685.3	742.3	809.6	890.5	989.5	1113.1	1271.9
	GSH adduct	9204	*709.0*	*768.0*	*837.7*	*921.4*	*1023.7*	*1151.5*	*1315.9*
Rho-Ub-**10**	unbound	8897	685.3	742.3	809.7	890.5	989.4	1113.0	1271.9
	GSH adduct	9204	*709.0*	*768.0*	*837.7*	*921.4*	*1023.7*	*1151.5*	*1315.9*
Rho-Ub-**Prp**	unbound	8887	684.5	741.4	808.8	889.6	988.3	1111.8	1270.4
	GSH adduct	9194	*708.2*	*767.2*	*836.8*	*920.4*	*1022.6*	*1150.3*	*1314.4*
Rho-Ub-**18**	unbound	8951	689.5	746.9	814.6	896.0	995.5	1119.8	1279.7
	GSH adduct	9258	713.1	772.5	842.5	926.8	1029.5	1158.2	1323.4
Rho-Ub-**VME**	unbound	8943	688.8	746.2	813.9	895.2	994.5	1118.7	1278.5
	GSH adduct	9250	712.5	771.8	841.8	926.0	1028.7	1157.2	1322.4

Data related to **Figure 7C**. Detection of Rho-Ub-ABPs, GSH–ABP adducts (+307 Da), and other ABP derivatives by LC-MS in ES+ mode; m/z = (M+ zH^+)/z. Values in *italics* are expected/calculated values, not detected.